3-D EM MODELLING USING THE COMPACT FINITE ELEMENT METHOD

A THESIS

submitted in fulfilment of the requirements for the award of the degree of

DOCTOR OF PHILOSOPHY

By

PRAVIN KUMAR GUPTA

Forwarded
M. Singhal
26.9.87

Professor & Head
Department of Earth Sciences
University of Roorkee
ROORKEE-247667

DEPARTMENT OF EARTH SCIENCES
UNIVERSITY OF ROORKEE
ROORKEE-247 667 (INDIA)

September, 1987

CANDIDATE'S DECLARATION

I hereby certify that the work which is being presented in the thesis entitled **3-D EM MODELLING USING THE COMPACT FINITE ELEMENT METHOD** in fulfilment of the requirement for the award of the DEGREE OF DOCTOR OF PHILOSOPHY submitted in the Department of Earth Sciences of the University is an authentic record of my own work carried out during a period from June 1984 to September 1987 under the supervision of **Prof. V.K. Gaur, Dr. A.P. Raiche** and **Prof. P.S. Moharir.**

The matter embodied in this thesis has not been submitted by me for the award of any other Degree.

P.K. Gupta

(PRAVIN KUMAR GUPTA)

This is to certify that the above statement made by the candidate is correct to the best of my knowledge.

V.K. Gaur

Prof. V.K. Gaur
N.G.R.I.,
Uppal Road
Hyderabad - 500 007
INDIA

A.P. Raiche

Dr. A.P. Raiche
Division of Mineral Physics
and Mineralogy, CSIRO,
Delhi Road, North Ryde - 2113
AUSTRALIA

P.S. Moharir

Prof. P.S. Moharir
Dept. of Earth
Sciences,
Univ. of Roorkee
Roorkee, U.P.,
INDIA

Date: 26.9.87

The candidate has passed the Viva-Voce examination held on.....
at..... The thesis is recommended for award of the Ph.D. Degree.

Signature of Guide/s

Signature of External Examiners

To

MAMTA, MANSI

AMMA and PITAJI

ACKNOWLEDGEMENTS

The sincere cooperation and help of my three supervisors Prof. Vinod K. Gaur, Dr. Art P. Raiche and Prof. Pramod S. Moharir rendered possible the completion of this thesis. I am gratefully indebted to Prof. Gaur for his wisdom, patience and ready advice which guided and encouraged me not only during the tenure of the present work but eversince my exposure to the world of geophysics. I would like to acknowledge my sincere gratitude to Dr. Raiche for valuable interest, advice and help in my work, and otherwise, during my stay in Australia and thereafter. I am grateful to Prof. Moharir for his illuminating suggestions and advice and also for the encouragement offered particularly during the final phase of this thesis.

My warm thanks are extended to Ki Ha Lee for his cooperation in providing the computer code HYB3D and the time domain results for comparison which made this work possible ; to Keeva Vozoff and Don F. Pridmore for their valuable suggestions during the discussions we had in Australia ; to Lincoln A. Bennett for his indispensable and valuable help particularly in decoding and debugging of computer codes of various algorithms developed ; and to San Filipo for providing a set of time domain results for comparison.

I am grateful to the Australian Minerals Industry Research Association (AMIRA) for financing my visit to the Division of Mineral Physics and Mineralogy, CSIRO, Australia, under one of their projects with Dr. Raiche and also to the Chief of the Division for inviting me and extending cooperation during my stay there.

I am thankful to Profs. V.K.S. Dave, K.N. Khattri and B.B.S. Singhal for their ready cooperation as Heads of the Department of Earth Sciences and for encouragement during the period of this work.

I am thankful to Pulok K. Mukherjee, Sujeet Sinha, Josodheer Das and Shantanu Sarkar for their unfailing and prompt assistance during the typing phase of the thesis and also for moral support all throughout.

Last but not the least important are Ashok K. Sharma and Kamesh Gupta who meticulously typed the manuscript and drafted the figures respectively.

PRAVIN KUMAR GUPTA

ABSTRACT

Numerical methods employed for 3-D electromagnetic (EM) forward modelling are : Finite Element Method (FEM), Integral Equation Method (IEM) and a Hybrid Method (HM) - Compact Finite Element Method (CFEM) - that amalgamates the positive features of the first two methods. FEM has the advantage of being able to deal with an arbitrary resistivity distribution. However, as the whole earth must be modelled, necessitating discretization of a large domain, the resulting stiffness matrix becomes rather large. IEM, on the other hand, can handle only confined targets buried in a layered earth. Here only the target need be discretized which makes the resulting coefficient matrix much smaller. In this case, however, we have the problem of singularities and of distributing the artificial charges arising at cell boundaries from the assumption of constant EM field in each cell. CFEM like IEM, can handle only confined targets and requires discretization of only the target alongwith an element thick veneer of the host medium. FEM is then used to solve for secondary fields and IEM to generate necessary boundary values. The two operations can be performed iteratively, in which case the coefficient matrix is banded, or a direct scheme can be developed where the coefficient matrix is not banded. In CFEM the coefficient matrix is not large and there are niether singularities nor artificial charges generated at the element boundaries because the EM field varies over the element. Although FEM is more versatile, this advantage becomes inconsequential as it can not be exploited in the present day computing environment.

This thesis deals with the development of three CFEM algorithms– HYBRIDC, SANGAM and SAMAYA. The first two enable one to compute solutions in the frequency domain and the third one in time domain. A brief outline of the thesis is as follows.

In the introductory chapter, the importance of numerical forward modelling in data inversion is discussed. The wide range of applications of EM methods is next presented. The scarcity of 3-D EM modelling results, particularly in time domain, is highlighted in the state-of-the-art review of the EM numerical modelling.

In chapter-II the EM theory is discussed in brief, the ranges of physical parameters : conductivity, dielectric permittivity and magnetic permeability encountered in the earth are discussed with a view to simplifying the general EM equations. Also presented in brief is an account of different EM response functions that are computed from observations for interpretation purposes.

In chapter-III, a classification of different numerical methods is presented. Weighted Residual Methods, in general, and FEM and IEM, in particular are discussed next. Finally, CFEM is discussed and its two variations, iterative and direct schemes, are formulated.

In chapter-IV, is presented an account of the development of the three CFEM algorithms HYBRIDC, SANGAM and SAMAYA that originated from an iterative HM algorithm HYB3D developed by Lee et.al. (1981, Geophysics, **46**, 796-805). The adapted version of HYB3D was named as HYBRIDB. The search routines, developed to eliminate the repetition in the computation of Green's functions that occurred in HYBRIDB, and the resulting modifications that led to the development of HYBRIDC are discussed next. HYBRIDC needs an order of magnitude less time than HYBRIDB. The development of SANGAM which implements direct scheme of CFEM and not the iterative one implemented by HYBRIDB and HYBRIDC, is discussed next. For the number of nodes that can be handled presently, SANGAM needs an order of magnitude less time than HYBRIDC. The results of a comparative study of the performances of HYBRIDB, HYBRIDC and SANGAM are then presented. Finally,

the development of SAMAYA is discussed.

In chapter-V the results of various studies made on SANGAM and SAMAYA are presented. The studies performed on SANGAM pertain to (i) mesh convergence, (ii) convergence of responses of a 3-D body, as its strike-length is progressively increased, to that of the corresponding 2-D body, (iii) no resistivity contrast case, (iv) reciprocity test and (v) comparison of SANGAM results with those obtained by using other algorithms. The studies conducted on SAMAYA pertain to i) identification of the range of frequencies for which frequency domain response need be computed, ii) identification of the minimum number of frequencies per decade necessary for stable transformation from frequency to time domain, iii) comparison of the transform routine results for a 1-D model with those obtained from a direct time domain algorithm for 1-D study, iv) comparison of the response of elongated 3-D body with those of a 3-D thin sheet like body, v) comparison of SAMAYA results with corresponding results obtained by using an IEM algorithm of San Filipo et.al. (1985, Geophysics, **50**, 798-809, 1144-1162), vi) the overburden effect and vii) the bore hole study.

Finally, in chapter-VI it is concluded that these algorithms offer new reliable software packages for forward 3-D EM modelling. Their possible use in catalogue preparation and development of definitive features of a 3-D anomaly is highlighted. Also discussed here is the possible future scope of work in the directions such as development of new matrix solvers exploiting more efficiently the sparsity and inherent structure of the matrix, use of a smaller set of digital filters in convolution operation and recourse to pipelining and parallel computing wherever possible.

CONTENTS

Page No.

CHAPTER - I

THE PERSPECTIVE

1.1 MOTIVATION

The interpretation of a set of observations is the climax of any scientific study. Through interpretation, an isomorphism is sought between the observations and the theoretical response of a putatively identified formal system (Hofstadter, 1982).

Definition : For interpretation of a geophysical data set, the formal system comprises of i) an appropriate physical model of the earth that incorporates, is consistent with, or at least, does not contradict the available geological and any other a-priori information ; the relevant physical laws in terms of which the consistency is determined and their mathematical formulation, ii) an appropriate computational methodology and iii) an efficient numerical software that would unambiguously compute the response of the chosen earth model to a given source-receiver system.

In literature, the computation of the response of a putatively identified formal system is termed as a 'direct' or 'forward' problem, while the identification of formal system(s) that would yield a response isomorphic to the given set of observations is termed an 'inverse' problem. Thus, any data interpretation problem is an inverse problem.

In geophysics, an inverse problem is conventionally understood as the search for the class of physical earth models that would generate a response isomorphic to the given set of observations within a prescribed approximation. This means that in order to solve a conventional geophysical inverse problem, it is sufficient only to satisfy the first requirement of the given definition

of a formal system. However, it may be stressed here that in the conventional concept of geophysical inverse problem articulation of the relevant physical law(s) is always presumed to be achieved a-priori although, at least in principle, the prevalent understanding of the physical laws and their mathematical formulation too may be subject to revision in the light of the experimental data. It may also be emphasized that in the conventional notion of the geophysical inverse problems, no specific consideration is given to the second and third requirements. This limited notion of geophysical inverse problem is justified in cases where analytical solution of the forward problem is sought because either the analytical solution is unique or a whole class of solutions can be derived and, if need be, substantiated using rigorous convergence and error analyses. Unfortunately, analytical solutions to many problems of interest do not exist and one has to seek recourse to numerical methods such as Finite Difference, Finite Element, Integral Equation, Hybrid etc., to obtain the solution of forward problems. Three basic characteristics of the numerical solution to a geophysical forward problem need be emphasized in order to illustrate how the use of numerical methods exposes the restricted nature of the conventional notion of geophysical inverse problems. Firstly, since any numerical solution is dependent upon the strategy and parameters of discretization of the domain under study, unlike the analytical solution, it may not be, and, in general, is not, unique. Secondly, finite register length effects due to quantization of i) input data, ii) coefficients and iii) intermediate computational results, render the results machine-dependent. Thirdly, although rigorous convergence and error analyses of numerical solutions are of utmost importance, they have rarely been carried out for 2-D/3-D geophysical modelling and inversion problems. Also, it would be appreciated that the results of error analysis are dependent on the strategy and parameters of discretization of the domain as well as of variables and constants, and may forbid certain

combinations of discretization options. These characteristics of numerical solutions call for an explicit incorporation of the second and third requirements of the formal system into the definition of an inverse problem.

The definition of the inverse problem proposed here explicitly states the dependence of derived earth model(s) on the computational methodology and the numerical software employed in solving the forward problem.

Since the solution to a forward problem is a prerequisite of solving an inverse problem, any progress made in the field of forward modelling, in turn, catalyzes new developments in the field of data interpretation. Development of appropriate computational methodologies and of efficient numerical software packages are the two fields where quite some progress has been made in recent years, particularly in geophysics. But a quite deal more still remains to be done. This is particularly true of 3-D modelling, because all available algorithms require enormous amount of computer storage and time. In today's world, where economic constraints are the most severe, development of evermore efficient and high precision numerical software packages is of considerable importance. The present study was taken up with this goal in mind resulting in the development of three forward modelling algorithms for 3-D electromagnetic studies of the geosphere.

1.2 WHY ELECTROMAGNETIC METHODS ?

The choice of electromagnetic (EM) methods for the present study was primarily motivated by the following factors :

a) A wide range of EM methods have been successfully employed in the fields of exploration, aeronomy and solid earth geophysics. For example, some important EM methods applied to geophysical problems are :

i) Frequency Domain Electromagnetic (FDEM),

ii) Time Domain Electromagnetic (TDEM),

iii) Magnetotelluric (MT) and

iv) Geomagnetic Deep Sounding (GDS).

b) EM methods find widespread application in diverse fields of earth investigations, notably,

i) Resource exploration such as

1) metallic ore deposits (vide articles by Brant et.al., Clayton, Hallof, Lacy et.al., Paterson, Podolsky, Salt, Strangway and White in Mining Geophysics Vol.I, Society of exploration geophysicists (1966), Poddar (1981, 1982), Macnae et.al. (1984), Butt (1985), Craven et.al. (1985), Peacock et.al. (1985), Rozenberg et.al. (1985), Silic et.al. (1985), Poddar et.al. (1986)),

2) ground water (vide Patra (1970), Koefoed et.al. (1976), Arora et.al. (1981), Palacky et.al. (1981), Palacky (1983), Dodds et.al. (1985)),

3) diamond bearing kimberlite pipes (vide Macnae (1979), Kamara (1981), Palacky (1983), Rai et.al. (1986)),

4) deep seated economic deposits overlain by thick magmatic or sedimentary cover (vide Anderson et.al. (1985)),

5) geothermal reservoirs (vide Adam (1976), Tripp et.al. (1978), Hoover et.al. (1978), Wright et.al. (1985)),

6) oil and gas bearing structures (vide Anderson et.al. (1985), Berkman et.al. (1985), Vozoff et.al. (1985)),

ii) Engineering applications (vide Patra (1970), Cauterman et.al. (1978), Lytle et.al. (1981), Haigh et.al. (1985)),

iii) Mining applications (vide Lytle et.al. (1976), Holmes et.al. (1977), Lytle et.al. (1979), Peacock et.al. (1985)),

iv) Archeological applications (vide Tabaagh (1985), Wynn (1986)),

v) Geological and stratigraphic mapping (vide Frischnecht (1966), Lytle et.al. (1979), Palacky (1981, 1983), Buselli (1985)),

vi) Study of subsurface tectonic structures (vide Hutton (1976a,b), Hutton et.al. (1977), Gough (1983), White et.al. (1985)) and

vii) Study of rock forming processes such as metamorphism, migmatization and granitization (vide Porstendorfer (1975), Adam (1976)).

c) Some of the EM software packages, existing at the time of commencement of the present study, were available to the author - The program HYB3D of the University of California, provided by K.H. Lee, The digital filter routines for computation of convolution integrals, Hankel, Sine and Cosine Transforms (vide Anderson (1979)), The programs RECTEM and OZPLAT of the Division of Mineral Physics and Mineralogy, CSIRO, Australia.

The EM algorithms developed in this thesis can be used to solve 3-D forward modelling problems pertaining to FDEM, TDEM, MT and GDS. Indeed, they may be readily adapted for application to any of the problems mentioned above.

1.3 THE CASE FOR 3-D EM FORWARD MODELLING

The current status of EM data interpretation is such that even when

there exists positive information from other studies that the target being investigated is three dimensional, the EM interpretation is mostly carried out using 1-D or sometimes, when feasible, 2-D approximation of the 3-D target model (e.g. refer to Gough (1973), Lytle et.al. (1979), Mbipom et.al. (1983), Kaikkonen et.al. (1984), Banks et.al. (1984), Ritz (1984), Berkman et.al. (1985), Cull (1985), Kurtz et.al. (1986)). The reason for this is twofold. Firstly, the available 3-D EM forward modelling algorithms require enormous amount of computer time and storage. Secondly, inversion methodologies have been adequately developed only for the 1-D case. Some 2-D inversion algorithms are also being used (e.g. Weidelt (1975), Jupp et.al. (1977) and Oristaglio et.al. (1980)), but for 3-D inversion of EM, only isolated indirect attempts have been made. However, 2-D EM forward modelling algorithms being sufficiently well developed to create confidence amongst field geophysicists, serious attempts are now afoot to develop viable 2-D EM inversion algorithms. Development of 3-D EM inversion methods, on the other hand, must await the availability of efficient 3-D EM forward modelling algorithms. Although the first endeavours in 3-D EM modelling started around 1972, it has gained momentum only during the past few years, as the review of literature, conducted in the next section, illustrates.

When the present study was launched in 1984, there were no published accounts in geophysical literature of 3-D TDEM modelling results. Since then, San Filipo et.al. (1985a, b) have published the results of their 3-D TDEM algorithm that is based on the integral equation method. A comparison of results of their algorithm with those of the TDEM algorithm developed in this thesis reveals a kind of complementarity between the two algorithms, which is discussed in chapter-V. Another result of a TDEM algorithm has been published by Newman et.al. (1986). It may be stressed here that although the efficiency

of the algorithms discussed subseqently in this thesis is greater than that of their predecessor, it still needs to be enhanced for 3-D EM modelling to become practical.

While 3-D inversion algorithms are still in being, the 3-D forward modelling algorithms can be used to prepare catalogues that would, in turn, suggest the distinguishing features of the response of a 3-D body. Furthermore, an attempt can be made to use these discriminant features for estimating the parameters of 3-D structures. In global MT and GDS methods, these 3-D algorithms can also be used for identifying and removing the effects of 3-D shallow heterogeneities, a procedure followed in Distortion Theory (vide Berdichevsky et.al. (1976), Park et.al. (1983), Park (1985)).

1.4 THE STATE-OF-THE-ART OF EM NUMERICAL MODELLING

About ten years ago, there were very few English language books dealing with EM methods - Keller and Frischnecht (1966), Rikitake (1966), Society of Exploration Geophysicists (1966, 1967) and Porstendorfer (1975). Besides these books there were few review articles - Keller (1971), Jones (1973), Ward et.al. (1973), Ward et.al. (1974), Hobbs (1975), Praus (1975) - which one could refer to for gaining insight into EM methods. However, since 1980, a number of textbooks and monographs have been published - Kaufman and Keller (1983, 1985) for FDEM and TDEM methods ; Patra and Mallick (1980) and Wait (1982) for FDEM, TDEM and MT methods ; Kaufman and Keller (1981) for MT method and Rokityanski (1982) and Berdichevsky and Zhdanov (1984) for MT and GDS methods. This spurt in publication of books on EM methods is indicative of growing interest in these methods. The books by Kaufman and Keller, Rokityanski and Berdichevsky and Zhdanov present illustrative accounts of and numerous references to the works of East European scientists, particularly the Soviet scientists - a feature that was

conspicuously missing in earlier works.

Ward (1980) presented an excellent account of the development of electrical, electromagnetic and magnetotelluric methods. In a seminar on Applied Geophysics in Tropical Regions, Hohmann (1983a), Nabighian (1983) and Vozoff (1983) contributed state-of-the-art papers on numerical modelling of EM methods, TDEM method and the MT method, respectively.

These review articles, alongwith the forementioned books, present an exhaustive account of i) various kinds of source excitations, ii) layered earth problems, iii) response of targets with simple geometries like sphere, cylinder, spheroid etc. and iv) response of arbitrary 2-D bodies. Of these, only books by Rokityanski (1982) and Berdichevsky and Zhdanov (1984) contain a discussion on distortion of deep MT and GDS anomalies by 3-D shallow hetrogeneities. Earlier, Berdichevsky and Dmitriev (1976) and Hewson-Brown and Kendall (1976) reviewed the problems in 3-D modelling and interpretation of MT and GDS data. Later, Hohmann (1983b) reviewed the state of the art of 3-D EM modelling with an emphasis on FDEM and MT methods. Notwithstanding these publications, there exists an acute scarcity of readily accessible literature on 3-D EM modelling. To fill this gap, an attempt has been made to review the 3-D literature in some detail in the next section. Subsequently in Sec 1.4.2, some recent developments of interest to 2-D EM modelling have been discussed and finally in sec. 1.4.3 some approximation methodologies, particularly in TDEM, have been discussed.

1.4.1 3-D EM modelling

The numerical methods employed in geophysics, particularly for 3-D EM modelling, are Finite Difference Method, Finite Element Method, Integral Equation Method, Hybrid Method, Electromagnetic Migration Method and

Summary Representation Method. A brief review of literature on the use of these methods in 3-D EM modelling follows.

1.4.1.1 Finite difference method (FDM)

The first results from a 3-D FDM algorithm were presented by Jones and Pascoe (1972) for solving the problem of geomagnetic perturbations due to a 3-D inhomogeneity. This algorithm was extended by L.R. Lines (Lines and Jones, 1973a, b) to incorporate variable sized grid and to permit the vertical discontinuities to extend to grid boundaries. Lines and Jones (1973a, b), Jones (1974) and Jones and Lokken (1975) used the new algorithm to study several island-coastline and channelling effect problems. Ramaswamy et.al. (1975) compared the results of this algorithm with the analogue model results, again for an island-coastline model. Jones and Vozoff (1978) used the 3-D FDM algorithm to compute and then compare principal axis directions and tipper azimuths for a few "perturbed 2-D" models to ascertain if one of these parameters is consistently a more reliable indicator of the strike direction. Zhdanov et.al. (1982) have presented a detailed account of boundary conditions relevant to 2-D and 3-D formulation of FDEM in case of FDM.

The author has not come across any 3-D FDEM or TDEM work based on FDM. However, Dey and Morrison (1979) and Hermance (1983) have used FDM in 3-D DC resistivity modelling. Further, there exists a number of papers on 3-D time domain EM modelling using FDM in the field of electromagnetic compatibility studies in aircraft design and radar studies. The first such algorithm was given by Yee (1966). Subsequently, Holland (1977) gave details of his algorithm THREDE. Recently, Taflove and Umashankar (1983) have compared the FDM algorithms with IEM ones. Ziolkowsky et.al. (1983) have presented and FDM algorithm, that employs a global lookback lattice truncation scheme, to take into consideration the unwarranted reflections

from grid boundaries.

1.4.1.2 Finite element method (FEM)

The first results of a 3-D FEM algorithm were published by Reddy et.al. (1977) for the MT case. Subsequently, Pridmore et.al. (1981) presented the 3-D results for DC resistivity and FDEM methods. Rijo (1983) has used FEM for 3-D resistivity and induced polarization modelling.

1.4.1.3 Integral equation method (IEM)

IEM is by far the most widely used numerical method in geophysical 3-D EM modelling. Although the IEM formulation of the 2-D FDEM problem was available in 1968 (vide Cermak and Silvester, 1968) yet the 3-D problem was first formulated in 1974 by Raiche (1974) and later by Weidelt (1975) and Hohmann (1975) independently. Weidelt applied his formulation to MT method while Hohmann applied his to Induced Polarization and FDEM methods.

Ting and Hohmann (1981) presented an exhaustive study of their IEM algorithm for the case of MT response of a 3-D body buried in a uniform half-space. This study included the results of convergence tests made and also a comparison of 3-D results with the results of limiting 1-D and 2-D approximations. Stodt et.al. (1981) used this algorithm for a detailed study of the telluric-magnetotelluric method. Wannamaker et.al. (1984a, b) extended the algorithm to incorporate the case of a 3-D body buried in a layered earth. The first of these papers deals with the FDEM case and it contains the expressions for the relevant Green's functions. The second paper, on the other hand, deals with the MT problem and it contains a detailed analysis of 3-D MT parameters like impedance and tipper tensors and also contains discussions on 3-D vs 1-D/2-D interpretation. Newman et.al. (1985) used this algorithm to study the problem of crustal magma chambers. San Filipo et.al. (1985a, b)

further extended the algorithm to solve the TDEM problem. They computed the retarded Green's functions by taking Inverse Laplace Transform of the corresponding frequency domain Green's functions. Using this algorithm they computed the effect of a conductive half-space on the TDEM response of a 3-D body buried in it. Newman and Hohmann (1985) have studied the bias of 1-D inversions of TDEM data observed over 3-D structures. They generated the 3-D data by taking Sine or Cosine transform, respectively of the imaginary or real part of the field values computed by the algorithm of Wannamaker et.al. (1984). Newman et.al. (1986) have presented TDEM results for a 3-D structure buried in a layered earth.

Besides Hohmann and his coworkers, several other groups have been developing IEM algorithms for 3-D EM studies. Cauterman et.al. (1978) developed an algorithm for computing the EM response of a 3-D inhomogeneity buried in a conductive half-space. They used it for the problem of identifying shallow underground quarries, by measuring the low frequency vertical electrical field within a borehole radiated by a horizontal electric dipole. Das and Verma (1981, 1982) developed their algorithm to compute 3-D FDEM response of a body buried in a layered half-space. They employed an efficient set of digital filters to compute the convolution integrals appearing in the expressions of Green's functions. By comparing their results with other published results, they established the efficacy of linear digital filter scheme. Degauque et.al. (1986) have used their algorithm to study the induced polarization effect when conductivity of the 3-D target is complex in nature and varies with frequency.

1.4.1.4 Hybrid method (HM)

An HM that amalgamates IEM and FEM was first formulated by Scheen (1978). He formulated the problem in terms of magnetic field intensity vector

and discussed the outlines of his algorithm EMMMMA. Lee et.al. (1981) formulated the problem in terms of electric field and presented the results of their algorithm HYB3D. They also presented a comparison of their results with 3-D model experiment results. Recently, Best et.al. (1985) gave the results of a modified version of the algorithm EMMMMA.

In the field of electromagnetic compatibility studies in aircraft design and radar, Taflove and Umashankar (1982) and Umashankar and Taflove (1982) developed an HM that amalgamates IEM and FDM.

1.4.1.5 Other methods

Zhdanov and Frenkel (1983) presented an EM migration method based on the "reverse" continuation of the transient EM fields into the conductive medium. They presented some 3-D results.

Tarlowski et.al. (1984) and James (1985) have developed algorithms based on Summary Representation Method of Polozhii (1965). Whereas James formulated a 3-D DC resistivity problem, Tarlowski et.al. formulated a 2-D EM problem. An interesting feature of the latter is the hybrid method they have developed by amalgamating this method with FEM.

Park (1985) developed a 3-D algorithm for MT studies by extending the generalized thin sheet algorithm of Rangnayaki and Madden (1980). He studied the distortion of deep MT sounding curves by 3-D structures. La Terroca et.al. (1985) used this algorithm for parameterization of impedance matrices to gain information about the geometry and conductivity of 3-D structures.

1.4.1.6 The thin sheet case

The thin sheet problem has attracted the interest of several workers. Dawson and Weaver (1979) extended the 2-D algorithm of Green and Weaver (1978) to the 3-D case. Their algorithm computes the 3-D induction effect in a

uniform thin sheet situated at the surface of a uniformly conducting half-space. McKirdy et.al. (1984) extended this algorithm to the case where the 3-D thin sheet is situated at the surface of a layered earth. Using these algorithms Weaver and his coworkers studied several island - coastline and channelling effect problems.

Lajoie and West (1976, 1977) studied the FDEM problem of a thin conducting sheet buried in a uniformly conducting half-space. They simulated some results for a fixed-transmitter loop FDEM method such as Turam method. Hanneson and West (1984) developed an algorithm similar to that of Lajoie and West for a layered half-space, with the freedom to be able to place the thin sheet in any layer. They also presented a comparison of their results with some analogue results. Weidelt (1981) studied dipole induction in a 3-D thin plate buried in a conductive half-space of a two layered earth. Lee (1986) converted Weidelt's algorithm to time domain.

It may be stressed here that all these studies were based on the IEM.

1.4.2 2-D EM Modelling

Since 3-D EM modelling is still economically unviable and is, truly speaking, still in a developing stage, a lot of work is being carried out in 2-D EM modelling, particularly in TDEM, where 3-D modelling results have started appearing only since 1985. Some of these works are therefore reported here.

Stoyer and Greenfield (1976) used FDM to simulate FDEM response of a 2-D earth to a magnetic dipole excitation. Goldman and Stoyer (1983) extended this work to the TDEM case. Goldman et.al. (1986) developed an FEM algorithm to simulate the TDEM response of an arbitrary 2-D resistivity distribution.

Oristaglio and Hohmann (1984) developed a total field 2-D TDEM algorithm based on FDM and Dufort - Frankel finite difference scheme for time stepping. Using this algorithm they studied in detail the diffusion of EM fields in a 2-D earth. Eaton and Hohmann (1984) used this algorithm for borehole studies. Adhijaja et.al. (1985) reformulated the Oristaglio-Hohmann algorithm in terms of secondary fields and studied the overburden and conductive host rock effects on a 2-D earth TDEM response.

1.4.3 Some Approximation Models

Even 2-D algorithms for bodies buried in a conductive host rock, particularly in TDEM case, are considered economically unviable. Continued efforts are therefore still being made to develop fast and economic algorithms to compute the response of 2-D earth models suspended in free space. Two such most popular programs are PLATE and SPHERE, developed at the University of Toronto (vide Dyck and West (1984)). Modified versions of these programs have been developed by several groups, for example OZPLAT is a modified version of PLATE developed by Gallagher (1985) at the Division of Mineral Physics and Mineralogy, CSIRO, Australia . These programs approximate the target by a thin plate or by a sphere in free space and compute the FDEM or TDEM response for various kinds of excitations.

Becker et.al. (1984) put forward an approximate scheme, whereby a TDEM anomaly is interpreted in terms of a single-turn closed loop in free space. In this scheme it is assumed that each anomaly is characterized by its amplitude and an average time constant.

Barnett (1984) gave an algorithm for TDEM data inversion where the body is approximated by an equivalent rectangular or circular current filament in a conductive host medium. He stated that whereas the forward modelling

problem using PLATE took 9 min his inversion algorithm took only 15 s on Vax - 11/780.

McNeill et.al. (1984), like Barnett, replaced a thin conducting plate buried in a conductive host rock by a single-turn wire loop and a distribution of current dipoles. Single-turn wire loop approximated the vortex current in the body, while the current dipole distribution approximated the galvanic current in the body. He presented a detailed analysis of these two components of the body response. Flores and Edwards (1985) used this approximation to calculate the low frequency 3-D MT response using a multiplate model.

West and Edwards (1985) have put forward a parametric theory for the approximate computation of the response of an anomalous 3-D body in a conductive host rock. To start with, they used the IEM formulation and subsequently approximated the computation of integral expressions of secondary fields by a representative point computation. They applied this algorithm to compute spectral response of an arbitrary EM prospecting system to a small conductive target buried in a conductive host.

1.5 THE THESIS OUTLAY

Brief contents of the thesis in subsequent chapters are given below.

In chapter-II a brief account of EM theory and relevant boundary conditions is presented. Further, the response parameters that are observed in different EM methods are discussed.

In chapter-III the numerical methods - Finite Element, Integral Equation and Hybrid - are presented. The iterative and direct schemes of Hybrid Method are formulated.

In chapter-IV the three algorithms HYBRIDC, SANGAM and SAMAYA, developed in this thesis are discussed and comparative study of the time requirements of FDEM algorithms is presented.

In chapter-V the various results are presented. These pertain to both FDEM and TDEM studies. Comparisons of the results of the algorithms developed here with those obtained by using other algorithms are also presented.

Finally, in chapter-VI a summary of the work carried out is presented, highlighting the main conclusions and exposing new grounds for future studies.

CHAPTER - II

ELECTROMAGNETIC THEORY AND METHODS

2.1 INTRODUCTION

Electromagnetic (EM) methods enable one to glean information about the subsurface EM structure by employing different kinds of instrumentation, field procedures, input source characteristics, output response functions and data processing and interpretation methodologies. This diversity in EM methods, when properly exploited, can be used with great advantage in enhancing their illuminating power. For example, the inherent non-uniqueness of the EM inverse problem can be reduced to a certain degree by simultaneously employing two or more compatible methods for studying a given situation. This becomes possible because the null parameter subspace, comprising the parameters not affecting the observations, may possess different dimensions, for different methods. When two or more methods are employed, the resultant null subspace is the intersection of null subspaces for individual methods. Hence,it possesses a dimension lower than or equal to that of individual null subspaces and thus reduces the degree of non-uniqueness. Further, the noise characteristics of different methods are independent. Thus when two or more methods are jointly employed, the noise may get reduced thereby enhancing the signal to noise ratio. However, this diversity also makes it imperative for a geophysicist to have a thorough understanding of the operational and physical aspects of different EM methods. The operational aspects of any survey method are concerned with such features as its sensitivity to the kind of target being sought and the nature of terrain, speed of data procurement, achievable data density for given budget, manpower and resources available. The physical aspects, on the other hand, deal with issues relating

to the nature of the source fields, of the induced currents in confined targets and in the host medium, of the relationship between electromagnetic properties of the subsurface and perturbations caused by it, of the resolving power, and the region of investigation. The choice of optimal EM method(s) that would yield maximum information about the subsurface in a given situation is made by going for an acceptable trade-off between the operational and physical features. The study of operational aspects is carried out by the methods of operations research and management science and does not come under the purview of this thesis. The study of physical aspects, on the other hand, is carried out by either mathematical or analogue modelling. Both these kinds of modelling require an exhaustive knowledge of EM theory as a prerequisite. Mathematical modelling being the subject of present study, a brief account of the fundamentals of EM theory is outlined in this chapter with a discussion of the physical parameters and their ranges relevant in the context of earth. Finally, a summary of the response functions that need be computed for data interpretation, from the observed EM fields for different EM methods, is presented.

2.2 FUNDAMENTAL EQUATIONS

The basis of EM theory is constituted by the Biot-Savart law for magnetic induction due to current, Faraday's law of EM induction, Coulomb's law of electrostatic force due to electric charges and the law of conservation of charge and continuity of current flow. These laws are mathematically expressed in terms of Maxwell's equations for continuous material medium, such as the earth, that are given below.

$$\nabla \times \mathbf{b} = \mu \mathbf{j} + \mu \frac{\partial \mathbf{d}}{\partial t} \tag{2.1}$$

$$\nabla \times \mathbf{e} = -\frac{\partial \mathbf{b}}{\partial t} \tag{2.2}$$

$$\nabla \cdot \mathbf{b} = 0 \tag{2.3}$$

$$\nabla \cdot \mathbf{d} = \rho_e \tag{2.4}$$

where **b**, **e** , **d** and **j** are respectively the magnetic induction in Tesla, the electric field intensity in V/m, the electric displacement in C/m^2 and the electric current density in A/m^2. ρ_e is the free electric charge density in C/m^3 and μ is the magnetic permeability of the medium in H/m. It can be easily verified that for piecewise continuous **b** and **d** which also possess continuous first and second derivatives, equation (2.3) can be derived from equation (2.2) while equation (2.4) can be derived from equations (2.1) and (2.5), the equation of continuity that states the law of conservation of charge,

$$\nabla \cdot \mathbf{j} + \frac{\partial \rho_e}{\partial t} = 0 \tag{2.5}$$

Thus, of the five equations, only the first two are independent and they involve four vectors thus rendering the system of equations grossly underdetermined. The two vector equations needed to render the system of equations determined are obtained from the constitutive relations that state the dependence of the various vectors on gross material properties : the electric conductivity, σ , and the dielectric permittivity, ϵ,

$$\mathbf{j} = \sigma \mathbf{e} \tag{2.6}$$

$$\mathbf{d} = \epsilon \mathbf{e} \tag{2.7}$$

where σ and ϵ are second order tensors and are functions of position **r**, time t, spectral angular frequency ω , temperature T, pressure P and strain S.

A third relation defines the magnetic field intensity vector **h**, commonly

mentioned in literature, as

$$\mathbf{b} = \mu \mathbf{h} \tag{2.8}$$

These relations need not be linear or single-valued. For example, σ and ϵ may be functions of **e**. In order to ascertain which of these functional dependences are of relevance in the context of the various EM methods, a discussion of geoelectromagnetic properties follows.

2.3 THE CONSTITUTIVE RELATIONS AND EM PARAMETERS OF EARTH

The constitutive relation (2.6) in the linear case may be recognised as a statement of Ohm's law.

In geophysical situations where an isotropic earth is considered, the parameters σ, ϵ and μ behave as scalars σ, ϵ and μ, respectively and are functions of position only. The only other functional dependence of importance in some situations is with respect to frequency. In some studies, however, the dependence of conductivity on temperature has been used to gather information about the thermal gradient in earth. Several texts have discussed these properties of rocks and minerals, notably Keller and Frischnecht (1966), Society of Exploration Geophysicists (1967). Here, only a brief discussion on the ranges of σ, ϵ and μ, that are widely encountered in the earth, is presented.

The parameter electrical conductivity, σ, or its inverse electrical resistivity, ρ, that is more popularly used in geophysical literature, has the widest range of all physical parameters of earth. The resistivity varies in the range 10^{-8} - 10^{13} Ohm m for different rocks and minerals. This wide range results from diverse physical phenomena that contribute to the conductivity of rocks. In the upper crust, the ionic conduction of electrolytes in the pores of rocks is the primary contributor to conductivity of rocks, while

in the lower crust and upper mantle, electronic mode of conduction is the primary contributor. In the former case, if it is desired to account for electrode and membrane polarization through a change in conductivity, it becomes frequency dependent and complex in nature. It has been shown that the anomaly caused by a target buried in a conducting host medium gets enhanced as the contrast in the resitivity values of the target and host medium increases. However, it asymptotically reaches a maximum value, rendering the cases, where the resistivity contrast is more than 1000, undiscernible from each other. Hence such cases can be modelled as if the target was suspended in free space.

The electric permittivity varies from its value ε_o for free space that is equal to $10^{-9}/36\pi$ F/m, to about 500 ε_o. However, for most earth materials it is less than 100 ε_o. These values contain contributions only due to the microscopic phenomena such as

i) the lengthening of the bonds between atoms, and

ii) the preferred orientation of the molecules along the direction of the field.

In case the macroscopic phenomena like electrode and membrane polarization are also taken into permittivity values, ε becomes very large and frequency-dependent.

Finally, the magnetic permeability, μ, in most geophysical situations equals its value for free space $\mu_o = 4\pi \times 10^{-7}$ H/m. Only for ferromagnetic minerals it goes upto 6 μ_o. In the case of remnant magnetization studies, however, μ becomes non-linear and multivalued due to the phenomenon of hysteresis.

2.4 THE EM BOUNDARY VALUE PROBLEM

In EM methods, the commonly used frequencies are less than 10^5 Hz, while the earth resistivity commonly encountered are less than 10^4 Ohm m. This means that the free charge density ρ_e in equation (2.5) dissipates in less than a microsecond. Hence, for observation times greater than a few microseconds after the source is switched off, the free charge density can be regarded as zero. Equations (2.4) and (2.5) then simplify to

$$\nabla . \mathbf{d} = 0 \tag{2.9}$$

$$\nabla . \mathbf{j} = 0 \tag{2.10}$$

Further, for frequencies less than 10^5 Hz, the displacement current term in equation (2.1) is an order of magnitude smaller than the conduction current term and hence can be neglected, so that equation (2.1), after using Ohm's law, gets simplified to

$$\nabla \times \mathbf{b} = \mu\sigma \mathbf{e} \tag{2.11}$$

Rewriting equation (2.2)

$$\nabla \times \mathbf{e} = - \frac{\partial \mathbf{b}}{\partial t} \tag{2.12}$$

Taking curl of each of these two equations, using the other equation together with the following identify that holds for any vector $\mathbf{v}$

$$\nabla \times (\nabla \times \mathbf{v}) = \nabla (\nabla . \mathbf{v}) - \nabla^2 \mathbf{v}$$

the equations satisfied by $\mathbf{b}$ and $\mathbf{e}$ can be obtained as

$$\nabla^2 \mathbf{b} - \mu\sigma \frac{\partial \mathbf{b}}{\partial t} = 0 \tag{2.13}$$

$$\nabla^2 \mathbf{e} - \mu\sigma \frac{\partial \mathbf{e}}{\partial t} = 0 \tag{2.14}$$

Here equations (2.7) and (2.9) have been used in deriving (2.14).

Equations (2.13) and (2.14) may be recognised to be diffusion equations.

The frequency domain EM equations can be obtained from the corresponding time domain equations by taking the Fourier transform of the latter. Fourier transform of a function f(t) is defined as

$$F(\omega) = \int_{-\infty}^{\infty} f(t)\ e^{-i\omega t}\, dt \tag{2.15}$$

while the inverse Fourier transform is defined as

$$f(t) = \frac{1}{2\pi} \int_{-\infty}^{\infty} F(\omega)\ e^{i\omega t}\, d\omega \tag{2.16}$$

Taking Fourier transform of equations (2.11) and (2.12), Maxwell's equations in the frequency domain become

$$\nabla \times \mathbf{B} = \mu\sigma \mathbf{E} \tag{2.17}$$

$$\nabla \times \mathbf{E} = -i\omega \mathbf{B} \tag{2.18}$$

while the boundary value problems are

$$\nabla^2 \mathbf{B} + k^2 \mathbf{B} = 0 \tag{2.19}$$

$$\nabla^2 \mathbf{E} + k^2 \mathbf{E} = 0 \tag{2.20}$$

These equations are the Helmholtz equations.

Before attempting a solution of any of the equations (2.13), (2.14), (2.19) or (2.20), like any other partial differential equation, necessary and sufficient boundary conditions must be identified. Equations (2.13) and (2.14) will require initial conditions also. These initial conditions may be that **e** or **b**, respectively are zero at t = 0 when the source is switched on. The requisite boundary conditions are discussed next.

2.5 THE BOUNDARY CONDITIONS

Since every text on EM theory contains a discussion on boundary conditions, these are only stated here.

If **n** is the normal to the boundary separating two media 1 and 2, that possess different physical properties like conductivity and dielectric permittivity, then the necessary and sufficient boundary conditions may be obtained by replacing the differential operator ∇ by **n** and by setting the time derivative to zero in equations (2.1) - (2.4)

i) the tangential components of **b** are discontinuous, discontinuity being equal to the surface current density $\mathbf{j}_s$, i.e.

$$\mathbf{n} \times (\mathbf{b}_1 - \mathbf{b}_2) = \mu \mathbf{j}_s \tag{2.21}$$

ii) the tangential components of **e** are continuous, i.e.

$$\mathbf{n} \times (\mathbf{e}_1 - \mathbf{e}_2) = 0 \tag{2.22}$$

iii) the normal components of **b** are continuous, i.e.

$$\mathbf{n}. (\mathbf{b}_1 - \mathbf{b}_2) = 0 \tag{2.23}$$

iv) the normal components of **d** are discontinuous, the discontinuity being equal to the surface charge density ρ_s, i.e.

$$\mathbf{n}. (\mathbf{d}_1 - \mathbf{d}_2) = \rho_s \tag{2.24}$$

The corresponding boundary conditions for frequency domain equations (2.19) and (2.20) are

i) $$\mathbf{n} \times (\mathbf{B}_1 - \mathbf{B}_2) = \mu \mathbf{J}_s \tag{2.25}$$

ii) $$\mathbf{n} \times (\mathbf{E}_1 - \mathbf{E}_2) = 0 \tag{2.26}$$

iii) $$\mathbf{n}. (\mathbf{B}_1 - \mathbf{B}_2) = 0 \tag{2.27}$$

and iv) $$\mathbf{n}. (\mathbf{D}_1 - \mathbf{D}_2) = \rho_s \tag{2.28}$$

The boundary conditions (a) (2.21) and (2.23), (b) (2.22) and (2.24), (c) (2.25) and (2.27) and (d) (2.26) and (2.28) are respectively employed to solve the partial differential equations (2.13), (2.14), (2.19) and (2.20). The boundary value problems can be solved numerically, by using any of the methods discussed in chapter-III.

It may be stressed here that, more often than not, particularly when closed form solutions to EM problems are being sought, it is easier to work with some judiciously defined vector and scalar potentials that are amenable to simpler boundary conditions. This would greatly reduce the computational effort. Ward (1967) has presented a detailed account of various vector and scalar potentials that have been employed in geophysics.

2.6 THE PARAMETERS ANALYZED IN EM METHODS

The equations (2.13), (2.14), (2.19) and (2.20), when solved in conjunction with respective boundary (and initial) conditions, yield unique EM vectors **b**, **e**, **B** and **E** respectively. However, in most of the EM methods, the parameters analyzed to gather information about the subsurface EM characteristics are not these field components but their functions. Hence it is in place to outline here the parameters analyzed in various EM methods.

In frequency domain EM methods, the parameters commonly analyzed are

i) the in-phase (real) and quadrature (out of phase or imaginary) components of the secondary field due to the induction current in earth, expressed as a percentage of the primary source field,

ii) the tilt angle - the angle through which the horizontal receiver coil must be rotated to generate minimum response from a vertical transmitter loop, and

iii) in case of two transmission frequencies,

$$\left(\frac{V_S}{V_R} - 1 \right) \times 100$$

where V_S is the EMF induced in the high frequency coil by the vertical component of the resultant field, and V_R is the EMF induced in the low frequency coil by the vertical component of the resultant field.

In time domain EM methods, the decay pattern of the voltage induced in the receiver coil during the off-period transmitter signal is analyzed. Rutter and Staltari (1984) have presented detailed accounts of frequency and time domain systems, data processing and interpretation.

In magnetotelluric method the parameter studied is **Z**, related to field components by

$$\mathbf{E}_t = \mathbf{Z}\ \mathbf{B}_t \times \mathbf{n} \qquad (2.29)$$

where $\mathbf{E}_t$, $\mathbf{B}_t$ are the tangential components of **E** and **B**, measured on the earth surface, while **n** is the unit vector normal to earth surface and pointing downwards.

It may be emphasized here that **Z** may behave as a second order tensor depending on the properties of the source and the anisotropy and the horizontal inhomogeneity of the earth. In such a case the components Z_{xx}, Z_{xy}, Z_{yx} and Z_{yy} are related to field components as follows

$$\begin{aligned} E_x &= Z_{xx} H_x + Z_{xy} H_y \\ E_y &= Z_{yx} H_x + Z_{yy} H_y \end{aligned} \qquad (2.30)$$

Estimation of the impedance tensor **Z** from the observed field components is one of the primary steps in MT data processing.

In geomagnetic deep sounding method, the parameters commonly used are

$$W = B_z/B_x \tag{2.31}$$

and

$$Q = I/E \tag{2.32}$$

where I and E are the contributions to the field from induction currents in the earth and from the current sources external to the earth, respectively.

The monographs by Kaufman and Keller (1981), Rokityanski (1982) and by Berdichevsky and Zhdanov (1984) discuss in detail the processing and interpretation of data procured by natural source EM methods. Similarly, the monographs by Kaufman and Keller (1983, 1985) and by Patra and Mallick (1980) present methods for interpretation of FDEM and TDEM data. For 3-D EM problems, which are merely alluded to in all the monographs cited here, only numerical solution is feasible. Hence, a discussion of some of the numerical methods is presented in the next chapter.

CHAPTER - III

THE NUMERICAL METHODS

3.1 INTRODUCTION

Forward 2-D and 3-D EM problems are amenable to analytic solution only in cases where the body has such a shape that each of its surfaces possesses, in some orthogonal coordinate system, a constant coordinate value, for example sphere, cylinder, spheroid and so on. In general, for arbitrary shape of bodies, numerical solution must be resorted to. Various numerical methods that can be employed to solve the problem are broadly classified into three groups :

(i) Differential Equation Methods (DEMs) like Finite Difference Method (FDM), Finite Element Method (FEM), Summary Representation Method (SRM),

(ii) Integral Equation Methods (IEMs) like surface IEM or volume IEM, and

(iii) Direct Discrete Methods (DDMs) like Electric Analogue Network Method or Graph Theoretic Field Modelling Method.

Besides, there exist some Hybrid Methods (HMs) where positive features of two different methods which may even belong to different groups, are efficiently amalgamated. The basic difference between these groups of methods can be understood in terms of the three fundamental components of the process of solving any physical problem :

(i) Identification of the physical processes that govern the system under study,

(ii) Development of the necessary differential and/or integral equations

and/or variational functional from the physical laws governing the processes involved, and

(iii) Discretization of the domain of problem, generation of a matrix equation by approximating the entities developed in step (ii) and solution of the matrix equation for the discrete values of the unknown variables.

The steps (i) and (iii) are performed with minor variations in all the methods while step (ii) is distinctly different for the various forementioned groups. Thus, in the case of DEMs either differential equations or variational functionals are developed, in IEMs integral equations are developed, while in DDMs step (ii) is altogether eliminated and the matrix equation is obtained directly from the approximation of the physical laws concerned.

In the EM study of the earth the forward problem has been solved using DEMs, IEMs and HMs. The DDMs have not so far been used, but have the potential of becoming alternative means for solving 3-D EM forward problem, as they are bound to offer a different trade-off amongst various advantages.

3.2 MATHEMATICAL DEVELOPMENT

The partial differential equations (2.13), (2.14), (2.19) and (2.20) satisfied by the vectors **b**, **e**, **B** and **E** respectively, were derived from Maxwell's equations for a homogeneous and source free region. If that is not the case, Maxwell's equations, as well as equations derived from them, need be modified. The new equations taking into account the electric and magnetic current sources $\mathbf{j}_p$ and $\mathbf{m}_p$ respectively, are

$$\nabla \times \mathbf{b} = \mu_o \sigma \mathbf{e} + \mu_o \mathbf{j}_p \tag{3.1}$$

$$\nabla \times \mathbf{e} = -\frac{\partial \mathbf{b}}{\partial t} - \mu_o \frac{\partial \mathbf{m}_p}{\partial t} \tag{3.2}$$

Taking divergence of these two equations, following equation can be obtained

$$\nabla \cdot \mathbf{e} = - \frac{\nabla \cdot \mathbf{j}_p}{\sigma} - \frac{\nabla \sigma}{\sigma} \cdot \mathbf{e} \tag{3.3}$$

$$\nabla \cdot \mathbf{b} = - \mu_o \nabla \cdot \mathbf{m}_p \tag{3.4}$$

It is easily verified that equations (3.1) - (3.4) reduce to Maxwell's equations for a homogeneous source-free region. Equations (3.1) - (3.4) lead to following two equations satisfied respectively by **b** and **e**

$$\nabla^2 \mathbf{b} + \sigma (\nabla \times \mathbf{b}) \times \nabla (1/\sigma) - \mu_o \sigma \frac{\partial \mathbf{b}}{\partial t}$$

$$= \frac{\mu_o}{\sigma} \nabla \times \mathbf{j}_p - \mu_o^2 \frac{\partial \mathbf{m}_p}{\partial t} \tag{3.5}$$

$$\nabla^2 \mathbf{e} + \nabla (\mathbf{e} \cdot \frac{\nabla \sigma}{\sigma}) - \mu_o \sigma \frac{\partial \mathbf{e}}{\partial t}$$

$$= \mu_o \frac{\partial \mathbf{j}_p}{\partial t} - \frac{1}{\sigma} \nabla (\nabla \cdot \mathbf{j}_p) + \mu_o \nabla \times (\frac{\partial \mathbf{m}_p}{\partial t}) \tag{3.6}$$

Equations (3.1) - (3.6) represent the total response of an inhomogeneous earth in terms of the EM field vectors **b** and **e**. However, since these equations are linear in **b** and **e**, it is possible and sometimes more convenient to consider the vectors **b** and **e** as comprising of two components each as given below

$$\mathbf{b} = \mathbf{b}_p + \mathbf{b}_s \tag{3.7}$$

$$\mathbf{e} = \mathbf{e}_p + \mathbf{e}_s \tag{3.8}$$

Here, $\mathbf{b}_p$ and $\mathbf{e}_p$ are the responses to impressed sources of a simple earth model, like layered earth, that is amenable to easy response computation and $\mathbf{b}_s$ and $\mathbf{e}_s$ are the responses of residual inhomogeneities. Let σ_p be conductivity values of the simple model, while σ_s represent the residual conductivity values of inhomogeneities. Thus

$$\sigma = \sigma_p + \sigma_s \tag{3.9}$$

at any point in the earth.

The equations satisfied by $\mathbf{b}_p$, $\mathbf{e}_p$, $\mathbf{b}_s$ and $\mathbf{e}_s$ can be obtained by substituting equations (3.7) - (3.9) in (3.1) - (3.6). The equations for primary field vectors $\mathbf{b}_p$ and $\mathbf{e}_p$ turn out to be

$$\nabla \times \mathbf{b}_p = \mu_o \sigma_p \mathbf{e}_p + \mu_o \mathbf{j}_p \tag{3.10}$$

$$\nabla \times \mathbf{e}_p = - \frac{\partial \mathbf{b}_p}{\partial t} - \mu_o \frac{\partial \mathbf{m}_p}{\partial t} \tag{3.11}$$

$$\nabla \cdot \mathbf{e}_p = - \frac{\nabla \cdot \mathbf{j}_p}{\sigma_p} - \frac{\nabla \cdot \sigma_p}{\sigma_p} \cdot \mathbf{e}_p \tag{3.12}$$

$$\nabla \cdot \mathbf{b}_p = - \mu_o \nabla \cdot \mathbf{m}_p \tag{3.13}$$

$$\nabla^2 \mathbf{b}_p + \sigma_p (\nabla \times \mathbf{b}_p) \times \nabla (1/\sigma_p) - \mu_o \sigma_p \frac{\partial \mathbf{b}_p}{\partial t} = \frac{\mu_o}{\sigma_p} \nabla \times \mathbf{j}_p - \mu_o^2 \frac{\partial \mathbf{m}_p}{\partial t} \tag{3.14}$$

$$\nabla^2 \mathbf{e}_p + \nabla (\mathbf{e}_p \cdot \frac{\nabla \sigma_p}{\sigma_p}) - \mu_o \sigma_p \frac{\partial \mathbf{e}_p}{\partial t} = \mu_o \frac{\partial \mathbf{j}_p}{\partial t} - \frac{1}{\sigma_p} \nabla (\nabla \cdot \mathbf{j}_p) + \mu_o \nabla \times (\frac{\partial \mathbf{m}_p}{\partial t}) \tag{3.15}$$

Similarly, the equations satisfied by $\mathbf{b}_s$ and $\mathbf{e}_s$ are

$$\nabla \times \mathbf{b}_s = \mu_o \sigma_p \mathbf{e}_s + \mu_o \mathbf{j}_s \tag{3.16}$$

$$\nabla \times \mathbf{e}_s = - \frac{\partial \mathbf{b}_s}{\partial t} \tag{3.17}$$

$$\nabla \cdot \mathbf{e}_s = - \frac{\nabla \cdot \mathbf{j}_s}{\sigma_p} - \frac{\nabla \sigma_p}{\sigma_p} \cdot \mathbf{e}_s \tag{3.18}$$

$$\nabla \cdot \mathbf{b}_s = 0 \tag{3.19}$$

$$\nabla^2 \mathbf{b}_s + \sigma_p (\nabla \times \mathbf{b}_s) \times \nabla (1/\sigma_p) - \mu_o \sigma_p \frac{\partial \mathbf{b}_s}{\partial t}$$

$$= \frac{\mu_o}{\sigma_p} \nabla \times \mathbf{j}_s \qquad (3.20)$$

$$\nabla^2 \mathbf{e}_s + \nabla \left(\mathbf{e}_s \cdot \frac{\nabla \sigma_p}{\sigma_p} \right) - \mu_o \sigma_p \frac{\partial \mathbf{e}_s}{\partial t}$$

$$= \mu_o \frac{\partial \mathbf{j}_s}{\partial t} - \frac{1}{\sigma_p} \nabla (\nabla \cdot \mathbf{j}_s) \qquad (3.21)$$

where $\mathbf{j}_s = \sigma_s \mathbf{e}$ (3.22)

A look at the three sets of equations : for **b** and **e**, equations (3.1) - (3.6), for $\mathbf{b}_p$ and $\mathbf{e}_p$, equations (3.10) - (3.15) and for $\mathbf{b}_s$ and $\mathbf{e}_s$, equations (3.16) - (3.21), reveals the similarity in their form. In this light the secondary field can be viewed as the response of the primary or the simple earth model to the secondary or scattering currents $\mathbf{j}_s$ generated by the residual inhomogeneities.

From the time domain equations (3.1) - (3.6) and (3.10) - (3.21), the corresponding frequency domain equations are obtained by taking Fourier Transform of each equation with the Fourier Transform pair for any variable v given by the following relations

$$V = \int_{-\infty}^{\infty} v \cdot e^{-i\omega t} dt \qquad (3.23)$$

$$v = \frac{1}{2\pi} \int_{-\infty}^{\infty} V \cdot e^{i\omega t} d\omega \qquad (3.24)$$

The frequency domain equations for **B** and **E** then are :

$$\nabla \times \mathbf{B} = \mu_o \sigma \mathbf{E} + \mu_o \mathbf{J}_p \qquad (3.25)$$

$$\nabla \times \mathbf{E} = -i\omega \mathbf{B} - i\omega \mu_o \mathbf{M}_p \qquad (3.26)$$

$$\nabla \cdot \mathbf{E} = \frac{-\nabla \cdot \mathbf{J}_p}{\sigma} - \frac{\nabla \sigma}{\sigma} \cdot \mathbf{E} \qquad (3.27)$$

$$\nabla \cdot \mathbf{B} = -\mu_o \nabla \cdot \mathbf{M}_p \tag{3.28}$$

$$\nabla^2 \mathbf{B} + \sigma(\nabla \times \mathbf{B}) \times \nabla(1/\sigma) - i\omega\mu_o\sigma\mathbf{B} = \frac{\mu_o}{\sigma}\nabla \times \mathbf{J}_p - i\omega\mu_o^2\mathbf{M}_p \tag{3.29}$$

$$\nabla^2 \mathbf{E} + \nabla\left(\mathbf{E} \cdot \frac{\nabla\sigma}{\sigma}\right) - i\omega\mu_o\sigma\mathbf{E} = i\omega\mu_o\mathbf{J}_p - \frac{1}{\sigma}\nabla(\nabla \cdot \mathbf{J}_p) + i\omega\mu_o\nabla \times \mathbf{M}_p \tag{3.30}$$

while for $\mathbf{B}_p$ and $\mathbf{E}_p$ the frequency domain equations are

$$\nabla \times \mathbf{B}_p = \mu_o\sigma_p\mathbf{E}_p + \mu_o\mathbf{J}_p \tag{3.31}$$

$$\nabla \times \mathbf{E}_p = -i\omega\mathbf{B}_p - i\omega\mu_o\mathbf{M}_p \tag{3.32}$$

$$\nabla \cdot \mathbf{E}_p = -\frac{\nabla \cdot \mathbf{J}_p}{\sigma_p} - \frac{\nabla\sigma_p}{\sigma_p} \cdot \mathbf{E}_p \tag{3.33}$$

$$\nabla \cdot \mathbf{B}_p = -\mu_o\nabla \cdot \mathbf{M}_p \tag{3.34}$$

$$\nabla^2 \mathbf{B}_p + \sigma_p(\nabla \times \mathbf{B}_p) \times \nabla(1/\sigma_p) - i\omega\mu_o\sigma_p\mathbf{B}_p = \frac{\mu_o}{\sigma_p}\nabla \times \mathbf{J}_p - i\omega\mu_o^2\mathbf{M}_p \tag{3.35}$$

$$\nabla^2 \mathbf{E}_p + \nabla\left(\mathbf{E}_p \cdot \frac{\nabla\sigma_p}{\sigma_p}\right) - i\omega\mu_o\sigma_p\mathbf{E}_p = i\omega\mu_o\mathbf{J}_p - \frac{1}{\sigma_p}\nabla(\nabla \cdot \mathbf{J}_p) + i\omega\mu_o\nabla \times \mathbf{M}_p \tag{3.36}$$

and finally for $\mathbf{B}_s$ and $\mathbf{E}_s$ the frequency domain equations are

$$\nabla \times \mathbf{B}_s = \mu_o\sigma_p\mathbf{E}_s + \mu_o\mathbf{J}_s \tag{3.37}$$

$$\nabla \times \mathbf{E}_s = -i\omega\mathbf{B}_s \tag{3.38}$$

$$\nabla . E_s = - \frac{\nabla . J_s}{\sigma_p} - \frac{\nabla \sigma_p}{\sigma_p} . E_s \tag{3.39}$$

$$\nabla . B_s = 0 \tag{3.40}$$

$$\nabla^2 B_s + \sigma_p (\nabla \times B_s) \times \nabla (1/\sigma_p) - i \omega \mu_o \sigma_p B_s = \frac{\mu_o}{\sigma_p} \nabla \times J_s \tag{3.41}$$

$$\nabla^2 E_s + \nabla (E_s . \frac{\nabla \sigma_p}{\sigma_p}) - i \omega \mu_o \sigma_p E_s = i \omega \mu_o J_s - \frac{1}{\sigma_p} \nabla (\nabla . J_s) \tag{5.42}$$

where

$$J_s = \sigma_s E \tag{3.43}$$

The partial differential equations (PDEs) derived here, together with the relevant boundary conditions, enable one to use various DEMs.

In order to derive an integral equation that would enable one to use volume IEMs, the J_s term in (3.42) is treated as a source current density and the appropriate Green's functions $G(r, r')$ are used to obtain the following expression for the secondary electric field

$$E_s(r) = \int_v G(r,r') J_s(r') \, d^3r'$$

or substituting for J_s from (3.43)

$$E_s(r) = \int_v G(r,r') \, \sigma_s(r') \, E(r') \, d^3r' \tag{3.44}$$

Now adding the primary field to both sides,

$$E(r) = E_p(r) + E_s(r) = E_p(r) + \int_v G(r,r') \, \sigma_s(r') E(r') \, d^3(r') \tag{3.45}$$

This is the integral equation which must be solved in IEM, the integra-

tion being confined to the volume of the target, for which σ_s is non-zero. Similar equation can be obtained for the vector **B**, if desired. The Green's function expressions have been derived by Hohmann (1975), Weidelt (1975), Lee et.al. (1981), Wannamaker et.al. (1984) and others for the frequency domain.

An integral equation for time domain problems can be similarly written in terms of the retarded Green's function as follows :

$$\mathbf{e}(\mathbf{r},t) = \mathbf{e}_p(\mathbf{r},t) + \int_0^t \int_v \mathbf{g}(\mathbf{r},\mathbf{r}',\, t-t')\, \mathbf{e}(\mathbf{r}',t')\, d^3\mathbf{r}'\, dt' \qquad (3.46)$$

with the initial condition that $\mathbf{e}(\mathbf{r},t)$ is zero for $t \leqslant 0$. San Filipo et.al. (1985) have derived expressions for $\mathbf{g}(\mathbf{r}-\mathbf{r}',\, t-t')$ and have discussed methods to compute them.

The EM problem formulated above can be solved by means of any one of the numerical methods mentioned earlier. Since the algorithms developed in this thesis are based on a Hybrid method, Compact Finite Element Method, that amalgamates FEM and volume IEM, only these methods are discussed below. Both FEM and IEM can be considered as special cases of, what are termed as, weighted residual methods (WRMs), which will be discussed first.

3.3 WEIGHTED RESIDUAL METHODS (WRM)

Let the spatial variation in any of the PDEs or integral equations derived above be written as

$$L\,\mathbf{u} = \mathbf{f} \qquad (3.47)$$

where L is the differential or integral operator, **u** is the unknown vector or scalar field and **f** is the known right hand side source term. For example, in equation (3.45)

$$\mathbf{L} = \mathbf{I} - \int_V \sigma_s(\mathbf{r}')\ \mathbf{G}(\mathbf{r},\mathbf{r}')\ d^3\mathbf{r}'$$

$$\mathbf{f} = \mathbf{E}_p$$

$$\mathbf{u} = \mathbf{E}$$

Approximating $\mathbf{u}$ in terms of a suitably chosen basis set comprising of n-terms,

$$\mathbf{u} \simeq \tilde{\mathbf{u}} = \sum_{i=1}^{n} a_i\, \mathbf{u}_i\,(\mathbf{r}) \tag{3.48}$$

and substituting this approximation of $\mathbf{u}$ in equation (3.47) yields

$$\sum_{i=1}^{n} a_i\ L\ \mathbf{u}_i + \boldsymbol{\epsilon} = \mathbf{f} \tag{3.49}$$

where, $\boldsymbol{\epsilon}$ is the error term. In WMRs the a's, which are arbitrary, are so chosen that the error term $\boldsymbol{\epsilon}$ is reduced to zero. For this purpose, a set of n complete independent weighting functions $\mathbf{w}_j(\mathbf{r})$ is chosen and a suitably defined inner product is taken of equation (3.49) with each $\mathbf{w}_j$:

$$\sum_{i=1}^{n} a_i \langle \mathbf{w}_j\ ,\ L\ \mathbf{u}_i \rangle + \langle \mathbf{w}_j, \boldsymbol{\epsilon} \rangle = \langle \mathbf{w}_j, \mathbf{f} \rangle\ , \quad j = 1,2,\ldots\ n \tag{3.50}$$

If for the complete set $\mathbf{w}_j$, the inner product $\langle \mathbf{w}_j, \boldsymbol{\epsilon} \rangle$ is zero for all j, it would mean that $\boldsymbol{\epsilon}$ itself is zero. Hence a's are chosen by setting these terms equal to zero in (3.50) which then reduces to

$$\sum_{i=1}^{n} a_i \langle \mathbf{w}_j, L\ \mathbf{u}_i \rangle = \langle \mathbf{w}_j, \mathbf{f} \rangle,\ j = 1,2,\ldots\ n \tag{3.51}$$

It can be written as a matrix equation

$$\mathbf{C}\ \mathbf{a} = \mathbf{b} \tag{3.52}$$

where $C_{ij} = \langle \mathbf{w}_i\ ,\ L\ \mathbf{u}_j \rangle$ and $b_i = \langle \mathbf{w}_i\ ,\ \mathbf{f} \rangle$

Solving matrix equation (3.52), the vector of unknown coefficients **a** can be obtained and then equation (3.48) yields the desired solution to the problem.

The crucial step in WRMs is the choice of basis functions $\mathbf{u}_i$'s and the weighting functions $\mathbf{w}_j$' s. Different choices lead to different methods. For example, FEMs generally employ the Galerkin technique (vide Zienkiewicz, 1977) where the basis and weighting functions are the same and in general low degree polynomial subsection functions, i.e. they are non-zero only over a small subdomain called elements. In IEM, on the other hand, pulse basis functions, resulting in a step approximation, and delta weight functions, are employed in geophysical literature. These two methods are discussed in some detail in the next two sections.

3.4 THE FINITE ELEMENT METHOD (FEM)

In FEM the domain of the problem is subdivided into small blocks, called elements, of uniform physical property. The elements may vary both in shape and size, the element size being smaller in regions of larger variation in physical property. The basis as well as weighting functions are low degree polynominals. For each element the number of basis functions employed is equal to the number of nodes for the element. The nodes are the representative points where the values of unknown variables are evaluated. These are, in general situated at corners and boundaries of the element but may, if desired, lie inside the element. For example, for the simplest 3-D element, tetrahedron, there are only four nodes and the approximation of a scalar unknown ϕ is given by

$$\phi = a_0 + a_1 x + a_2 y + a_3 z \tag{3.53}$$

Here the four basis functions are 1,x,y and z.

For the four nodes, the nodal values of unknown are given by

$$\phi_i = a_o + a_1 x_i + a_2 y_i + a_3 z_i \ , \quad i = 1,2,3,4$$

x_i, y_i, z_i and ϕ_i being x, y and z coordinates and the nodal value at the ith node.

Treating these four equations as a set of simultaneous equations, the coefficients a_o, a_1, a_2 and a_3 can be evaluated in terms of ϕ_i, x_i, y_i and z_i. Substituting these expressions of a's in (3.53), a new approximation is obtained with nodal values of the unknown ϕ as coefficients, i.e.

$$\phi = \Sigma N_i \phi_i \tag{3.54}$$

where N_i's are linear polynomials, known as shape functions, and have the property that at any node the corresponding shape function has a value unity while the others are zero.

In this thesis, the 8-nodes brick type elements are used for which the linear approximation can be written as

$$\phi = a_o + a_1 x + a_2 y + a_3 z + a_4 xy + a_5 xz + a_6 yz + a_7 xyz$$

This, in terms of shape functions, obtained as in the case of a tetrahedron, can be rewritten as

$$\phi = \sum_{i=1}^{8} N_i \phi_i \tag{3.55}$$

where

$$N_i = \frac{1}{8a^2b^2c^2} (a^2 + x x_i)(b^2 + y y_i)(c^2 + z z_i)$$

with a, b and c being respectively half of the brick lengths along the x, y and z coordinate axes.

In the case of a vector unknown **u**, each of its components is expressed in terms of an equation like (3.55). Thus

$$u_p = \sum_{i=1}^{8} N_{ip}\, u_{ip} \quad , \quad p = x, y, z \tag{3.56}$$

Substituting this expression of **u** in equation (3.51), with appropriate definition of L and **f**, derived from the PDE to be solved, and using shape functions themselves as the weighting functions, an element stiffness matrix eqn. similar to equation (3.52) is obtained. Assembling all stiffness matrix eqns. one obtains a global stiffness matrix equation

$$\mathbf{K}\,\mathbf{u} = \mathbf{f} \tag{3.57}$$

where

$$K_{ij} = \langle N_i , L\, N_j \rangle$$
$$f_i = \langle N_i , f \rangle$$

and u_i's are the unknown nodal values to be evaluated by solving equation (3.57).

3.5 The Integral Equation Method (IEM)

In IEM, the domain to be discretized is the target body which is divided into N cubic cells of dimension Δ and the scattering current, $\mathbf{J}_s = \sigma_s \mathbf{E}$, is assumed constant in each cell. This means that pulse basis functions are employed. The integral equation (3.45) is approximated by a finite summation

$$\mathbf{E} = \mathbf{E}_p + \sum_{n=1}^{N} \left(\int_{v_n} \mathbf{G}(\mathbf{r}, \mathbf{r}')\, d^3\mathbf{r}' \right) \cdot \mathbf{J}_s^n \tag{3.58}$$

The integration over the tensor Green's function can be carried out numerically or analytically over the volumes and surfaces of the cells (hohmann, 1975) to obtaine the equation

$$\mathbf{E} = \mathbf{E}_p + \sum_{n=1}^{N} \Gamma(\mathbf{r}, \mathbf{r}_n) \cdot \mathbf{J}_s^n \qquad (3.59)$$

where $\mathbf{J}_s^n$ is the polarization current in the cell n having the centre $\mathbf{r}_n$, Γ is the dyadic Green's function for a small volume of current.

When $\mathbf{E}$ is evaluated at the centre of the mth cell, (3.59) can be written as

$$\mathbf{E}^m = \mathbf{E}_p^m + \sum_{n=1}^{N} \Gamma_{mn} \mathbf{J}_s^n$$

$$\text{or} \quad \frac{1}{\sigma_s} \mathbf{J}_s^m = \mathbf{E}_p^m + \sum_{n=1}^{N} \Gamma_{mn} \mathbf{J}_s^n$$

Rearranging various $\mathbf{J}$ terms, the following matrix equation is obtained

$$\mathbf{Z} \cdot \mathbf{J}_s = \mathbf{E}_p \qquad (3.60)$$

where

$$Z_{mn} = \frac{1}{\sigma_s} \delta_{mn} - \Gamma_{mn} \qquad (3.61)$$

Once $\mathbf{J}_s$ is obtained by solving the matrix equation (3.60), the field $\mathbf{E}$ can be obtained at any point by means of equation (3.45).

3.6 THE COMPACT FINITE ELEMENT METHOD (CFEM)

The IEM mesh models only the target and thus results in a smaller order matrix equation in comparison to stiffness matrix eqn. of FEM where the whole earth need be modelled. However, in IEM, the use of pulse basis function dependence of field variables within the cell results in artificial charges at cell boundaries, which are then distributed uniformly over the cell volume (Hohmann, 1975). Further, for mesh boundary nodes there exists a singularity which is artificially circumvented. These features sometimes result in an ill-conditioned matrix. In FEM, this problem is not faced, since linear or higher order field dependence is employed and the mesh boundary is

not the target boundary. The hybrid method, CFEM amalgamates the positive features of both IEM and FEM.

In CFEM, a FEM grid is generated on and around the target with only one element lying out side the target anywhere along its boundary. Some grids are shown in Fig. 5.1. The FEM is used to solve for the secondary electric field E_s using the definitions of L and **f** as given by equation (3.42). It may be emphasized here that equation (3.42) gets simplified for FEM, as for each element the conductivity is constant. The resulting stiffness matrix equation may be written as

$$K E_s = -S \tag{3.62}$$

In order to be able to solve equation (3.62), it is essential that the RHS vector S be known inside the mesh of the modelled domain, while the secondary field vector E_s must be known all over the boundary. The former can be computed easily, while the latter is obtained using the IEM, wherein the secondary field at any point is expressed in terms of the total field values inside the target mesh as follows :

$$E_s(r) = \int_V \Gamma(r, r')\ \sigma_s(r')\ [E_s(r') + E_p(r')]\ d^3r' \tag{3.63}$$

Using the FEM grid and Galerkin method, equation (3.63) can be reduced to the following matrix equation

$$E_s^b = G E_s^i + S_p \tag{3.64}$$

where S_p results from E_p terms in equation (3.63) and suffixes b and i refer to boundary and internal nodes respectively.

Partitioning equation (3.62) in terms of boundary and internal nodes, it can be written as

$$\begin{bmatrix} K_{ii} & K_{ib} \\ K_{bi} & K_{bb} \end{bmatrix} \begin{bmatrix} E_s^i \\ E_s^b \end{bmatrix} = - \begin{bmatrix} S_i \\ S_b \end{bmatrix} \tag{3.65}$$

The first of these equations yields

$$K_{ii}\ E_s^i + K_{ib}\ E_s^b = - S_i \tag{3.66}$$

or

$$E_s^i = K_{ii}^{-1}\ (K_{ib}\ E_s^b + S_i) \tag{3.67}$$

Alternatively, substituting for E_s^b from equation (3.64)

$$E_s^i = - (K_{ii} + K_{ib}\ G)^{-1}\ (S_i + K_{ib}\ S_p) \tag{3.68}$$

Equation (3.67) in conjunction with equation (3.64) defines the iterative scheme, while equation (3.68) defines the direct scheme. Once E_s is obtained, equation (3.64) can be used to obtain fields at the receiver positions.

The two schemes, iterative and direct, are implemented in the algorithms HYBRIDC and SANGAM, discussed in the next chapter.

3.7 NUMERICAL SCHEMES FOR TDEM COMPUTATIONS

There are two possible ways to compute the TDEM responses. One way is to deal directly with time domain equations and use some kind of a time stepping. The other is to compute the FDEM results at a requisite number of frequencies and then inverse Fourier transform the results to time domain. San Filipo et.al. (1985) used the direct approach working with the IEM equation (3.46). However, they computed the retarded tensor Green's functions by taking the inverse Laplace transform of the frequency domain tensor Green's functions.

In this thesis the second approach is followed. Newman et.al. (1986) have also followed this approach. Here the Sine (Cosine) transform of the

imaginary (Real) component of frequency domain field values is taken. For a step turn off of source the transformation can be written as

$$\frac{d\,\mathbf{b}(t)}{dt} = \frac{2}{\pi} \int_0^\infty \text{Im}\,[\mathbf{B}(\omega)]\,\text{Sin}\,(\omega t)\,d\omega \tag{3.69}$$

or

$$\frac{d\,\mathbf{b}(t)}{dt} = \frac{2}{\pi} \int_0^\infty \text{Re}\,[\mathbf{B}(\omega)]\;\text{Cos}(\omega t)\,d\omega \tag{3.70}$$

Anderson (1979) has given digital filters to compute these integrals efficiently.

Algorithm SAMAYA discussed in the next chapter implements these schemes.

CHAPTER - IV

THE COMPACT FINITE ELEMENT ALGORITHMS

4.1 MOTIVATION AND OUTLINE

As stated in the perspective, the goal of the present study was to develop efficient 3-D EM modelling software, based on the hybrid method (HM) - Compact Finite Element Method (CFEM)' - of numerical solution of partial differential equations, for both frequency and time domains. When this study was initiated, there already existed at the University of California, Berkeley, a 3-D FDEM modelling program based on the iterative scheme of CFEM, developed by Lee et.al. (1981). A copy of the CDC-7600 Code HYB3D, of this program was given by Lee to A.P. Raiche, one of the supervisors of this thesis. This code was the launching pad for the present study which was initiated by translating the CDC-7600 Code HYB3D into the code HYBRIDB that was implementable on VAX-11/780, the computer on which this study was carried out.

For a test model, HYBRIDB took 1 hr 7 min on a Vax 11/780 computer. The next task was to significantly reduce the run-time of HYBRIDB in order to be able to undertake any meaningful study using this program. This led to the development of the improved program HYBRIDC which took only 27 min 10s for the test model. The program SANGAM which implements the direct scheme for CFEM as against the iterative one, was developed next. It further shortened the time to 7 min 47s for the test model, thereby achieving an increase of efficiency by a factor of 8.6 in comparison with the starting program HYBRIDB. Encouraged by the success of SANGAM, the program SAMAYA was developed for the time domain. These algorithms are discussed in this chapter. The three frequency domain programs, HYBRIDB, HYBRIDC

and SANGAM, are dercribed first, followed by results of a comparative study of these algorithms. Finally, the time domain algorithm SAMAYA is discussed.

4.2 FREQUENCY DOMAIN CFEM ALGORITHMS

4.2.1 Basic Features

All three algorithms, HYBRIDB, HYBRIDC and SANGAM, are capable of dealing with an earth model, where the target comprises three or fewer arbitrarily shaped bodies buried in the half-space of a two layered earth. The programs employ a right-handed coordinate system with z-positive upwards for FE computations while the layered earth responses are computed with a left-handed coordinate system with z-positive downwards. Hence, relevant coordinate transformations are made when subprograms calculating layered earth responses are called.

The coordinates of the front left top corner of the FE mesh are always taken as (0, 0, -d) where d is the depth to the top of the target below the air-earth interface, z = 0. In case there is a plane of symmetry in the source-receiver-target configuration, it should be selected as a y = constant plane. The programs can exploit the existence of another plane of symmetry, only if it happens to be orthogonal to the first one.

In these programs, the source type options available are i) vertical magnetic dipole, ii) horizontal magnetic dipole and iii) TE or TM mode plane wave. SANGAM has the additional option of admitting polygonal loop source. However, in this thesis, results using only a rectangular loop, which is commonly used in transient EM exploration, have been presented.

All these programs can, of course, be formulated either in terms of the electric field intensity **E** or in terms of the magnetic induction **B** and provisions

for doing so, indeed, exist in HYBRIDB and HYBRIDC. However, the **B** option is essentially redundant because the **E** formulation is more stable on account of the numerical curl operation that must be performed to calculate the scattering currents in the former case. Accordingly, the **B** option was not incorporated in SANGAM. Similarly, the option of using the quadrature method for computing convolution integrals appearing in the expressions of Green's functions was not incorporated in SANGAM, as it tends to be more time consuming than the option of digital filters. However, the former option can readily be revived, if desired.

The programs HYBRIDB, HYBRIDC and SANGAM require, respectively, four, six and seven random access I/O files for storing intermediate results.

A breakup of various subprograms in HYBRIDB, HYBRIDC and SANGAM is given in appendix. In order to elucidate the characteristics of these algorithms, the main program of HYBRIDB is discussed in brief and the changes made in HYBRIDC and SANGAM are described next.

4.2.2 The Main programs of HYBRIDB, HYBRIDC and SANGAM

The program HYBRIDB starts with the reading of parameters for mesh generation. The array dimensions are checked next. If these are not sufficient, the program stops with the relevant message, else, subprograms JCHECK and KCHECK are called. The former checks if there, indeed, exist integral number of nodes in every block comprising uniformly sized elements, while the latter checks whether the computed number of total nodes in any direction is same as given in data or not. If any check fails the program stops with the relevant message, else, it calls subprograms NBLOC and NODLOC. The former computes the number of elements in each block while the latter computes the coordinates of the nodes of each element. Again the

array dimensions are checked. This completes the phase of mesh generation, steps 1-7 in flow chart of HYBRIDB given in Fig. 4.1.

Next the symmetry parameter, the frequency, the layered earth parameters and the data pertaining to source type, their number and positions and the receiver positions are read. The subprogram MCHECK is called to check whether the interfaces of the layered earth model coincide with nodes having same z-coordinate or not. If not, the program stops with the message, else, it reads the number of bodies. If number of bodies is greater than three, it stops with that message, else, it reads the body parameters for each body and calls LCES to identify the elements constituting this body. This completes the phase of model creation, steps 8-16 in flow chart, Fig. 4.1.

Next, the subprograms DIMEN and ELEMEN are called to create the element stiffness matrices. The subprogram LDES assembles these matrices. The subprogram BDES sets up the necessary boundary conditions, arising as a result of symmetry of the problem and RHS sets up the right hand side vector of the matrix equation. The matrix solver BANDEX solves the matrix equation saving the upper and lower triangular matrices created during Gaussian elimination. This completes the first FEM computations for the first source, steps 17-24.

Next, the subprogram GBASE is called to create a 2-D (r, z) grid where the convolution integrals, (CIs) need be computed. The subprogram BASE, then, computes these CIs as well as the coefficient arrays for bicubic spline interpolation. The subprogram INTEGR performs the computations corresponding to the IEM part of CFEM and renders the new boundary values. Next, the right hand side vector is modified in the light of new boundary values and the resulting new matrix equation is solved. The iteration between FEM and IEM components continues till either the convergence is achieved or the number of iterations exceeds the given maximum. In latter case, the program stops with a message.

Fig. 4.1 Flow chart of the main program of algorithm HYBRIDB

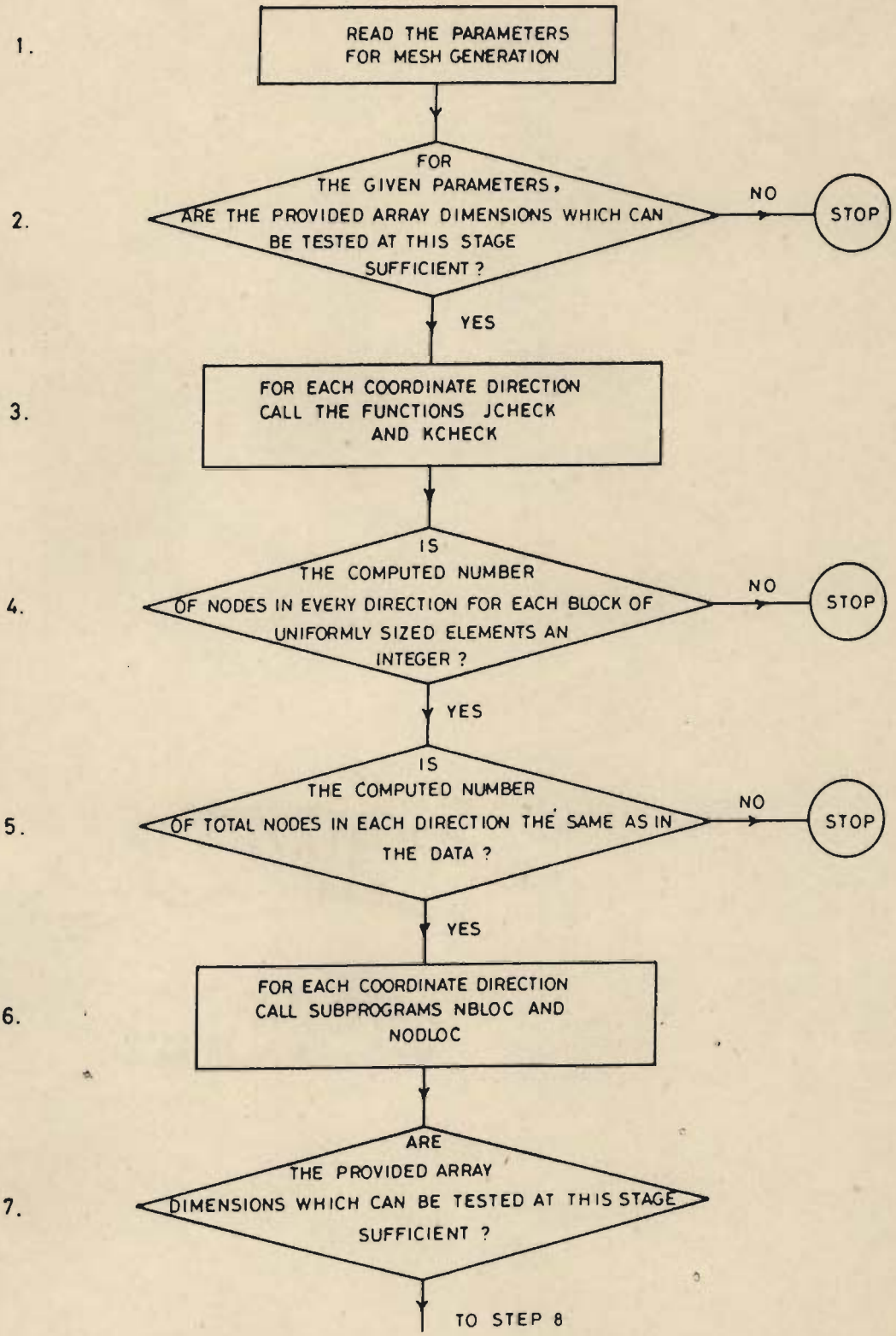

Contd.....

Fig. 4.1 (Contd.....)

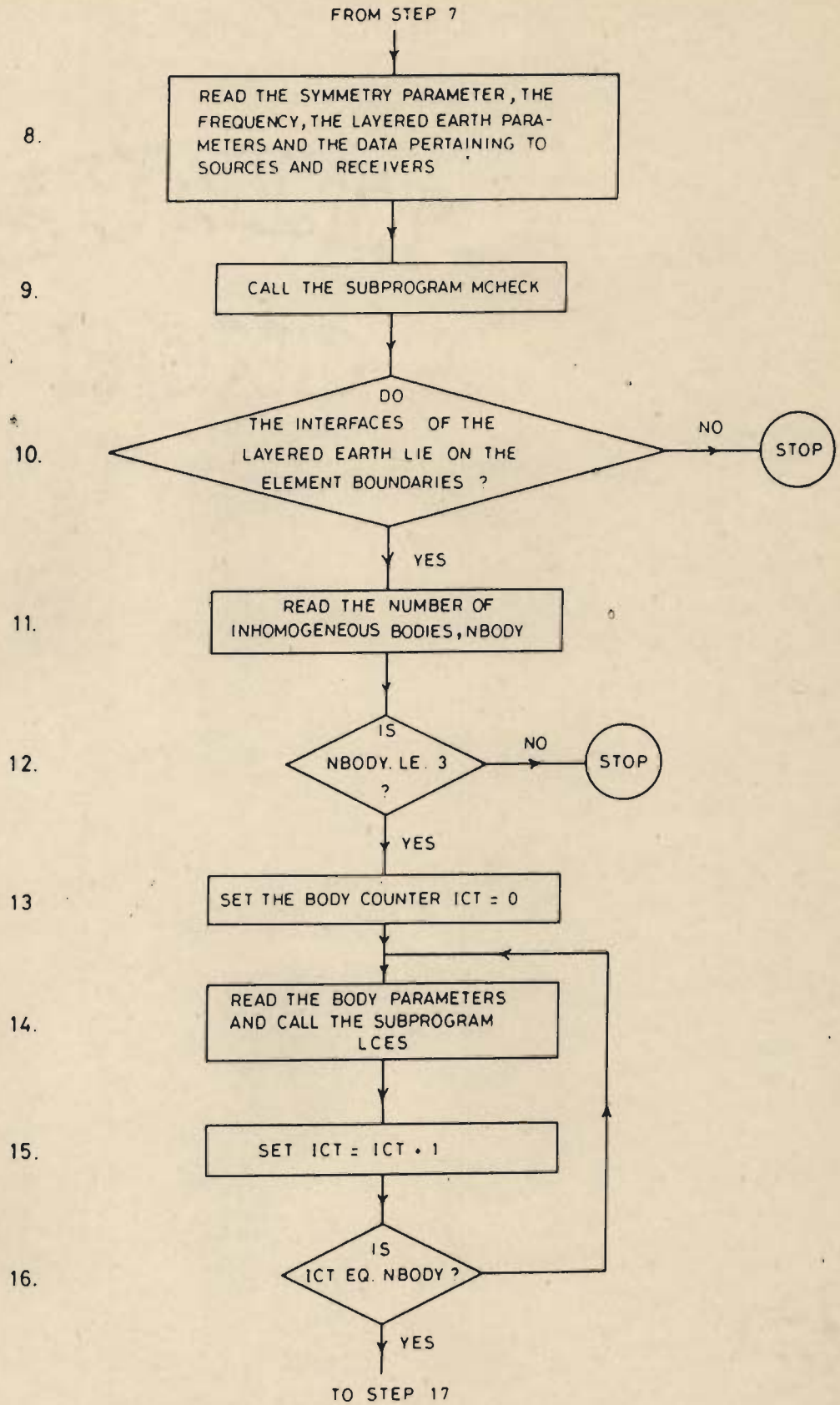

Contd.....

Fig. 4.1 (Contd.....)

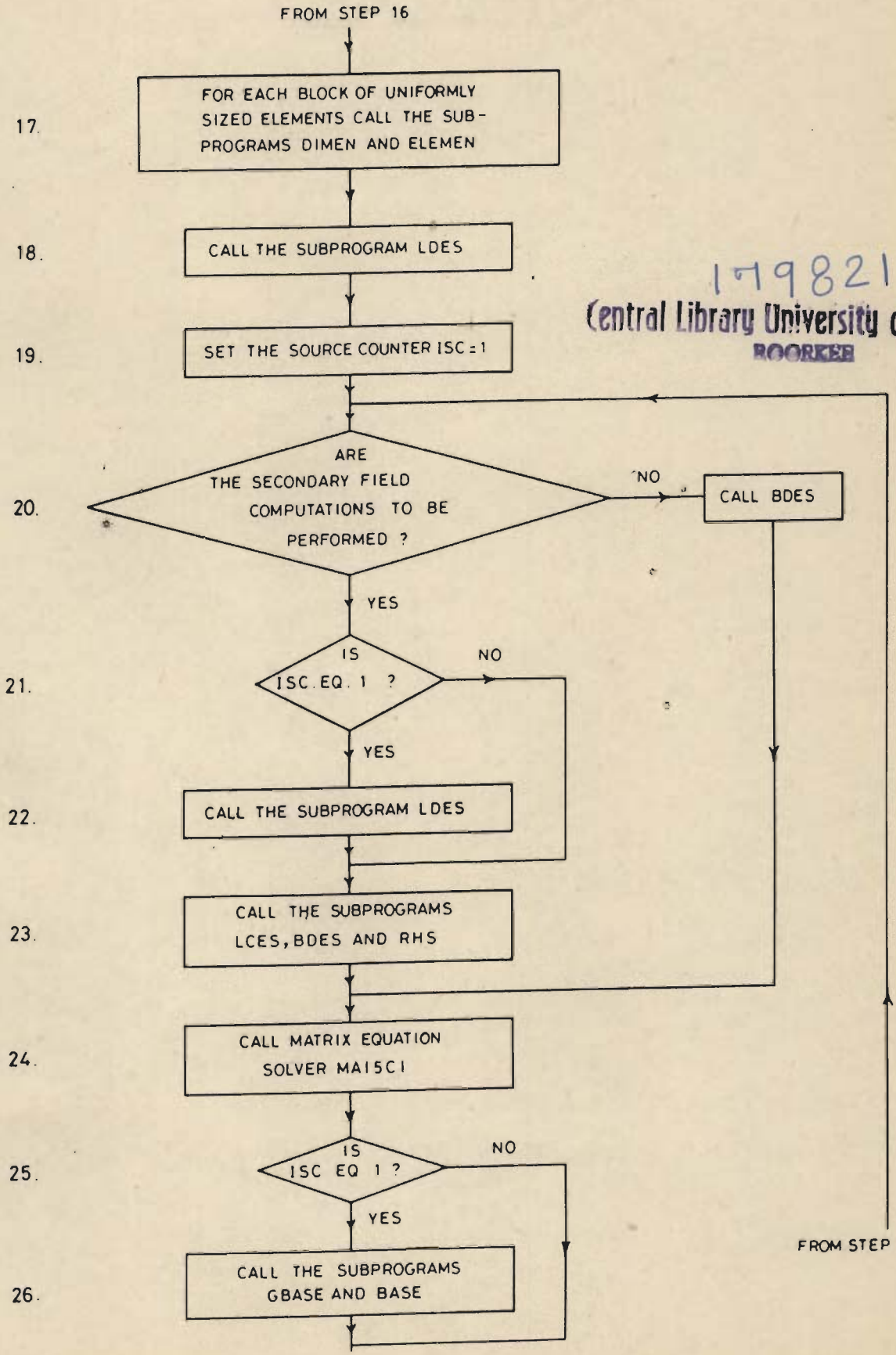

Contd.....

Fig. 4.1 (Contd.....)

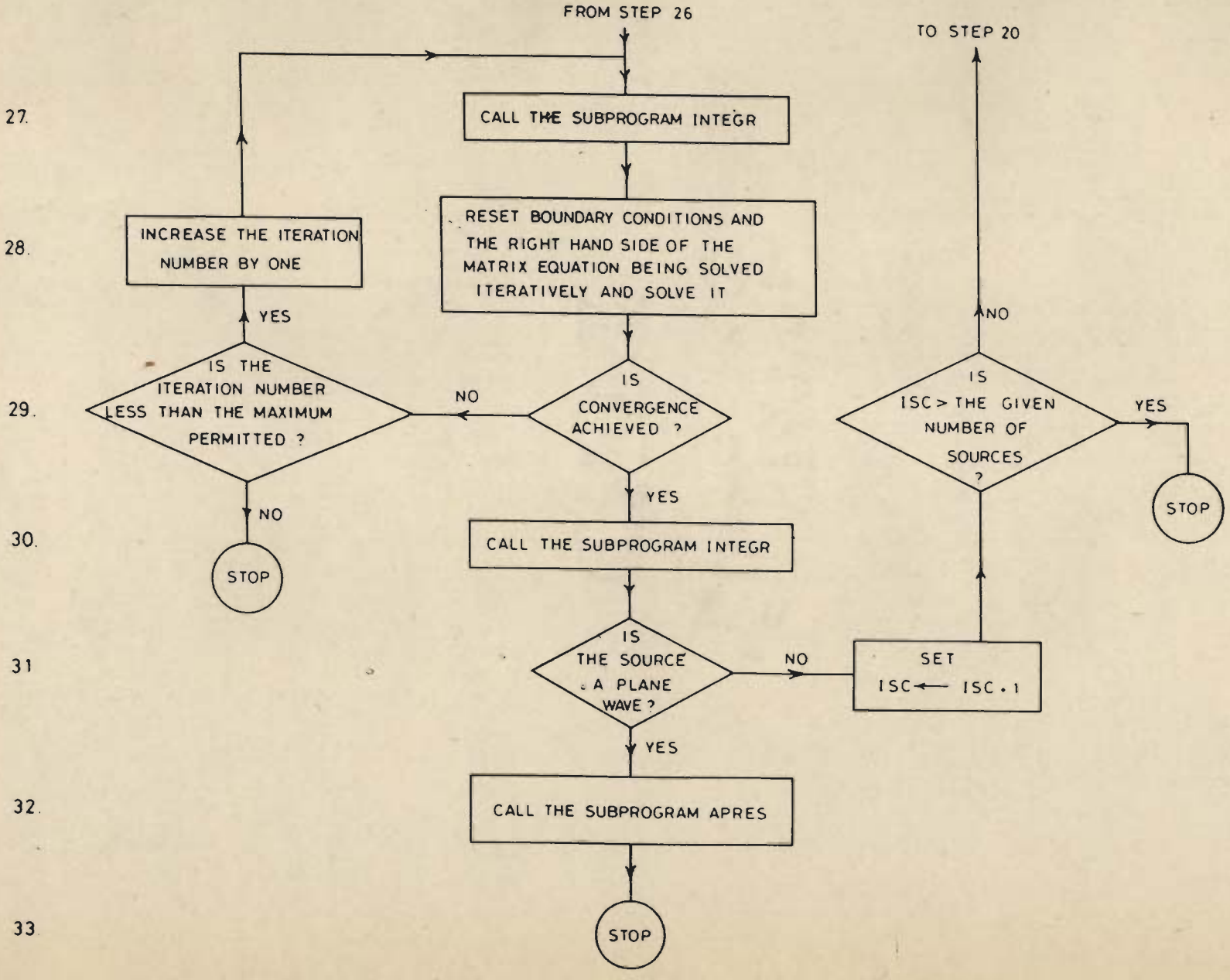
FROM STEP 26
27.
CALL THE SUBPROGRAM INTEGR
28.
RESET BOUNDARY CONDITIONS AND THE RIGHT HAND SIDE OF THE MATRIX EQUATION BEING SOLVED ITERATIVELY AND SOLVE IT
INCREASE THE ITERATION NUMBER BY ONE
YES
29.
IS THE ITERATION NUMBER LESS THAN THE MAXIMUM PERMITTED ?
NO
IS CONVERGENCE ACHIEVED ?
NO
YES
30.
STOP
CALL THE SUBPROGRAM INTEGR
31
IS THE SOURCE A PLANE WAVE ?
NO
SET ISC ← ISC + 1
YES
32.
CALL THE SUBPROGRAM APRES
33.
STOP
TO STEP 20
NO
IS ISC > THE GIVEN NUMBER OF SOURCES ?
YES
STOP

Finally, for MT case the apparent resistivity and other parameters of interest are computed. The complete flow chart is given in Fig. 4.1

In HYBRIDC main program, only changes were that i) the subprogram GBASE was replaced by the subprogram BASRG which generates a 1-D r-grid where the CIs need be computed and the subprogram BASE was called in the subprogram GREEN and not in main itself.

The main program of SANGAM differes significantly from that of HYBRIDB or of HYBRIDC, particularly in the last phase i.e. after step 18 in the flow chart of HYBRIDB. This part of the main program is described in the flow chart given in Fig. 4.2. Major changes are that the subprograms RHS, GBASE and BASE are replaced by TOOHEY, BASRG and GFNS. Then subroutine INTEGR, after the subroutine BMAT assembles the coefficient matrix and the right hand side vector. The matrix solver BANDEX is replaced by MATINV. Since SANGAM implements the direct scheme of CFEM, the iterative steps of HYBRIDB are deleted.

4.2.3 Development of HYBRIDC

A detailed examination of all the (r, z) pairs used as arguments in the computation of convolution integrals (CIs) in HYBRIDB revealed an enormous amount of repetition. For example, out of a total of 9346 (r, z) pairs for which CIs were actually computed for the test model, only 611 were distinct and of these, only 14 had distinct z-values. For all the models tried, the ratio of the total number of pairs to the number of distinct pairs was at least 2, as can be seen from Table 4.1.

On the basis of this revelation, the following strategy was adopted for the development of HYBRIDC :

i) Identify distinct (r, z) pairs, as well as distinct z-values and create a

Fig. 4.2 Partial flow chart of the main program of algorithm SANGAM

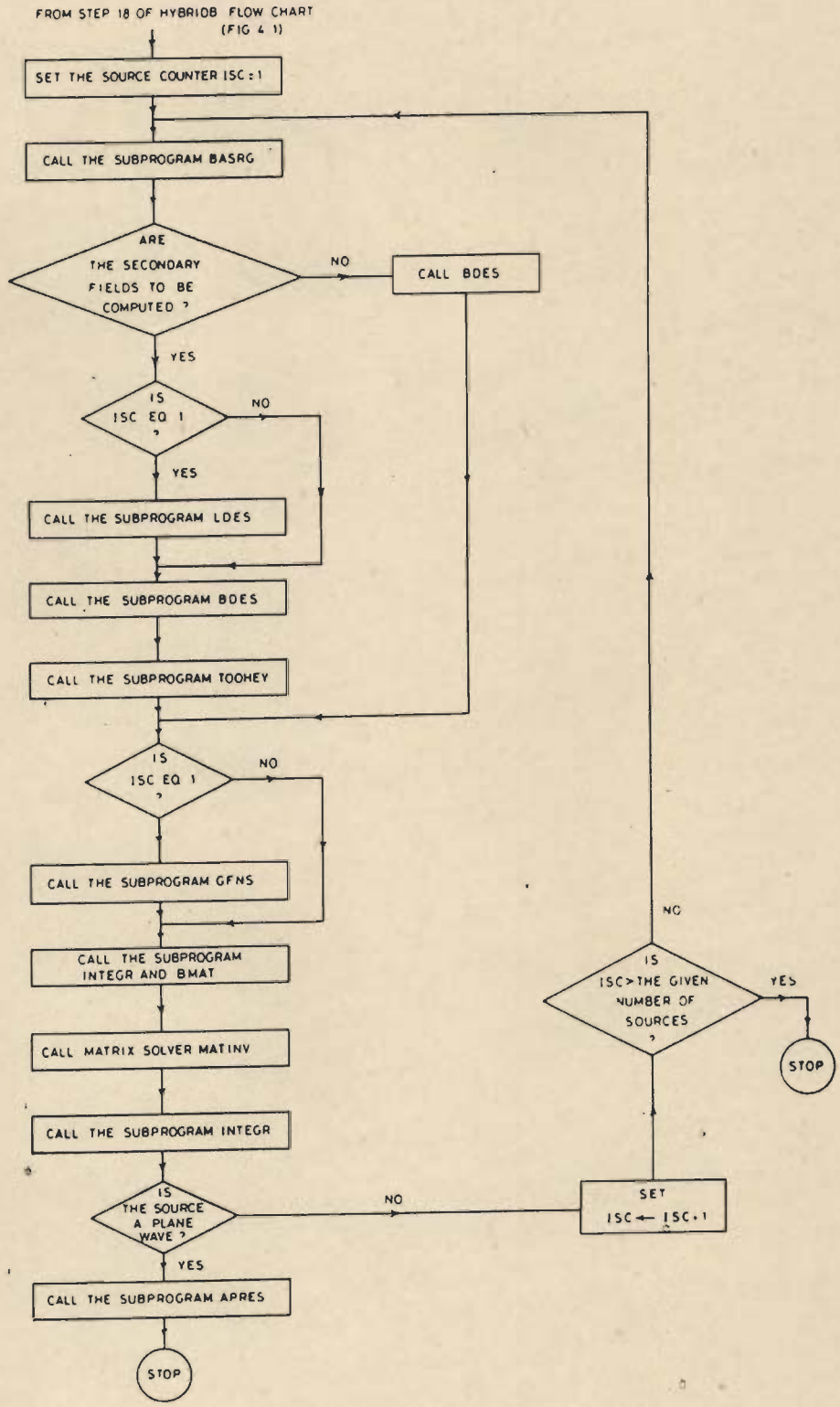

pointer table that would allocate a specific position to each (r, z) pair, for which CIs are to be computed, in the set of distinct (r, z) pairs,

ii) Use 1-D base r-grid and 1-D cubic spline interpolation, instead of the 2-D base (r, z) - grid and the 2-D bicubic spline interpolation employed in HYBRIDB, and

iii) Compute and store the CIs for the distinct (r, z) pairs and read the CIs values for every repeating (r, z) pair.

This strategy led to the development of three new subprograms: GRFIND for step (i), BASRG for step (ii) and GRINT for step (iii). Further, three subprograms CUBSPL, CUBINT and CUBVAL were adapted for 1-D cubic spline interpolation from the programs of Carl de Boor (1978) and the three subprograms of HYBRIDB - BASE, GREEN and INTEGR were rewritten in the light of 1-D interpolation. Unlike HYBRIDB, where BASE was called in the main program in HYBRIDC, it was called in subprogram GREEN and only for distinct z-values. The subprogram GBASE of HYBRIDB which generated the 2-D base (r, z) grid and the subprograms OBCSPY, OPSPLY, SOLVYR, SPL and SPLYN which performed the bicubic spline interpolation, thus became redundant under the new scheme.

Another improvement was made in HYBRIDC over HYBRIDB. In the latter the CIs having Bessel functions J_0 and J_1 as kernels were computed by the two subprograms ZHANK0 and ZHANK1 which used two different sets of digital filters. These subprograms were replaced in HYBRIDC by the subprogram ZHANKS which was more efficient and which used only one set of digital filters (vide Anderson, 1979). ZHANKS together with ZAVE, which let one use the results of previous computations performed on ZHANKS, enhances the efficiency of HYBRIDC.

4.2.3.1 The search algorithm GRFIND

The distinct (r, z) pairs where CIs are to be computed can not be listed a-priori from the input data, in any straightforward manner. The argument values of each pair are complicated functions of i) position of the FE mesh in the earth, ii) position of receivers or of mesh boundary nodes and iii) order of the numerical quadrature over the element. Hence the problem was resolved by developing the search routine GRFIND, where distinct pairs are identified, and linked lists of r and z values are constructed. Further, the pointer lists are generated which, for any given (r,z) pair, provide the index for the table of CIs.

The component r of the distinct pair (r, z) is always entered in the list R while the component z is entered in the list Z only if z is distinct. The pointer array PR links each distinct z value in list Z to values of r with which it forms pairs. Figure 4.3 shows the data structure of the linked lists with their associated pointer table.

Since the number of distinct z-values is found to be very small, the z-search is carried out sequentially. On the other hand the number of r-values that pair with a given z-value may be very large. Further, it was observed that, in general, every pair had its r-value close to that of the previous pair within each sublist R_z, with something like a Gaussian probability distribution centred about the r-value of the previous pair. Hence the r-search was carried out in a leap frog manner - searching first within ± 10 entries around the r-value of the previous pair, then searching from the first entry in R_z to the lower limit of the first search step and finally from the upper limit of the first search step to the last entry of R_z. The flow chart is given in Fig. 4.4.

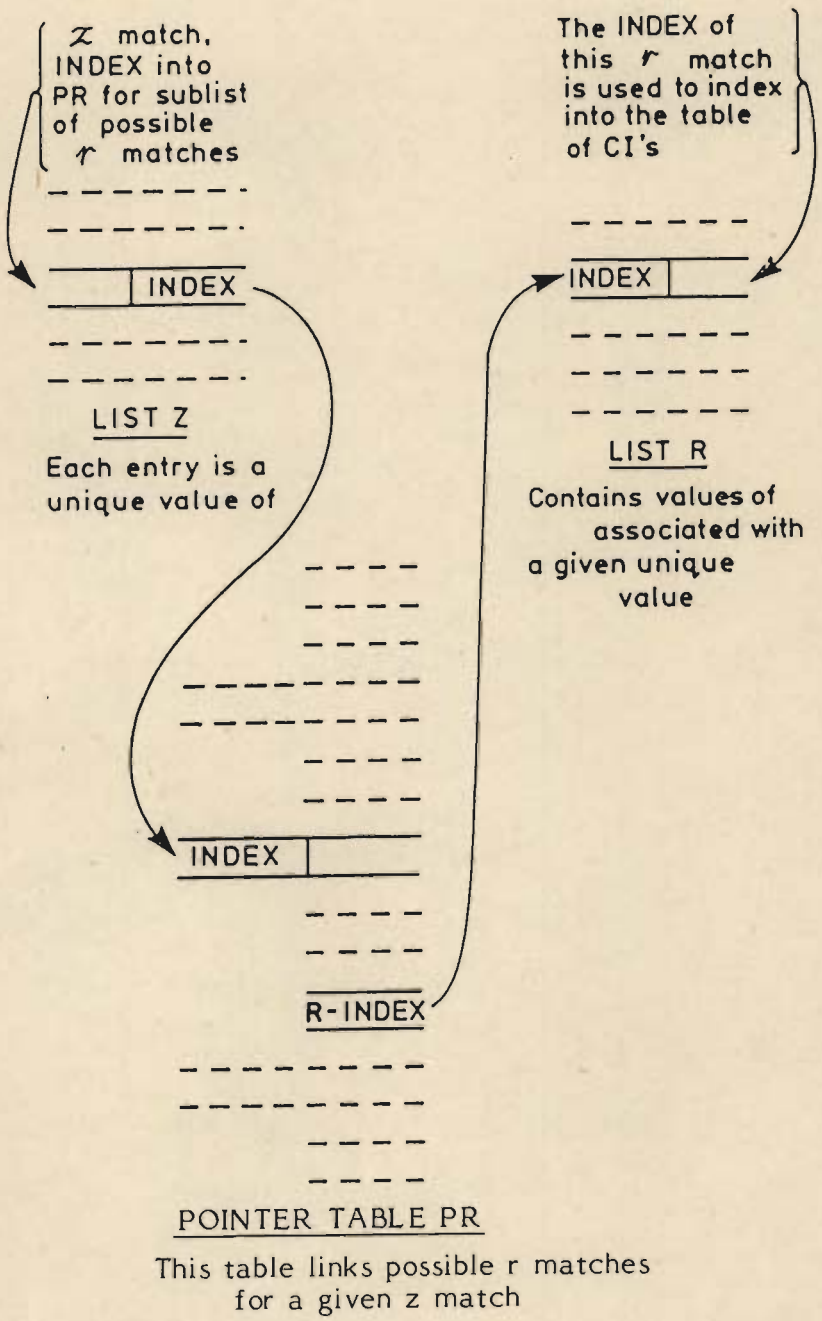

Fig. 4.3 A match in the list of unique z values gives the index of the pointer table entry in PR. PR defines the sublist entries of list R. These are the possible values of r for the matched z value. If the search in list R is successful, the matched value gives the index of the required CI's in the stored table.

Fig. 4.4 Flow chart of the search subroutine GRFIND

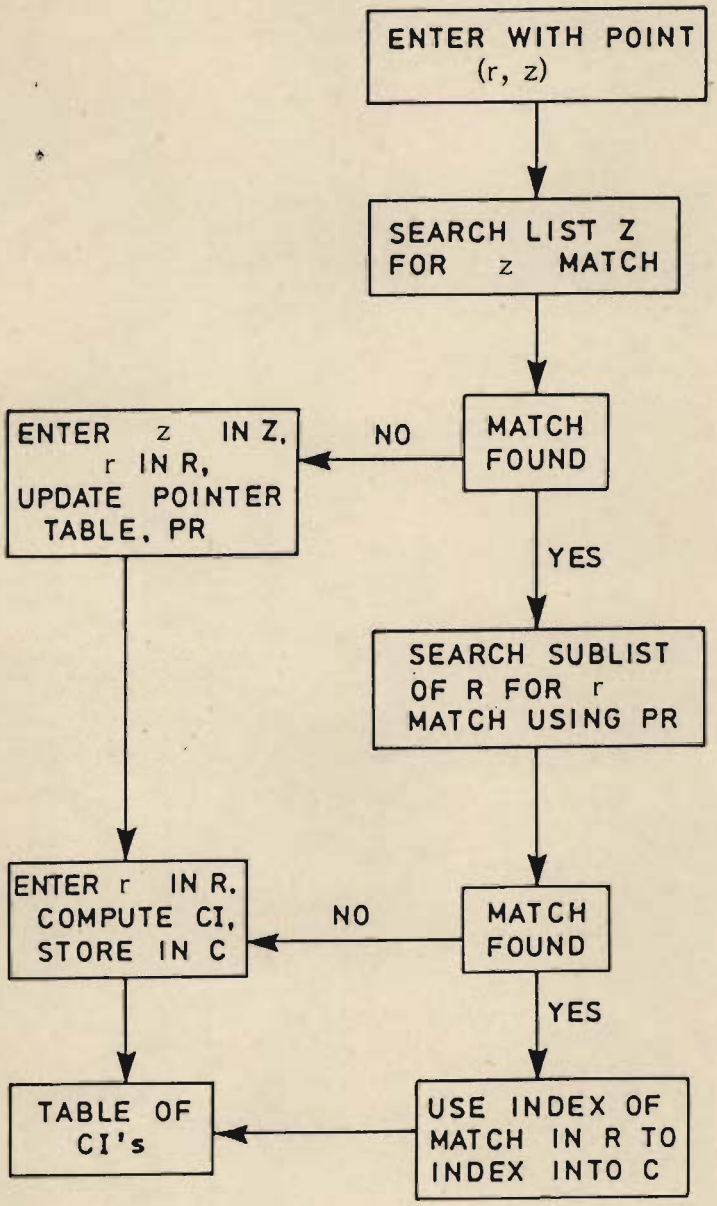

4.2.4 Development of SANGAM

An a-priori estimate of the number of multiplicative operations required for solving the matrix equation solution component of the direct and iterative schemes of CFEM can be obtained from the number of internal and boundary nodes in the FE mesh. These estimates, however, do not suggest a clear preference in favour of either scheme. In order to resolve this issue, the development of a direct CFEM algorithm SANGAM was undertaken. This development, however, unlike the case of HYBRIDC, necessitated a restructuring of the main program, as discussed earlier ; and rewriting of the major subprograms BANDEX, BDES, INTEGR, LCES, LDES, RHS, TOOHEY and GREEN. Further, two new subprograms GFNS and BMAT were written. The former computes and stores all the necessary Green's functions before the commencement of IE computations, a strategy that led to a more efficient use of the large arrays. The latter subprogram generated the final coefficient matrix and the right hand side vectors by assembling various submatrices and vectors in accordance with the relation (3.68). The resulting coefficient matrix and right hand side vector are input to the matrix equation solver MATINV.

SANGAM has the following new features :

i) The source type option includes the polygonal loop source, and

ii) The bore-hole option is incorporated by letting the receiver be anywhere in the earth but outside the target body.

Feature (i) led to the incorporation of the Gaussian integration steps in BDES and to the addition of BLOCK DATA BLDGIN which contains the weights and abscissa values for different orders of quadrature. Feature (ii) led to the development of COMPLEX FUNCTIONS H00A, H10A, H10AA, H20A and H20AA which perform kernel computations for the relevant CIs.

A preliminary study made on HYBRIDC to evluate the relative performance of the convolution and quadrature methods, revealed that the latter is, in general, significantly more time consuming. However, in some extreme cases, where better accuracy is desirable, irrespective of the time factor, the quadrature method may yield marginally better results. One such case is that of extreme resistivity contrst between the target and the host. However, even for this case, the improvement in results does not justify the additional amount of time needed. Hence, the option for using the quadrature method was altogether dropped in SANGAM, resulting in the deletion of subprograms AJ0, AJ1, ANINT, CIMPS and DQG8. The option of using the secondary B-field formulation was also dropped in SANGAM for reasons already stated in section 4.2.1.

4.2.5 Comparison of HYBRIDB, HYBRIDC and SANGAM

A comparative study of the relative performance of the three programs HYBRIDB, HYBRIDC and SANGAM was made on a number of models. Various descriptions of models, including cases of extreme resistivity contrast, were chosen for this study. Of these, eight models have been selected for illustrating the relative performance of these programs.

Parameters of these models, as well as the performance data of the three programs, are given in Table 4.1. A comparative analysis of these brings out the following features :

1. The search reduction factor is the primary contributor to improvement in the efficiency of HYBRIDC compared with that of HYBRIDB. Model 1 and 3 entries seem to contradict this observations. However, this seeming paradox can be explained by noting the fact that in HYBRIDC, the only saving over HYBRIDB accrue in the computation of Green's

Table 4.1 Comparison of the Three Algorithms HYBRIDB, HYBRIDC and SANGAM for Eight Models

Parameters		Model 1	Model 2	Model 3	Model 4	Model 5	Model 6	Model 7	Model 8
No. of NODES	x,y,z	5,4,5	3,3,4	6,9,6	5,6,8	5,12,4	4,5,6	4,5,6	4,4,5
	Internal	27	8	128	90	88	48	48	27
	boundary	73	28	196	150	152	72	72	53
Res. Ohm m	layer	100	100	13.7	120.48	200	100	100	7
	host	100	100	13.7	120.48	200	100	100	10
Layer thickness		10	10	15	15	500	250	250	1000
BODY	Number	1	1	1	1	1	1	1	2
	Dimens. (km^3)	.05x.1x.1	.05x.1x.1	.5x1.5x.5	.03x095x.19	2.5x2x1	.5x1x2	.5x1x2	.5x.5x.05 .25x.25x.05
	Res. Ohm m	5	5	1.821	2.7	5	0.5	5	100 100
	Burial depth(m)	50	50	200	30	750	500	500	1050 1000
Res. contrast		20	20	7.5	44.6	40	200	20	.07 .1
SOURCE	Type	VMD	MT	VMD	VMD	MT	MT	MT	MT
	Number	2	1	2	3	1	1	1	1
No. of receivers		13	13	2	7	15	15	15	10
Frequency		20	20	0.15	15	1	0.01	0.1	0.1
SKIN DEPTH	layer	1125	1125	4807	976	7113	50300	15910	4208
	host	1125	1125	4807	976	7113	50300	15910	5030
	body	251.5	251.5	1752.6	213.4	1125	3556.7	3556.7	15906.3
Max. Iterations		30	30	18	60	30	30	30	30

(Contd.....)

Table 4.1 (Contd.....)

Parameters		Model 1	Model 2	Model 3	Model 4	Model 5	Model 6	Model 7	Model 8
NO. OF GREEN's FNS.	Boundary nodes,	84114	8064	1778625	864243	1313658	373356	373356	83538
	Receivers	33471	10926	6300	63630	126540	75510	66258	21042
TOTAL (r, z) PAIRS	Boundary nodes,	9346	896	197625	96027	145962	41484	41484	9282
	Receivers	3719	1214	700	7070	14060	8390	8390	2338
DISTINCT (r, z) PAIRS	Boundary nodes,	612	352	47712	27230	11224	18564	18565	617
	Receivers	557	259	176	2502	2044	2838	2462	435
DISTINCT z-values	Boundary nodes,	14	8	32	70	8	32	32	12
	Receivers	10	5	9	14	5	13	11	10
SEARCH REDUC-TION FACTOR	Boundary nodes,	15.27	2.55	4.14	3.57	13.00	2.23	2.23	15.04
	Receivers	6.68	4.69	9.00	2.83	6.88	2.96	3.41	5.37
CPU TIME (h.m.s.)	HYBRIDB	1.06.56	0.17.59	14.07.34	12.26.55	-	-	-	-
	HYBRIDC	0.27.10	0.08.58	03.22.20	06.32.43	2.16.26	0.52.38	0.52.23	0.19.10
	SANGAM	0.07.47	0.03.14	01.27.18	00.47.55	0.48.15	0.25.35	0.24.57	0.06.20
TIME REDUC-TION FACTOR	$\frac{\text{HYBRIDB}}{\text{HYBRIDC}}$	2.46	2.01	4.19	1.90	-	-	-	-
	$\frac{\text{HYBRIDC}}{\text{SANGAM}}$	3.49	2.77	2.32	8.20	2.83	2.06	2.10	3.03
	$\frac{\text{HYBRIDB}}{\text{SANGAM}}$	8.60	5.56	9.70	15.59	-	-	-	-
REFERENCES		K.H. Lee (1986)	-	HYB3D manual	HYB3D manual	Wannamaker et.al.(1984, Fig. 4)	Hohmann (1983 b, Fig. 9)	Mozeley (1982, Fig. 4.4)	K. Vozoff private comm.

functions which are performed only once, irrespective of the number of sources and iterations, other time-requirements remaining the same.

2. The ratio of the number of boundary nodes to the number of internal nodes and the number of iterations needed for convergence in the iterative scheme are the primary factors controlling the relatively better performance of SANGAM over HYBRIDC. This is corroborated by entries for model 4.

4.3 TIME DOMAIN CFEM ALGORITHM - SAMAYA

After the success of SANGAM, the 3-D TDEM program SAMAYA based on CFEM was developed. The frequency domain field values were transformed to obtain the time domain results. In the process of development, the main program of SANGAM was again restructured, making provision for computations for a number of frequencies and storing the final results and then calling the time domain conversion control routine TDM which was written afresh. TDM has an option of either computing the Sine-transform of imaginary components of the field values or the Cosine transform of the real components of the field values. The Sine-transform routine SINTRN, as well as the Cosine-transform routine COSTRN, were adapted from the corresponding digital filter routines of W.L. Anderson. The filter coefficients for these two subprograms are respectively contained in the two BLOCK DATA SINBLD and COSBLD respectively.

SAMAYA has the option of frequency or time domain computations. Further, in time domain, it has the option of computing the time variation of either the field values or their time derivatives. It can also compute the time variation of current. The program also has an option for the pulse ramp integration.

APPENDIX

SUBPROGRAMS OF THE ALGORITHMS HYB3D, HYBRIDB, HYBRIDC, SANGAM AND SAMAYA

Various subprograms comprising the algorithms HYB3D, HYBRIDB, HYBRIDC, SANGAM and SAMAYA are given in the Table A.1. Here a (x) and (-) in any column, representing one of the five algorithms, shows the presence and absence respectively of the corresponding subprogram in that algorithm. Two or three crosses mean that the corresponding subprogram has been re-written once or twice respectively. As far as the numbers of various types of subprograms in different algorithms are concerned these are given in Table A.2. Finally, in Table A.3 the subprograms deleted or introduced in different algorithms with respect to the previous column algorithm are given.

Table A.1 Subprograms of Various Algorithms

Sl. No.	Subprogram	HYB-3D	HYB-RIDB	HYB-RIDC	SAN-GAM	SAM-AYA	Outline
1	2	3	4	5	6	7	8
1	AJ0	x	x	x	-	-	Computes the Bessel function J_0 needed for the quadrature in integration of the convolution integrals (CIs).
2	AJ1	x	x	x	-	-	Computes the Bessel function J_1 needed for the quadrature integration of CIs.
3	ANINT	x	x	x	-	-	Computes the CIs using quadratures.
4	APRES	x	x	x	x	x	Computes the apparent resistivity and other parameters for an MT source.
5	BANDEX	-	x	x	-	-	Decomposes the banded stiffness matrix into LU factors and solves it.
6	BASE	x	x	xx	xx	xx	(x) Computes the CIs on the base (r, z) - grid and the necessary coefficients for bicubic spline interpolation. (xx) Computes the CIs on the base r-grid and the necessary coefficients for cubic spline interpolation.
7	BASRG	-	-	x	x	x	Computes the base r-grid.
8	BDES	x	x	x	xx	xx	(x) Calculates and stores the boundary values. (xx) The same as for (x), includes the polygonal loop source computations.
9	BLDGIN	-	-	-	x	x	Block data for Gaussian integration.
10	BMAT	-	-	-	x	x	From matrices $\mathbf{K}_{ii}$, $\mathbf{K}_{ib}$ and $\mathbf{G}$ and vectors $\mathbf{S}_i$ and $\mathbf{S}_p$ generates the matrix $(\mathbf{K}_{ii} + \mathbf{K}_{ib}\mathbf{G})$ and the vector $(\mathbf{S}_i + \mathbf{K}_{ib}\mathbf{S}_p)$ which are the inputs to matrix solver MATINV. Boundary conditions are also implemented here.
11	CIMPS	x	x	x	-	-	Subroutine for quadrature integration, called in ANINT.
12	COSTRN	-	-	-	-	x	Performs the Cosine transform operations.
13	COSBLD	-	-	-	-	x	Block data of filter coefficients for Cosine transform.
14	CUBINT	-	-	x	x	x	Identifies the two successive r-grid points which limit the point of interpolation.
15	CUBSPL	-	-	x	x	x	Generates the cubic spline interpolation coefficient arrays.

Contd.....

Table A.1 (Contd.....)

1	2	3	4	5	6	7	8
16	CUBVAL	-	-	x	x	x	Interpolates the CI value for a given point.
17	DIMEN	x	x	x	x	x	Computes the dimensions of the elements of a given block.
18	DIRACC	-	x	x	x	x	Manages the direct access I/O files.
19	DQG8	x	x	x	-	-	Subroutine for quadrature integration called by ANINT.
20	E	x	x	x	x	x	Computes the parameters u_1, u_2, AES etc. (vide, Pridmore, 1978) for the complex functions E10A and E20A.
21	E00A	x	x	x	x	x	These complex functions compute the various convutes needed in the computation of different CIs for electric field evaluation (vide Pridmore (1978) and Lee et.al. (1981)).
22	E00B	x	x	x	x	x	
23	E01A	x	x	x	x	x	
24	E01B	x	x	x	x	x	
25	E10A	x	x	x	x	x	
26	E10B	x	x	x	x	x	
27	E11	x	x	x	x	x	
28	E11A	x	x	x	x	x	
29	E11B	x	x	x	x	x	
30	E12	x	x	x	x	x	
31	E13	x	x	x	x	x	
32	E14	x	x	x	x	x	
33	E15	x	x	x	x	x	
34	E16	x	x	x	x	x	
35	E17	x	x	x	x	x	
36	E1Z	x	x	x	x	x	
37	E20A	x	x	x	x	x	
38	E20B	x	x	x	x	x	
39	E21	x	x	x	x	x	
40	E21A	x	x	x	x	x	
41	E21B	x	x	x	x	x	
42	E22	x	x	x	x	x	
43	E23	x	x	x	x	x	
44	E24	x	x	x	x	x	
45	E25	x	x	x	x	x	
46	E26	x	x	x	x	x	
47	E2Z	x	x	x	x	x	
48	EE	x	x	x	x	x	Computes the E-field at a point (x,y,z) inside an element using the FE shape functions.

Contd.....

Table A.1 (Contd.....)

1	2	3	4	5	6	7	8
49	ELEMEN	x	x	x	x	x	Computes the stiffness matrix elements using basement conductivity for the mesh elements.
50	EXPAND	x	x	x	-	-	Returns the elements of a particular row of coefficient matrix as needed by BANDEX or MA15C1.
51	EXTRA	-	x	x	xx	xx	The entry point in BANDEX (x) or MATINV (xx) for performing back substitution.
52	FIELD	x	x	x	x	x	Computes parameters needed in VLOOP.
53	FIELDH	x	x	x	-	-	Computes parameters needed in HLOOP.
54	FIELDP	x	x	x	x	x	Computes the electric field inside the earth for the magnetic dipole sources.
55	FIELDS	x	x	x	x	x	Computes the electric field inside the earth for a plane wave source.
56	GBASE	x	x	-	-	-	Generates the 2-D (r, z) grid for the computation of CIs in BASE.
57	GFNS	-	-	-	x	x	Computes and stores all the Green's functions needed in the integral equation part.
58	GREEN	x	x	xx	xxx	xxx	(x) · Computes the Green's functions for a (r,z) pair by either computing or interpolating, over a 2-D (r,z) grid, the CIs. (xx) same as for (x) but interpolation is over a 1-D r-grid. (xxx) same as for (xx) with the H-field option deleted.
59	GRFIND	-	-	x	x	x	Identifies whether the arguments of the given (r,z) pair are repeating or not.
60	GRINT	-	-	x	x	x	Interpolates the CIs from their values for base grid points.

Contd.....

Table A.1 (Contd.....)

1	2	3	4	5	6	7	8
61	H00A	-	-	-	x	x	These complex functions compute the various convolutes needed in the computation of different CIs for magnetic field evaluation (vide Pridmore (1978) and Lee et.al. (1981)).
62	H01	x	x	x	x	x	
63	H02	x	x	x	x	x	
64	H03	x	x	x	x	x	
65	H04	x	x	x	x	x	
66	H05	x	x	x	x	x	
67	H06	x	x	x	x	x	
68	H10A	-	-	-	x	x	
69	H10AA	-	-	-	x	x	
70	H11	x	x	x	x	x	
71	H12	x	x	x	x	x	
72	H13	x	x	x	x	x	
73	H14	x	x	x	x	x	
74	H15	x	x	x	x	x	
75	H16	x	x	x	x	x	
76	H20A	-	-	-	x	x	
77	H20AA	-	-	-	x	x	
78	H21	x	x	x	x	x	
79	H22	x	x	x	x	x	
80	H23	x	x	x	x	x	
81	H24	x	x	x	x	x	
82	H25	x	x	x	x	x	
83	H26	x	x	x	x	x	
84	HLOOP	x	x	x	xx	xx	Computes the VMD response of the layered earth at any point.
85	INTEGR	x	x	xx	xxx	xxx	(x) Performs the IE computations of the CFEM. (xx) as for (x) but with new subroutine GREEN that incorporates the search. (xxx) as for (xx) but it also generates various submatrices needed to obtain the final coefficient matrix in the direct scheme of CFEM.
86	JCHECK	x	x	x	x	x	Checks for an integer number of nodes in any direction and in any block.

Contd.....

Table A.1 (Contd.....)

1	2	3	4	5	6	7	8
87	KCHECK	x	x	x	x	x	Checks whether the computed number of nodes in a given direction agrees with the input data or not.
88.	LCES	x	x	x	xx	xx	(x) Identifies the elements encompassing the anomalous bodies. (xx) same as for (x) but rewritten for direct scheme.
89	LDES	x	x	x	xx	xx	(x) Creates the total and the upper and lower secondary field stiffness matrices and writes them respectively on units 4, 9 and 10 for the iterative scheme of CFEM. (xx) Creates the total or secondary field stiffness matrix and writes them respectively on units 4 and 10 for the direct scheme of CFEM.
90	M	x	x	x	x	x	Computes the parameters needed in E10B, E1Z, E20B and E2Z.
91	MA15C1	x	-	-	-	-	Matrix solver for iterative scheme of CFEM.
92.	MATINV	-	-	-	x	x	matrix solver for direct scheme of CFEM.
93	MCHECK	x	x	x	x	x	Checks whether layered model interfaces coincide with the nodes or not.
94	NBLOC	x	x	x	x	x	Calculates the number of elements in each block.
95	NFIND	x	x	x	x	x	Computes the number of nodes between two coordinate values.
96	NODLOC	x	x	x	x	x	Computes coordinates of element nodes.
97	OBCSPY	x	x	-	-	-	Generates the coefficient arrays for bicubic spline interpolation of CIs.
98	OPSPLY	x	x	-	-	-	Bicubic spline routine called by OBCSPY.
99	PRINT1	x	-	-	-	-	Array print out routine.
100	PRINTT	x	xx	xx	xx	xx	Array print out routine.
101	QEXP	x	-	-	-	-	Computes the exponential of a complex argument.
102	R0	x	x	x	x	x	Compute the convolutes for CIs needed for field evaluations respectively in air, layer and basement.
103	R1	x	x	x	x	x	
104	R2	x	x	x	x	x	

Contd.....

Table A.1 (Contd.....)

1	2	3	4	5	6	7	8
105	RANDOM	x	-	-	-	-	Manages random access I/O files.
106	REDUCE	-	-	x	x	x	Look for the duplication of the size of the element respectively in all, x, y and z directions.
107	REDUCX	x	x	-	-	-	
108	REDUCY	x	x	-	-	-	
109	REDUCZ	x	x	-	-	-	
110	RHS	x	x	x	-	-	Generates the right hand side of the stiffness matrix eqn.
111	RWREC	-	x	x	x	x	Computes the number of records to be handled by the I/O file manager DIRACC.
112	SINTRN	-	-	-	-	x	Performs the Sine transform operations.
113	SINBLD	-	-	-	-	x	Block data of filter coefficients for Sine transform.
114	SOLVYR	x	x	-	-	-	Bicubic spline interpolation routines.
115	SPL	x	x	-	-	-	
116	SPLYN	x	x	-	-	-	
117	TANC	x	x	x	x	x	Computes Tangent of a complex argument.
118	TDM	-	-	-	-	x	Transforms the frequency domain data to time domain.
119	TEMODE	x	x	x	x	x	Computes the RTE parameter (vide, Pridmore, 1978).
120	TEXP	-	x	x	x	x	Computes the exponential of a complex argument.
121	TEUL	x	x	-	-	-	Called by the quadrature integration routine ANINT.
122	TOOHEY	x	x	x	xx	xx	(x) Creates the RHS vectors for the secondary field FE stiffness matrix equation after implementing the boundary conditions and symmetry. (xx) as for (x) but rewritten for direct scheme of CFEM.
123	UU	x	x	x	x	x	Computes the parameter $u_i = (\lambda^2 - k_i^2)^{1/2}$.
124	VLOOP	x	x	x	xx	xx	Computes the response of the layered earth to a HMD.

Contd.....

Table A.1 (Contd.....)

1	2	3	4	5	6	7	8
125	ZAVE	-	-	x	x	x	Modifies previously computed CIs for the case where two convolutes are algebraically related.
126	ZHANK0	x	x	-	-	-	Performs convolution operation for CIs respectively with J_o, J_1 and both kernels.
127	ZHANK1	x	x	-	-	-	
128	ZHANKS	-	-	x	x	x	

Table A.2 Description of Number of Various Types of Subprograms in Various Algorithms

Sl.No.	Subprogram	HYB-3D	HYB-RIDB	HYB-RIDC	SANGAM	SAMAYA
1	FUNCTION	6	6	7	5	7
2	COMPLEX FUNCTION	55	55	55	59	59
3	SUBROUTINE	39	39	35	32	33
4	BLOCK DATA	-	-	-	1	3
5	ENTRY	-	1	1	1	1
	TOTAL	100	101	98	98	103

Table A.3 The Subprogram Added or Deleted in Various Algorithms

Sl. No.	Operation	HYB-3D	HYBRIDB	HYBRIDC	SANGAM	SAMAYA
1	added	-	5,18,51,111, 120	7,14,15,16,59, 60,106	9,10,57,61, 68,69,76,77, 92	12,13,112, 113,118
2	deleted	-	91,99,101, 105	56,97,98,107, 108,109,114, 115,116,121	1,2,3,5,11,19, 50,53,110	-

CHAPTER - V

RESULTS AND DISCUSSION

5.1 INTRODUCTION

The reduction in computer-time requirements of the frequency domain iterative and direct CFEM algorithms HYBRIDC and SANGAM was discussed in the previous chapter. However, these algorithms can not be used confidently unless their stability and accuracy have been established. These aspects are discussed in this chapter. Here results of various excercises performed on SANGAM and the time domain algorithm SAMAYA, are discussed. The excercises covered such aspects as mesh convergence, strike-length convergence, reciprocity test, no-contrast case, stability and accuracy of transformation from frequency to time domain and so on. Besides, comparisons were made of the results obtained using SANGAM and SAMAYA with those worked out using already existing algorithms.

5.2 MESH CONVERGENCE STUDY

Mesh convergence studies are of crucial importance for proving the efficacy of any numerical field problem algorithm. For SANGAM these studies were made for an MT source. The base model chosen was a 100 x 100 x 50 m^3 cuboid target of resistivity 0.5 Ohm m buried at a depth of 60 m in a half-space of resistivity 100 Ohm m, and the frequency was 0.01 Hz corresponding to which the respective skin depths of the host medium and target would be 50300 m and 3557 m. Although this study has been conducted only for MT, to reduce the computational effort involved, it is felt that the mesh convergence results would be broadly valid for other sources also. Apparent resistivities were computed at the earth's surface along a profile in the

x-direction at seven points which were 0, 50, 100, 150, 200, 250 and 300 m distant from the point of intersection of the two planes of symmetry. The plan and section views of the three grids used for the convergence study are given in Fig. 5.1. All three grids exploit the two planes of symmetry so that only one fourth of the body need be used for computations, and the mesh is created only around a 50 x 50 x 50 m^3 cube. The coarsest grid comprises of 3, 3 and 4 nodes in x, y and z directions respectively with the internodal distance of 50 m. The second grid with 4, 4 and 5 nodes was obtained by halving the internodal distance to 25 m and the third grid with 6, 6 and 7 nodes was obtained by further halving the internodal distance to 12.5 m. No further refinement of the grid was attempted owing to restrictions on available computer time/storage. It may be stressed here that the number of nodes in any direction in the second (third) grid does not bear the relationship that one would expect after the operation of halving the internodal distance with the corresponding number of nodes in the first (second) grid. This is so because only a single element layer of the host medium is needed around the target for generating the CFEM mesh. Hence the outer one of the two halves of every bounding element side is dropped from the finer mesh as shown in Fig. 5.1.

In order to study the mesh convergence property of the algorithm in some detail, a number of experiments was performed by changing the size, depth of burial, resistivity of the target and the frequency. Table 5.1 presents the results for nine such experiments. These results are plotted in Fig. 5.2.

The first three sets of results correspond to the base model A1 and to the models A2 and A3 derived from A1 by increasing all corresponding distances by factors of 4 and 10, respectively. Thus in A2 (A3) the body is a 400 x 400 x 200 m^3 (1000 x 1000 x 500 m^3), the depth to the top of the

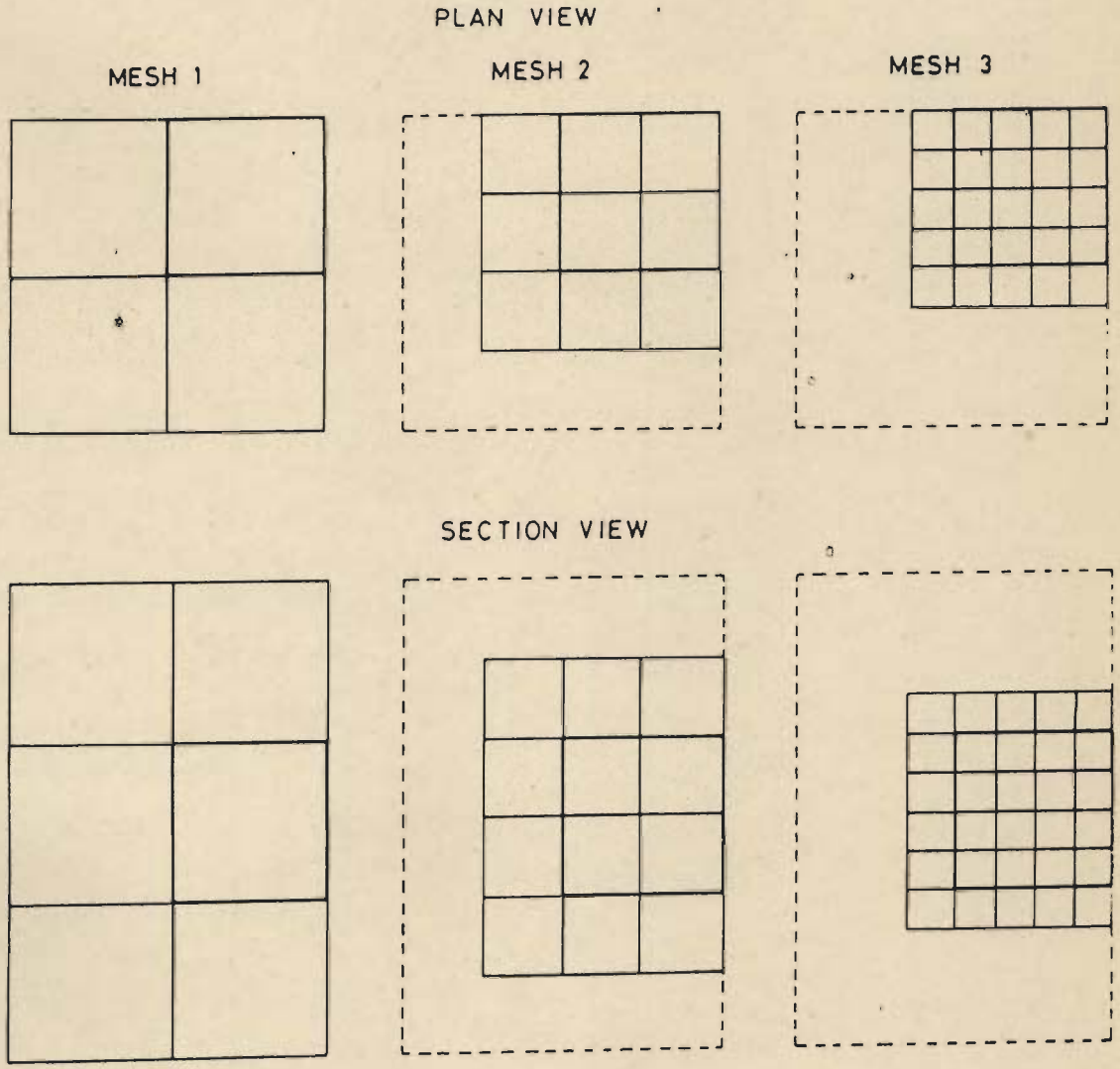

Fig. 5.1 The plan and section views of the three meshes used for convergence studies.

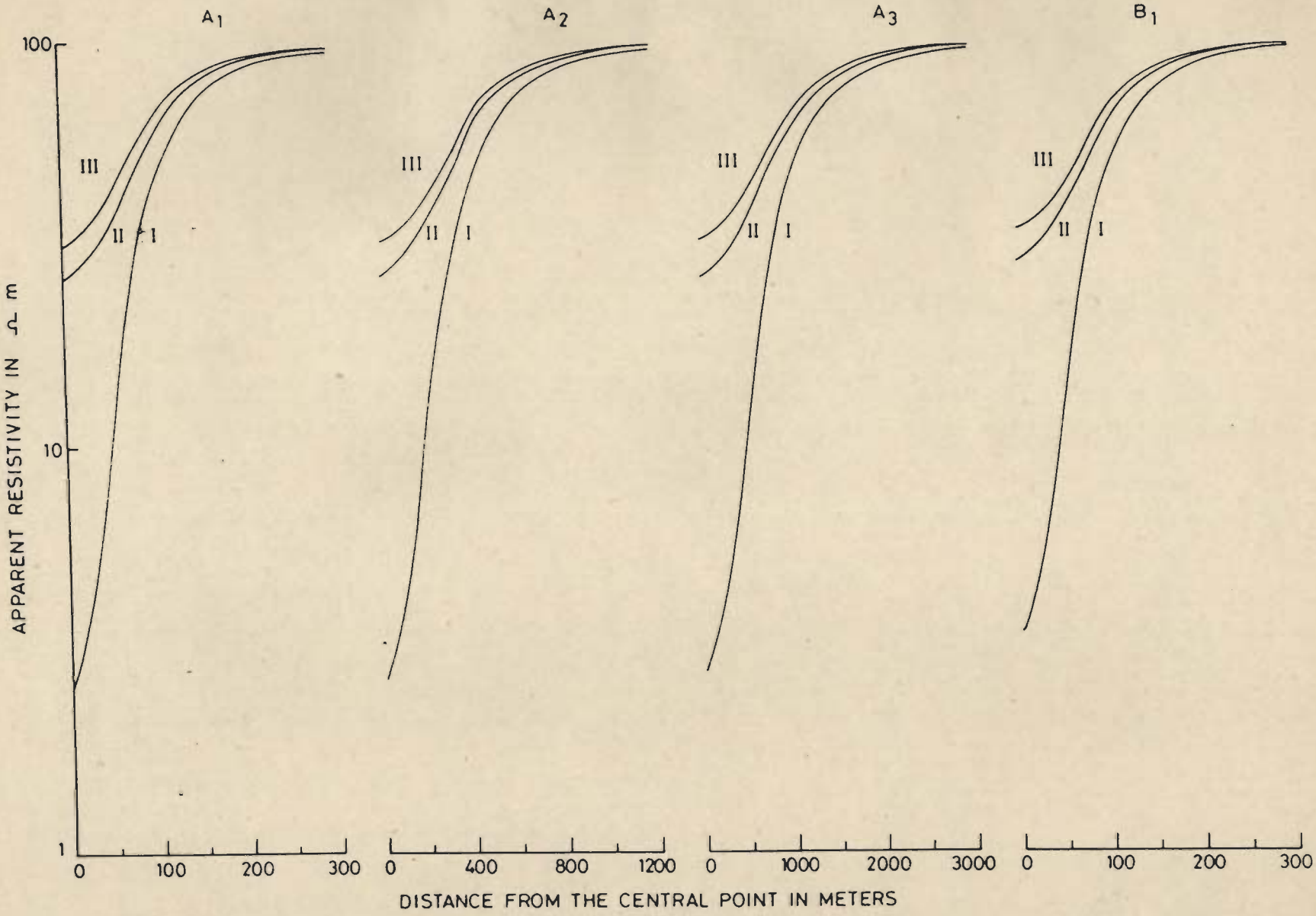

Fig. 5.2(a) The apparent resistivity curves illustrating mesh convergence for models A1, A2, A3 and B1. Curves I, II and III correspond to coarse, medium and fine meshes respectively.

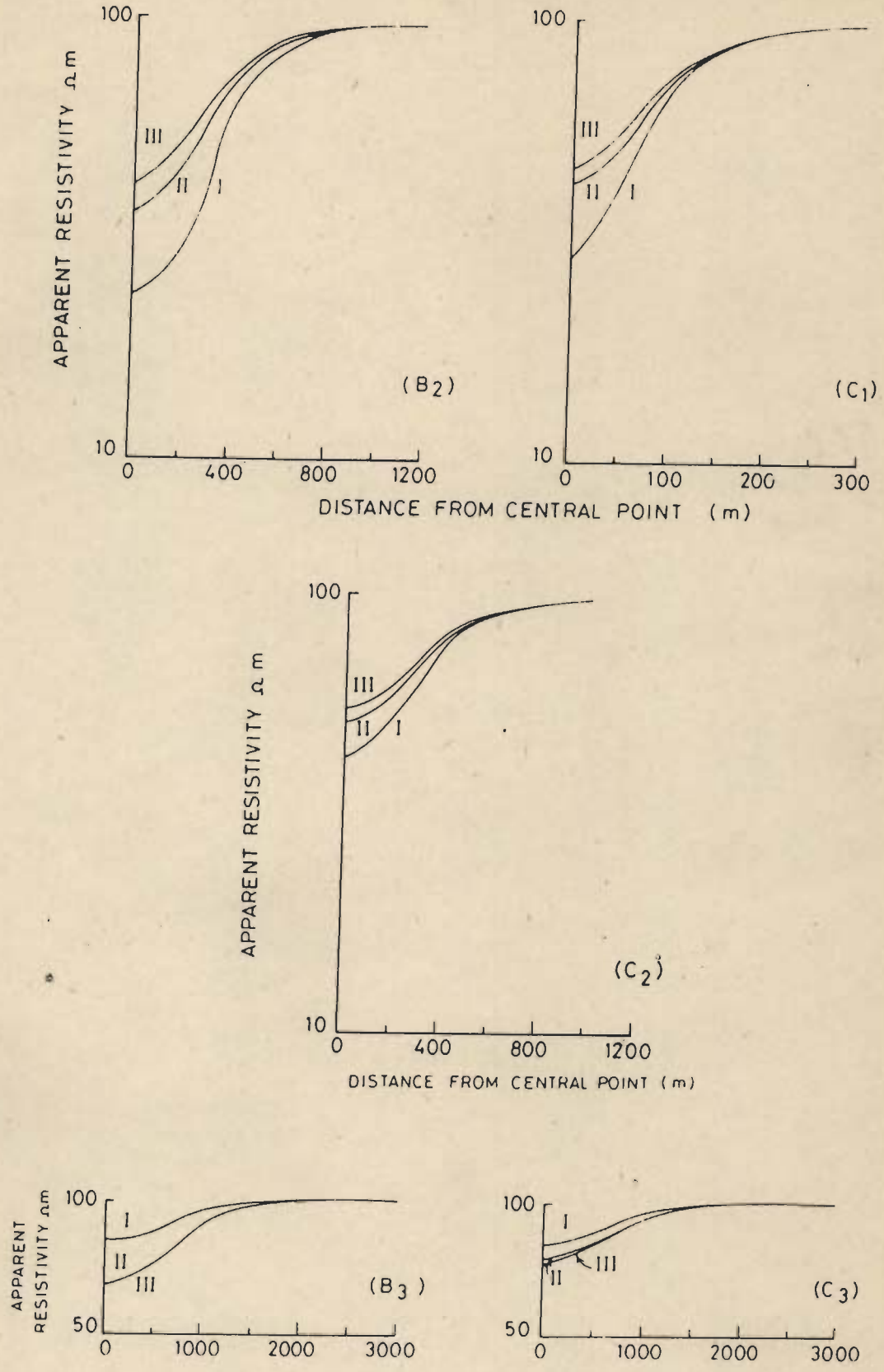

Fig. 5.2(b) The apparent resistivity curves illustrating mesh convergence for models of groups B (B2, C1, C2) and C (B3, C3). Curves I, II, and III correspond to coarse, medium and fine meshes respectively.

Table 5.1 The Apparent Resistivity Profiles (values in Ohm m) Generated by Using the Three Grids for Each of the Nine Models Employed to Study the Mesh Convergence Characteristics of the Algorithm SANGAM

Rec. Pos.	Grid I	II	III	Rec. Pos.	I	II	III	Rec. Pos.	I	II	III
	Model A1				Model A2				Model A3		
-0	2.610	25.86	31.43	0	2.654	26.03	31.62	0	2.747	26.37	32.00
50	11.64	33.92	40.69	200	11.73	34.09	40.87	500	11.91	34.44	41.23
100	45.09	59.82	65.28	400	45.23	59.97	65.42	1000	45.51	60.27	65.70
150	72.58	80.02	83.14	600	72.70	80.12	83.22	1500	72.94	80.33	83.41
200	85.90	89.82	91.42	800	85.99	89.89	91.49	2000	86.16	90.02	91.60
250	92.11	94.36	95.22	1000	92.17	94.41	95.26	2500	92.29	94.50	95.32
300	95.18	96.58	97.11	1200	95.23	96.61	97.13	3000	95.31	96.68	97.19
	Model B1				Model B2				Model B3		
0	3.480	28.41	34.24	0	20.34	36.35	42.34	0	82.29	65.64	65.25
50	13.12	36.55	43.39	200	28.80	45.29	51.39	500	85.21	72.34	72.53
100	47.18	62.04	67.34	400	59.32	69.52	73.50	1000	95.60	89.38	88.87
150	74.32	81.51	84.44	600	81.92	86.13	88.10	1500	100.3	97.80	97.26
200	87.11	90.78	92.24	800	91.63	93.43	94.34	2000	101.1	100.1	99.85
250	92.94	94.99	95.75	1000	95.75	96.61	97.01	2500	100.9	100.6	100.4
300	95.78	97.02	97.47	1200	97.60	98.08	98.30	3000	100.7	100.6	100.5
	Model C1				Model C2				Model C3		
0	29.11	42.37	46.40	0	42.19	50.47	53.91	0	81.48	76.01	74.57
50	42.29	51.36	55.11	200	53.38	58.85	61.94	500	86.21	82.06	80.81
100	69.01	72.79	75.07	400	75.80	77.82	79.54	1000	95.42	93.38	92.46
150	85.52	87.11	88.26	600	89.17	89.89	90.70	1500	99.49	98.72	98.24
200	92.80	93.60	94.15	800	94.83	95.16	95.52	2000	100.5	100.2	100.2
250	96.06	96.51	96.80	1000	97.29	97.46	97.63	2500	100.6	100.5	100.2
300	97.66	97.92	98.10	1200	98.47	98.55	98.64	3000	100.4	100.4	100.2

target is 240 m (600 m) and the points of observation are 0, 200 (500), 400 (1000), 600 (1500), 800 (2000), 1000 (2500) and 1200 (3000) m from the point of intersection of the planes of symmetry. The next three sets of results correspond to models B1, B2 and B3, derived, respectively from models A1, A2 and A3 by changing the frequency from 0.01 Hz to 20 Hz, the corresponding skin depths in the host medium and in the target being 1125 m and 80 m, respectively. Finally, the last three sets of results correspond to models C1, C2 and C3 derived, respectively from models B1, B2 and B3 by changing the target resistivity from 0.5 Ohm m to 5 Ohm m. Thus, for these models the resistivity contrast is 20 while the skin depth in the target is 252 m.

Although the two step grid refinement carried out here is insufficient to prove the mesh convergence characteristics of the algorithm in general, yet the results presented in Table 5.1 do establish unambiguously the converging trend of results of the three grids for all the nine models studied. Further, these results as plotted in Fig. 5.2 reveal following two features :

1. The response at the receiver position 0 is most sensitive to the coarseness of the grid. This sensitivity gets lower and lower as the points of observation get farther and farther.

2. For models A1, A2, A3, B1, B2, C1 and C2, the peak amplitude of anomaly is maximum for the coarsest grid and approaches a lower limiting value as the grid becomes finer. On the other hand, for models B3 and C3, the peak amplitude of anomaly is the least for the coarsest grid and approaches a higher limiting value as the grid becomes finer.

In order to study the relative performance of the grids for different models, the following parameters were heuristically identified and computed from the results presented in Table 5.1.

1. The difference between the corresponding values of apparent resistivity ρ_a obtained by using consecutive grids - $(R_2 - R_1)$ and $(R_3 - R_2)$,

2. The ratio of the corresponding values of ρ_a obtained by using consecutive grids - (R_2/R_1) and (R_3/R_2), and

3. The percentage variation in the values of ρ_a obtained by using grids 1 and 2 from the corresponding values for grid 3 which were treated as the limiting values - $(R_3 - R_1)x100/R_3$, $(R_3 - R_2)x100/R_3$.

Here, R_i represents the apparent resistivity value at an observation point for the ith grid. The outcome of these computations is presented in Table 5.2, while the average values of these parameters for various models are given in Table 5.3.

It is obvious from these that the degree of convergence achieved for various models varies. In fact on the basis of the percentage variation averages presented in column 7 of Table 5.3 the nine models can be classified into three distinct groups - fair convergence group I, good convergence group II and excellent convergence group III. Group I comprises models A1, A2, A3 and B1, group II comprises models B2, C1 and C2 and group III comprises models B3 and C3.

Having thus classified the models, the next step is to identify a set of model parameters that would enable a similar classification. This would highlight the correlation between this set of model parameters and the degree of convergence achieved. Table 5.4 presents the results of such a study which was by no means exhaustive. Two model characteristics that were identified are :

1. The ratio, A, of the skin depth in the host medium (h) to that in

Table 5.2 The Heuristically Identified Parameters (refer to text, p.78) Computed from the Data of Table 5.1, R_i being the Apparent Resistivity Value at a Given receiver Position for the ith Grid

Rec. No.	R_2-R_1	R_3-R_2	R_2/R_1	R_3/R_2	$\frac{\lvert R_3-R_1\rvert}{R_3}$ %	$\frac{\lvert R_3-R_2\rvert}{R_3}$ %	Model
1	2	3	4	5	6	7	8
1	23.25	5.57	9.91	1.22	91.7	17.7	
2	22.28	6.77	2.91	1.20	71.4	16.6	
3	14.73	5.46	1.33	1.09	30.9	8.4	A1
4	7.44	3.12	1.10	1.04	12.7	3.8	
5	3.92	1.6	1.05	1.02	6.0	1.8	
6	2.25	0.86	1.02	1.01	3.3	0.9	
7	1.40	0.53	1.01	1.01	2.0	0.5	
1	23.38	5.59	9.81	1.22	91.6	17.7	
2	22.36	6.78	2.91	1.20	71.3	16.6	
3	14.74	5.45	1.33	1.09	30.9	8.3	A2
4	7.42	3.10	1.10	1.04	12.6	3.7	
5	3.90	1.60	1.05	1.02	6.0	1.7	
6	2.24	0.85	1.02	1.01	3.2	0.9	
7	1.38	0.52	1.01	1.01	2.0	0.5	
1	23.62	5.63	9.60	1.21	91.4	17.6	
2	22.53	6.79	2.89	1.20	71.1	16.5	
3	14.76	5.43	1.32	1.09	30.7	8.3	A3
4	7.39	3.08	1.10	1.04	12.6	3.7	
5	3.86	1.58	1.04	1.02	5.9	1.7	
6	2.21	0.83	1.02	1.01	3.2	0.9	
7	1.37	0.51	1.01	1.01	1.9	0.5	

(Contd.....)

Table 5.2 (Contd.....)

1	2	3	4	5	6	7	8
1	24.93	5.83	8.16	1.21	89.8	17.0	
2	23.43	6.84	2.79	1.19	69.8	15.8	
3	14.86	5.3	1.31	1.09	29.9	7.9	
4	7.19	2.93	1.10	1.04	12.0	3.5	B1
5	3.67	1.46	1.04	1.02	5.6	1.6	
6	2.05	0.76	1.02	1.01	2.9	0.8	
7	1.24	0.45	1.01	1.00	1.7	0.5	
1	16.01	5.99	1.79	1.16	52.0	14.1	
2	16.49	6.10	1.57	1.13	44.0	11.9	
3	10.20	3.98	1.17	1.06	19.3	5.4	
4	4.21	1.97	1.05	1.02	7.0	2.2	B2
5	1.80	0.91	1.02	1.01	2.9	1.0	
6	0.86	0.4	1.01	1.01	1.3	0.4	
7	0.48	0.22	1.00	1.00	0.7	0.2	
1	-16.64	-0.4	0.80	0.99	26.1	0.6	
2	-12.87	0.19	0.85	1.00	17.5	0.3	
3	- 6.22	-0.51	0.93	0.99	7.6	0.6	B3
4	- 2.5	-0.54	0.98	0.99	3.1	0.6	
5	- 1.0	-0.25	0.99	1.00	1.3	0.3	
6	- 0.3	-0.2	1.00	1.00	0.5	0.2	
7	- 0.1	-0.1	1.00	1.00	0.2	0.1	

(Contd.....)

Table 5.2 (Contd.....)

1	2	3	4	5	6	7	8
1	13.26	4.03	1.46	1.10	37.3	8.7	
2	9.07	3.75	1.21	1.07	23.3	6.8	
3	3.78	2.28	1.05	1.03	8.1	3.0	
4	1.59	1.15	1.02	1.01	3.1	1.3	C1
5	0.8	0.55	1.01	1.01	1.4	0.6	
6	0.45	0.29	1.00	1.00	0.8	0.3	
7	0.26	0.18	1.00	1.00	0.4	0.2	
1	8.28	3.44	1.20	1.07	21.7	6.4	
2	5.47	3.09	1.10	1.05	13.8	5.0	
3	2.02	1.72	1.03	1.02	4.7	2.2	
4	0.72	0.81	1.01	1.01	1.7	0.9	C2
5	0.33	0.36	1.00	1.00	0.7	0.4	
6	0.17	0.17	1.00	1.00	0.3	0.2	
7	0.08	0.09	1.00	1.00	0.2	0.1	
1	-5.47	-1.44	0.93	0.98	9.3	1.9	
2	-4.15	-1.25	0.95	0.98	6.7	1.5	
3	-2.04	-0.92	0.98	0.99	3.2	1.0	
4	-0.77	-0.48	0.99	1.00	1.3	0.5	C3
5	-0.3	0.0	1.00	1.00	0.3	0.0	
6	-0.1	-0.3	1.00	1.00	0.1	0.3	
7	0.0	-0.2	1.00	1.00	0.0	0.2	

Table 5.3 The Averages of the Parameters of Table 5.2 in Case of the Nine Models

Model	R_2-R_1	R_3-R_2	R_2/R_1	R_3/R_2	$\frac{\lvert R_3-R_1\rvert}{R_3}$ %	$\frac{\lvert R_3-R_2\rvert}{R_3}$ %
A1	10.7	3.4	2.6	1.1	31.1	7.1
A2	10.8	3.4	2.6	1.1	31.1	7.1
A3	10.8	3.4	2.6	1.1	31.0	7.0
B1	11.1	3.4	2.3	1.1	30.2	6.7
B2	7.1	2.8	1.2	1.1	18.3	5.0
B3	5.6	0.3	0.94	1.0	8.4	0.4
C1	4.1	1.7	1.1	1.0	10.6	3.0
C2	2.5	1.4	1.0	1.0	6.2	2.2
C3	1.8	0.6	0.98	0.99	3.0	0.8

Table 5.4 The Characteristic Model Parameters in Case of the Nine Models

Model	Skin-depth in host (h)	Skin-depth in target (t)	Thickness of target (s)	h/t = A	Truncated (1+s/t) = B	A/B
A1	50300	3557	50	14.1	1	14.1
A2	50300	3557	200	14.1	1	14.1
A3	50300	3557	500	14.1	1	14.1
B1	1125	80	50	14.1	1	14.1
B2	1125	80	200	14.1	3	4.7
B3	1125	80	500	14.1	7	2.0
C1	1125	252	50	4.5	1	4.5
C2	1125	252	200	4.5	1	4.5
C3	1125	252	500	4.5	2	2.2

the target (t), and

2. The ratio of the thickness of the target (s) to the skin depth in the target. This ratio was employed to define the second parameter B as the truncated integer value of (1 + s/t).

The ratio (A/B) given in column 7 of Table 5.4 satisfies the classification given earlier. Smaller the value of A/B, better the convergence, hence this ratio can be used as a guideline while creating the mesh to ensure reasonably convergent results. It may be emphasized here that since the study is heuristic and by no means exhaustive this ratio should only be treated as a thumb-rule and convergence studies must be carried out, wherever possible.

The mesh convergence study presented here was carried out for a uniform mesh. However, a judicious mesh for any model will be, in general, non-uniform. It will be fine towards the boundary of the target and coarser within. Further, the mesh must be finer for high frequency cases. The optimal element size is controlled by the skin depth in the target. It is believed that the mesh convergence characteristics of the algorithm will be upheld in these cases also.

5.3 STRIKE-LENGTH CONVERGENCE STUDY

For any 3-D field modelling algorithm, an important check for accuracy and consistency is that for any elongated body, the results for increasing strike-length should converge to corresponding 2-D results. For SANGAM, the first model chosen for such a study was that used by Ting and Hohmann (1981, Fig. 8) who presented the results of a similar study they had carried out for their 3-D Integral equation algorithm. The model comprises a cuboid target of vertical cross-section 1000 x 2000 m^2 and resistivity 5 Ohm m buried in a half-space of resistivity 100 Ohm m, at a depth of 500 m. The plane wave

frequency was taken as 0.1 Hz. Apparent resistivity was computed along a profile parallel to the x-axis for four values of strike length 4, 8, 12 and 16 km. The results are plotted in Fig. 5.3(A). It may be stressed here that these show better convergence than obtained by Ting and Hohmann (1981).

The second model was derived from the first by changing the plane-wave frequency from 0.1 Hz to 0.01 Hz. The corresponding results are plotted in Fig. 5.3(B). Finally, the third model was derived from the second by changing the target resistivity from 5 Ohm m to 0.5 Ohm m. The results for this model are plotted in Fig. 5.3(C). The results of Fig. 5.3 are replotted in Fig. 5.4 as apparent resistivity vs the strike length for various observation points along the profile. A look at this figure reveals that the convergence of results is not monotonous for most of the observation points in all three cases.

It may be emphasized here that the mesh used for the three models was the same, the element side measuring between 500 - 1000 m. In order to check the degree of coarseness of the mesh, the parameters A/B were computed for all models and were found to be 4.47, 4.47 and 14.1. This suggested that the first two models lied in the second group while the third model lied in the first group. Hence, the average percentage variation would be 10% for the first two models and 30% for the third. These values were based on the assumption that the mesh used corresponded to the coarsest. Since 30% was an unacceptably high deviation from the convergence limits, model 3 was further studied using three different meshes. The element side of these second, third and fourth meshes respectively varied between 200 - 1000 m, 250 - 500 m and 150 - 500 m. As expected, with these grids, strike-length could not be extended upto 20 km as was done in case of first mesh. In fact, for second, third and fourth meshes the sets of strike lengths for which

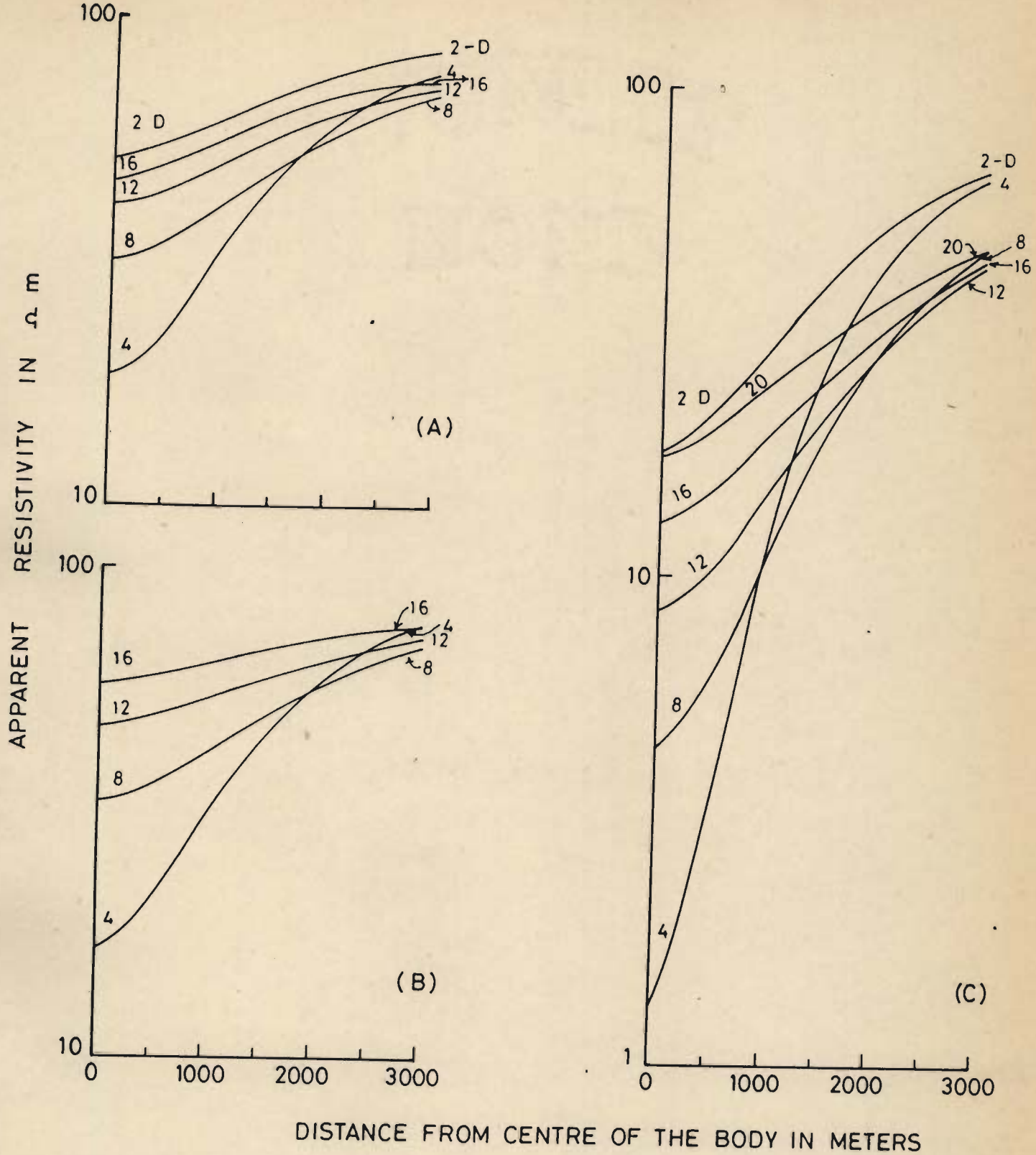

Fig. 5.3 The apparent resistivity curves for various strike-lengths (in km.) for the three models studied. The mesh used in all these cases had element side measuring between 500 - 1000 m.

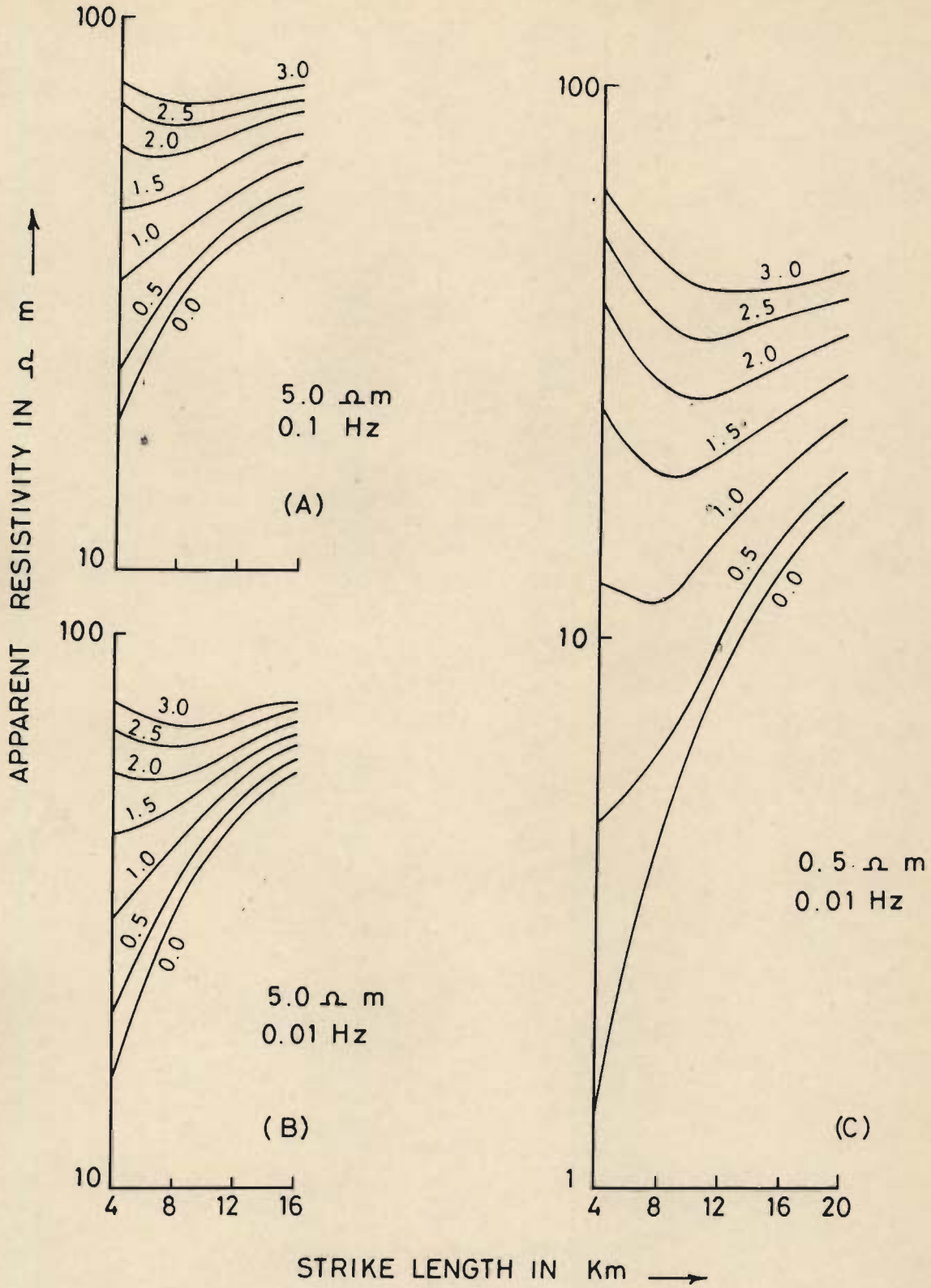

Fig. 5.4 The apparent resistivity vs strike-length curves for various receiver positions (in km. from the central point) for the three models studied. The mesh used in all these cases at element side measuring between 500 - 1000 m.

results were computed were i) 1, 1.5, 2, 2.5, 3, 3.5, 4, 5, 6 km, ii) 1, 2, 4, 6 km and iii) 1, 1.5, 2, 2.5, 3, 3.5 km. For comparison, the results for the first mesh were also computed for strike lengths 1, 2, 3, 5 and 6 km. All these are plotted in Fig. 5.5 and again in Fig. 5.6 where the format of Fig. 5.4 has been used.

Figure 5.6(c) shows the anomalous oscillatory behaviour of the first mesh results in the initial parts of the curves for observation points 0.0 and 0.5 km. However, such a behaviour is absent from the corresponding results for the second, third and fourth meshes. Hence, these oscillations must be due to coarseness of the mesh. Another feature that emerges is that for no observation point the convergence is monotonous. Rather, there exists, for each observation point, a strike length, S_m, where the apparent resistivity value is minimum. For any model, S_m is found to shift to the right as the observation point recedes from the centre. Thus, S_m has a minimum value at the central point and it gradually increases at points farther away. S_m at a fixed point on the profile is also found to vary with the model. For the three models it gradually increases from model 1 to model 3.

A correlation between S_m and the model parameters can, possibly, be discovered empirically. The rigorous study required for this purpose was not taken up because of time constraints. The product of resistivity contrast value and skin depth in the host medium, which is 31806, 100600 and 100600 m, respectively for models 1, 2 and 3, increases from model 1 to 3 as does S_m. This correlation suggests an interesting possibility that S_m may, in some way, depend on this product.

5.4 NO-CONTRAST CASE

Another check made on the algorithm SANGAM was to verify the convergence of the buried target response to that of a half-space as the

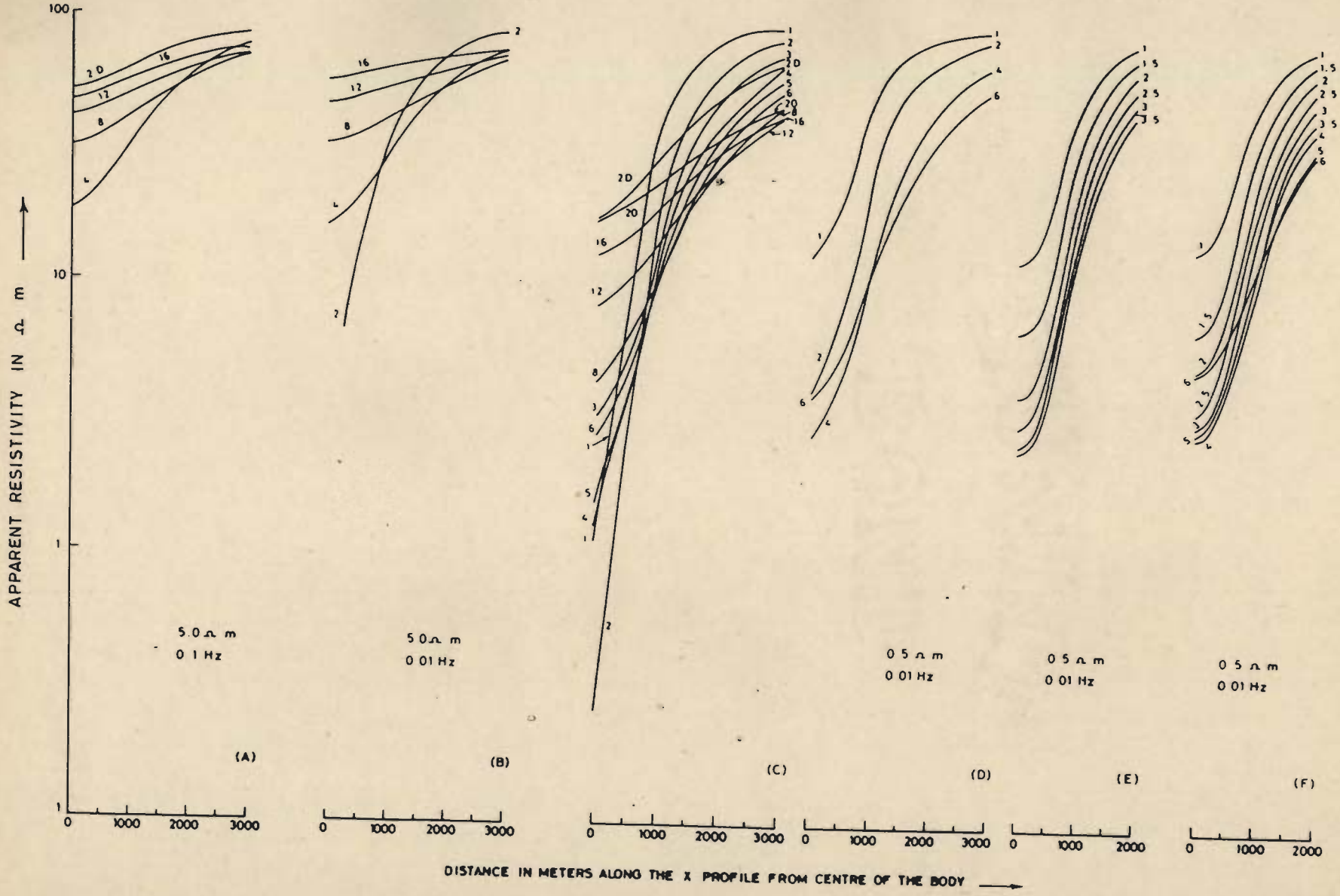

Fig. 5.5 The apparent resistivity curves for various strike-lengths (in km.) for the three models studied. The mesh element side measured between 500 - 1000 m in case of A,B and C, between 250-500 m, 150-500 m and 200-1000 m in case of D,E and F respectively.

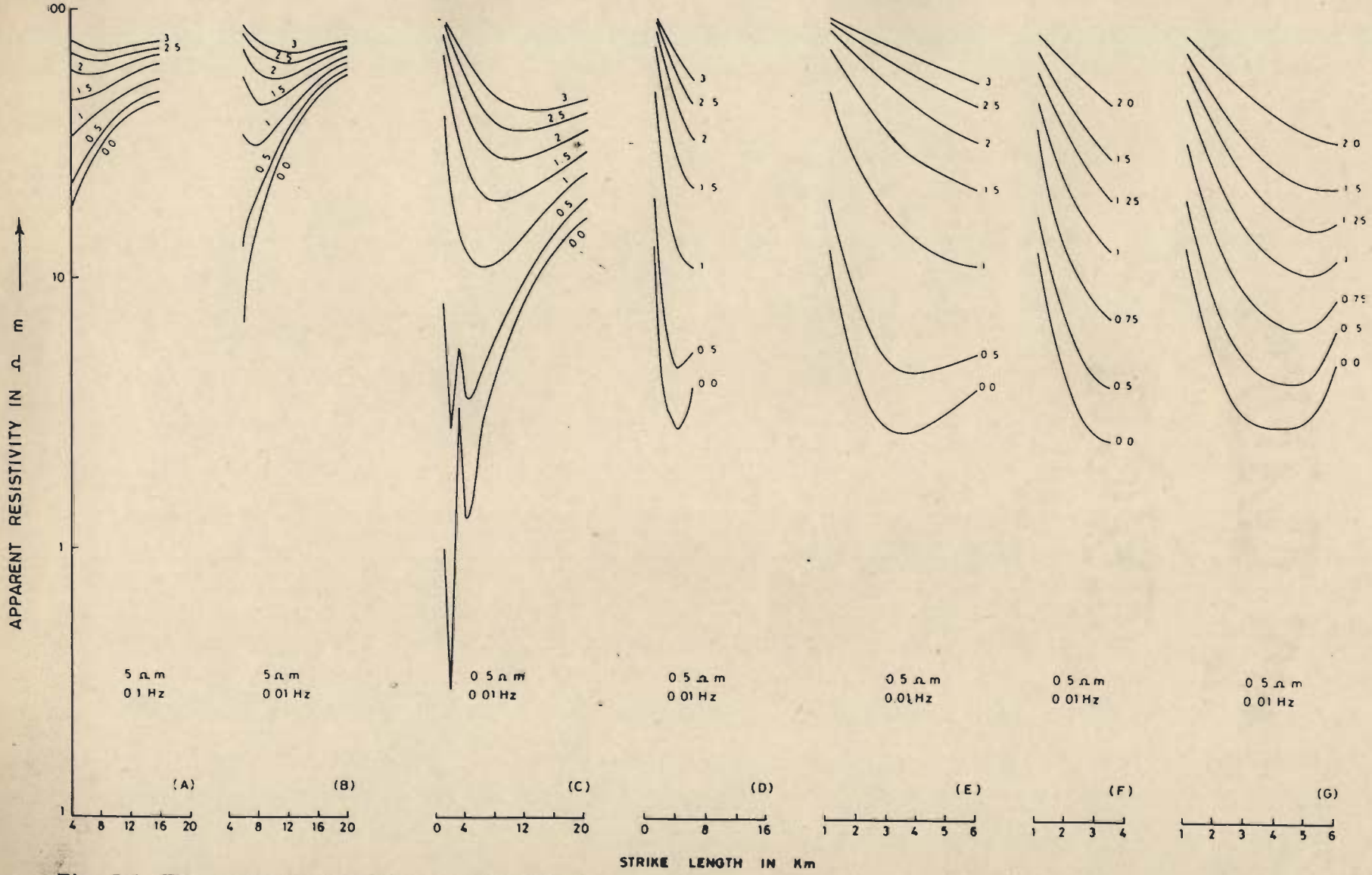

Fig. 5.6 The apparent resistivity vs strike-length curves for various receiver positions (in km. from the central point) for the three models studied. The mesh element side measured between 500-1000 m in case of A,B and C and between 250-500 m, 150-500 m and 200-1000 m in case of E,F and G respectively. The set D is same as set E but on the same scale as used for sets A, B and C.

resistivity contrast was reduced to 1. The 1000 x 1000 x 2000 m^3 cuboid target used for this study had a resistivity of 99 Ohm m and it was buried at a depth of 500 m in a half-space of resistivity 100 Ohm m. The plane wave frequency used was 0.01 Hz. The apparent resistivities were computed at 11 points along a profile parallel to the x-axis, starting from the point of intersection of the two planes of symmetry - 0, 125, 250, 375, 500, 750, 1000, 1250, 1500, 1750 and 2000 m. The maximum deviation of apparent resistivity from host resistivity was 0.31% while the average deviation was 0.2%.

5.5 THE RECIPROCITY TEST

An important test for consistency of an EM field modelling algorithm is the reciprocity test. Accordingly, if the source and receiver positions were to be interchanged, the z-component of the secondary field should remain unchanged. It may be stated here that for this test to hold, the receiver and source should be horizontally coplanar. For testing SANGAM, the model chosen was the one subsequently used for the time-domain studies. This model comprises a 20 x 400 x 120 m^3 cuboid target of resistivity 0.4 Ohm m, buried in a half-space at a depth of 40 m. The source was a vertical magnetic dipole and the frequency of operation equal to 1 Hz. Two cases were studied with host resistivities 100 Ohm m and 300 Ohm m, respectively. For the latter case, two meshes were used - first being the same as for the former while the second was generated by halving the internodal distances of the first mesh. The percentage deviation in the real and imaginary parts of the z-component of the magnetic field (given in brackets in the following table) from the respective mean values for two sets of source-receiver positions are given below :

Field Component	Host resistivity	100 Ohm m		300 Ohm m Coarse mesh		300 Ohm m Fine Mesh	
Re (H_z)		$\begin{bmatrix} -4.2E-15 \\ -4.3E-15 \end{bmatrix}$	2%	$\begin{bmatrix} -8.9E-16 \\ -9.0E-16 \end{bmatrix}$	1%	$\begin{bmatrix} -1.2E-15 \\ -1.2E-15 \end{bmatrix}$	0%
Im (H_z)		$\begin{bmatrix} -1.3E-12 \\ -1.3E-12 \end{bmatrix}$	0%	$\begin{bmatrix} -7.1E-13 \\ -7.1E-13 \end{bmatrix}$	0%	$\begin{bmatrix} -9.4E-13 \\ -9.4E-13 \end{bmatrix}$	0%

5.6 COMPARISON OF SANGAM RESULTS WITH THE RESULTS FROM OTHER SOURCES

A number of models for which results had already been obtained using other algorithms was studied using SANGAM. The models were 1, 3, 4, 5, 6 and 7 given in Table 4.1 of chapter-IV, where the computer run-times for these models were compared with those for HYBRIDB and HYBRIDC. For models 1, 3 and 4, numerical values of the results from the Hybrid Code HYB3D runs on CDC-7600 were available to the author which enabled a term by term comparison.

For model 1, maximum deviation of SANGAM results from the corresponding HYB3D results was less than 0.1%.

For model 3, of the 24 possible comparisons of the corresponding real and imaginary parts of the field components H_x, H_z and E_y from the two programs, in the 4 worst cases the percentage deviations were 22, 5, 2 and 1%. For the remaining 20 comparisons the average percentage deviation was 0.3%. Since the two codes were run on different machines, having different round-off and accuracy characteristics, it may be safely presumed that on average there will be a constant deviation, on that account. However, this average deviation shall result in higher percentage deviation for lower absolute

values. This indeed was the case : large percentage deviation cases had absolute values in the range 10^{-17} - 10^{-16} against other values that ranged between 10^{-13} - 10^{-16}.

For model 4, of the 48 comparisons made, only 2 had percentage deviations greater than 10% (38, 13), 6 between 5-10% (9, 8, 7.4, 6.8, 5.8, 5.8), 12 between 1-5% (4.4, 4, 4, 3.2, 2.8, 2, 2, 2, 2, 2, 1.7, 1.6) and the rest less than 1% averaging to 0.40%. Here again, as for model 3, larger deviations corresponded to smaller absolute values.

The SANGAM results for model 5 were compared with the corresponding 3-D integral equation algorithm and 2-D results in Fig. 5.7. This figure was obtained by posting the SANGAM results on fig. 6 of the paper by Wannamaker et.al. (1984 a). There seems to be greater deviation in SANGAM results for the x-component of the magnetic field.

Finally, the SANGAM results for models 6 and 7 were compared with the corresponding integral equation algorithm, HYB3D and 2-D results in Figs. 5.8 and 5.9. These figures were again obtained by posting the SANGAM results on Figs. 4.4 and 4.5 of the thesis by Mozeley (1982). Figures 5.8 and 5.9 highlight the improvement effected in SANGAM results over the HYB3D results. The former, unlike the latter, compares well with the integral equation results.

5.7 PRELIMINARY TIME-DOMAIN STUDIES

Once the algorithm SANGAM was validated, the transform routines SINTRN and COSTRN were rigorously tested before being incorporated in the time domain algorithm SAMAYA. First, the results from the transform routine SINTRN for the layered earth frequency domain responses were compared with the corresponding results obtained from the direct time domain layered earth algorithm RECTEM developed by A.P. Raiche. The percentage

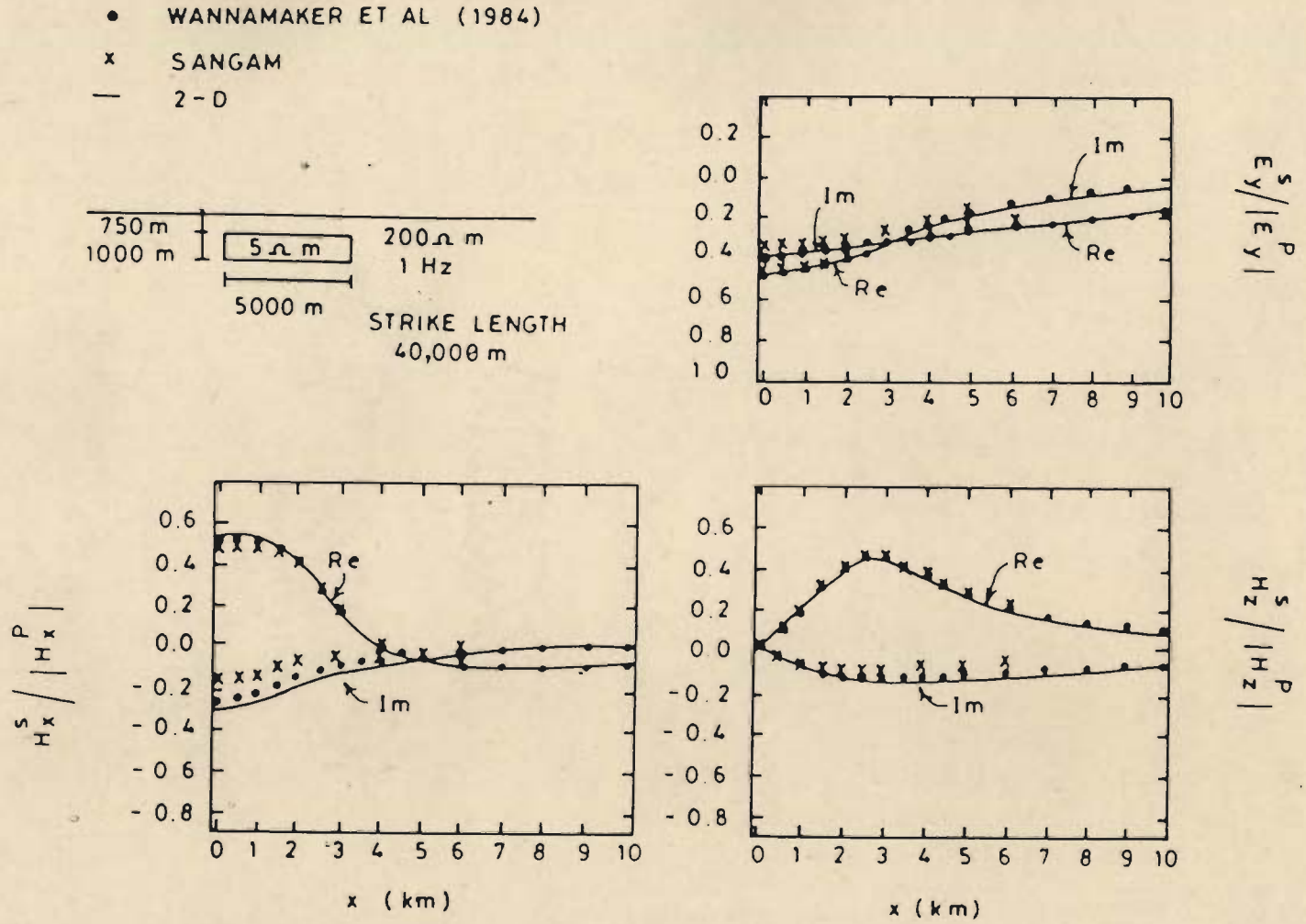

Fig. 5.7 Comparison of SANGAM results for the model 5 with the corresponding results presented in Fig. 6 of Wannamaker et.al. (1984).

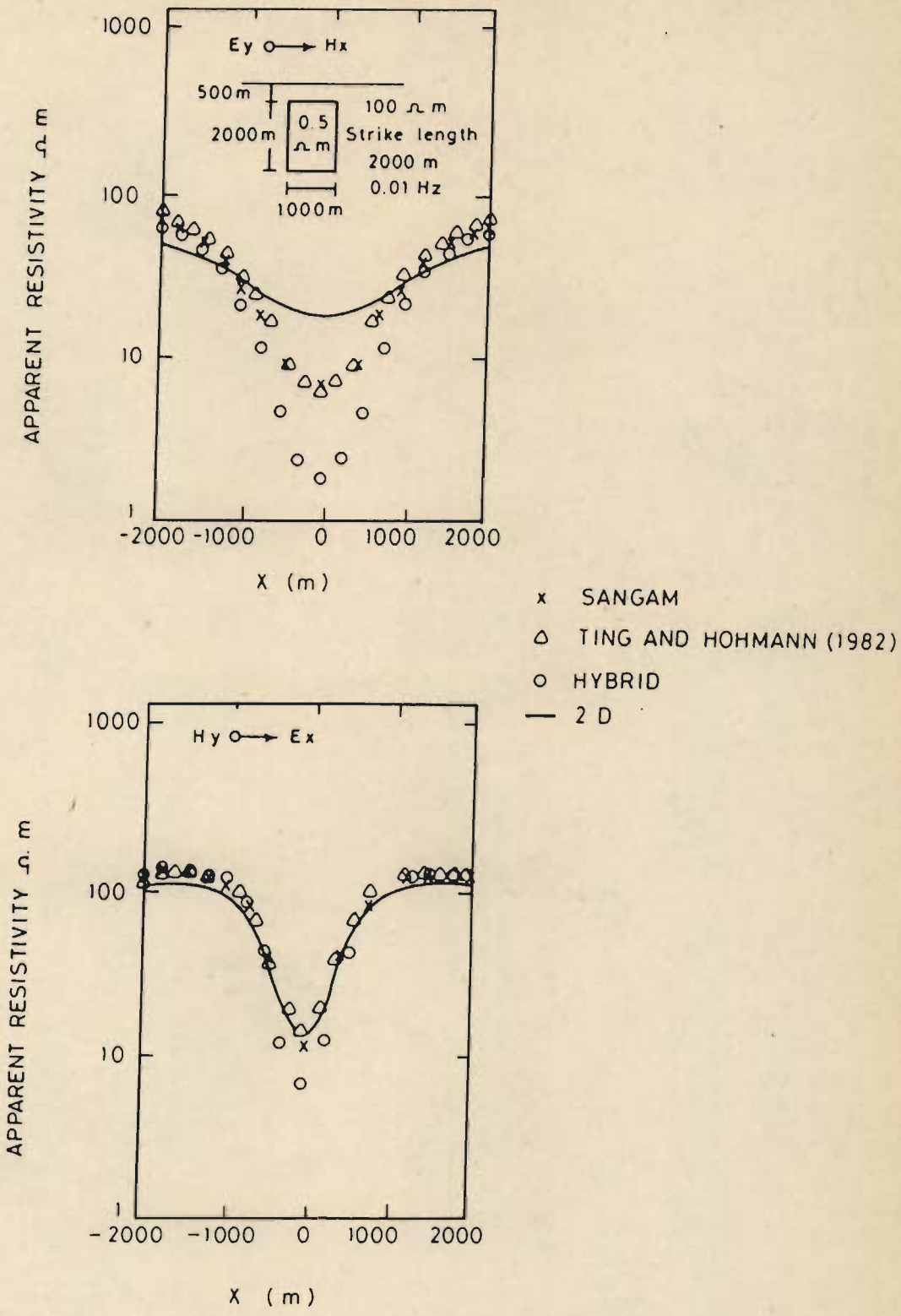

Fig. 5.8 Comparison of SANGAM results for the model 6 with the corresponding results presented in Fig. 4.4 of Mozley (1982).

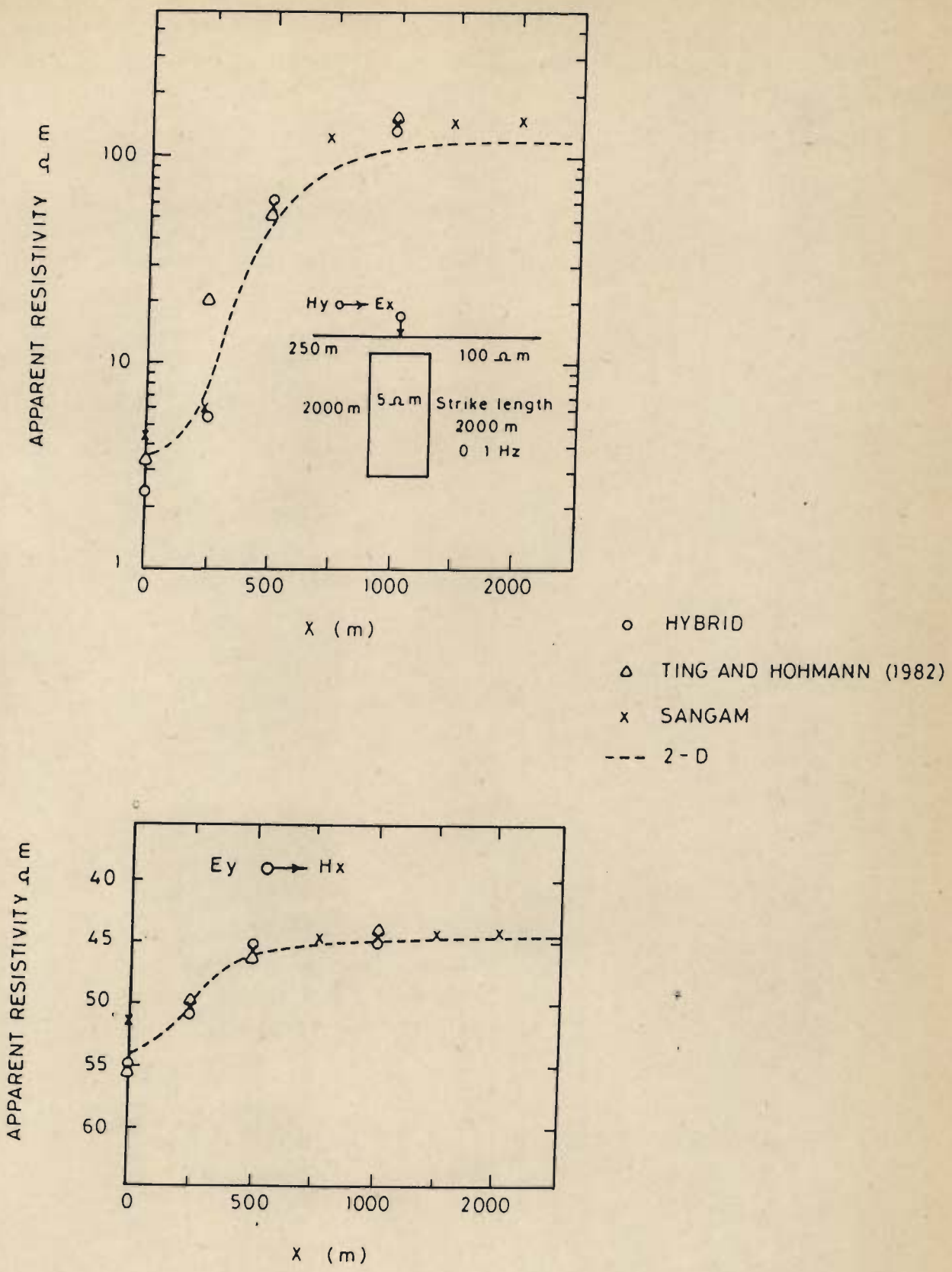

Fig. 5.9 Comparison of SANGAM results for the model 7 with the corresponding results presented in Fig. 4.5 of Mozley (1982).

variation in the two sets of results was less than 0.1% for early times (<5 mS) and did not exceed 1% at later times. It was observed that for low resistivity values, the results were in better agreement than those for high resistivity values. Then, a comparison was made between the results obtained from Sine-transforming imaginary part, using SINTRN, and Cosine-transforming real part, using COSTRN, of the frequency domain values of the x and z-components of the field of magnetic induction. The agreement was excellent, percentage variation being less than 0.1%.

Next, a study was made to identify the shortest frequency range and the minimum number of freqencies per decade for which the frequency responses must be computed in order to obtain stable and accurate results after transformation. For this purpose the base model chosen was an elongated 20 x 400 x 120 m^3 cuboid, buried in a half-space at a depth of 40 m. Six cases were studied by changing the target and host resistivities : 0.4 or 5 Ohm m for the former, and 300, 100 or 30 Ohm m for the latter. The six cases, thus formed, were arranged in decreasing order of resistivity contrasts, 750, 250, 75, 60, 20 and 6 respectively. The observation points on the profile parallel to x-axis and passing through the centre of the strike were -110, -90, -70, -50, -30, -20, -10, 0, 10, 20, 30, 50, 70, 90 and 110 m from the centre. The rectangular loop source, 300 x 600 m^2, was placed symmetrically about the profile with nearest side being 120 m from the centre. The current ramp had a duration of 0.2 mS. The model is illustrated in Fig. 5.10.

Figure 5.11 presented the logarithmic plots of imaginary parts of x- and z-components of both primary and secondary fields for a frequency range 10^{-4} - 10^{6} Hz and for two cases with resistivity contrast of 750 and 250. These plots suggests that the frequency range 10^{-2} - 10^{6} encompasses all the salient features of various curves. It may be stated here that this is a

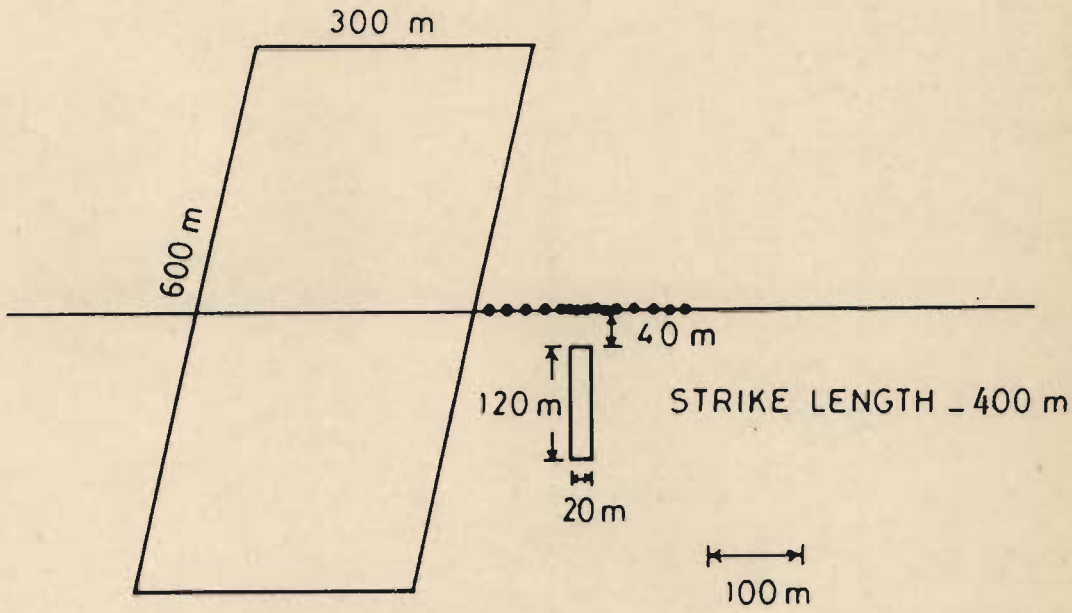

Fig. 5.10 The schematic diagram showing positions of source loop, target and receivers for various models used in time-domain studies.

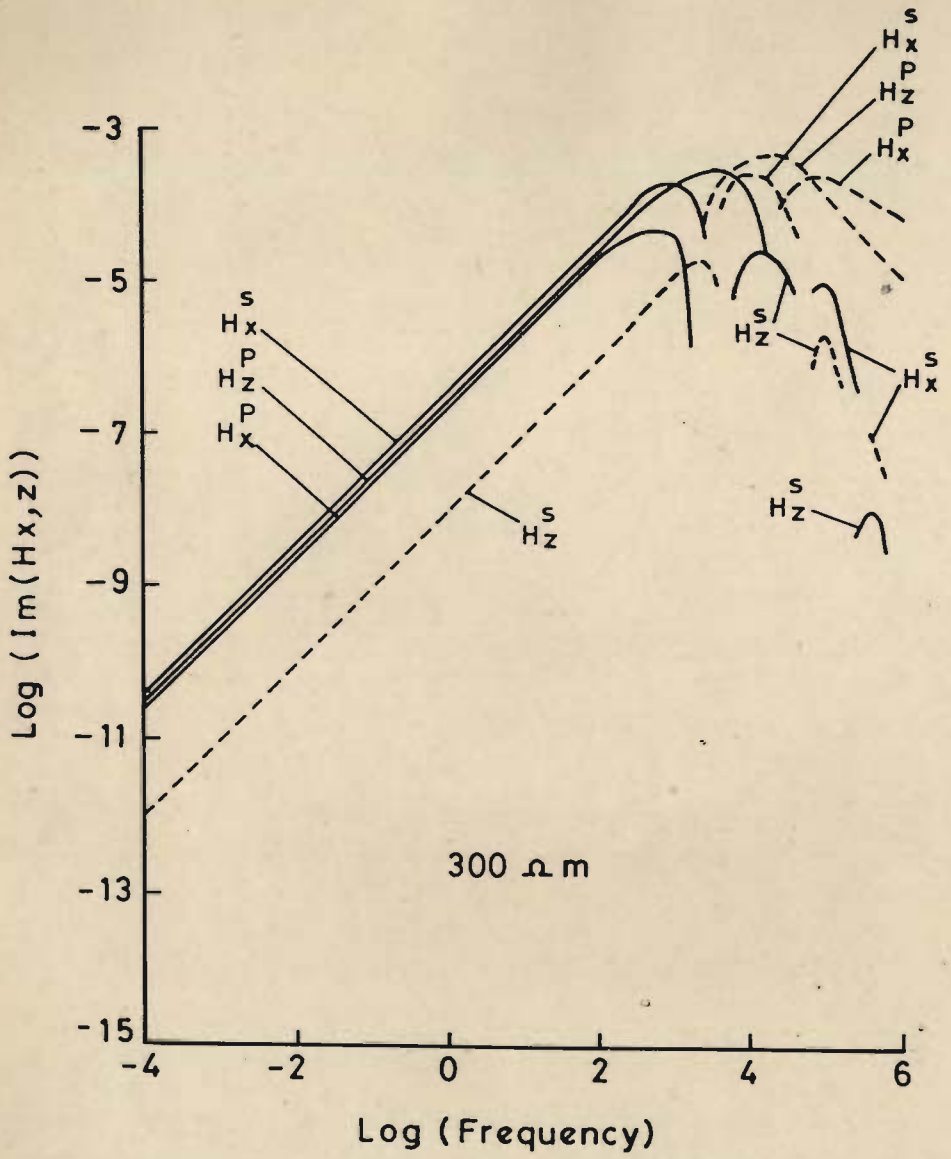

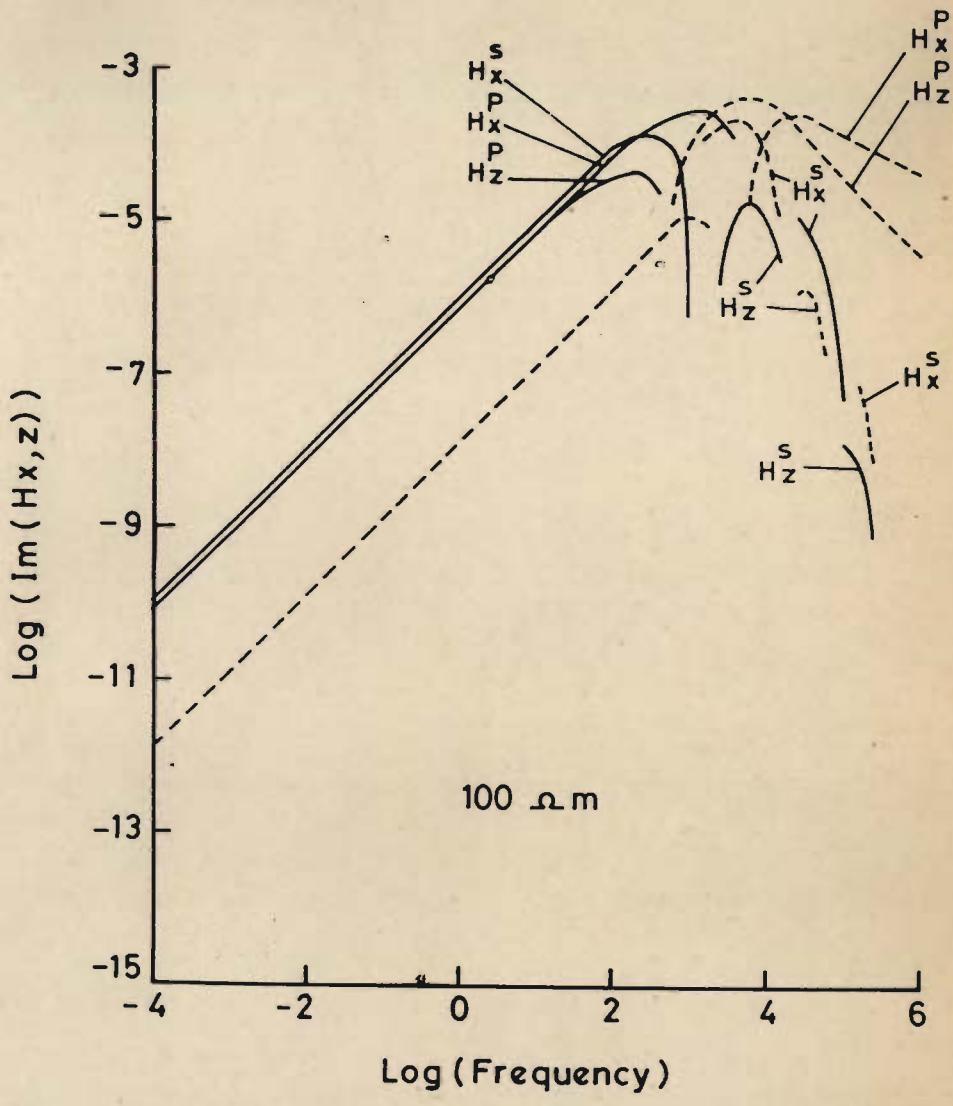

Fig. 5.11(a) The logarithmic plots of imaginary parts of the x- and z-components of the primary and secondary magnetic field for two resistivity contrasts 750 and 250 and for the receiver positioned at the centre.

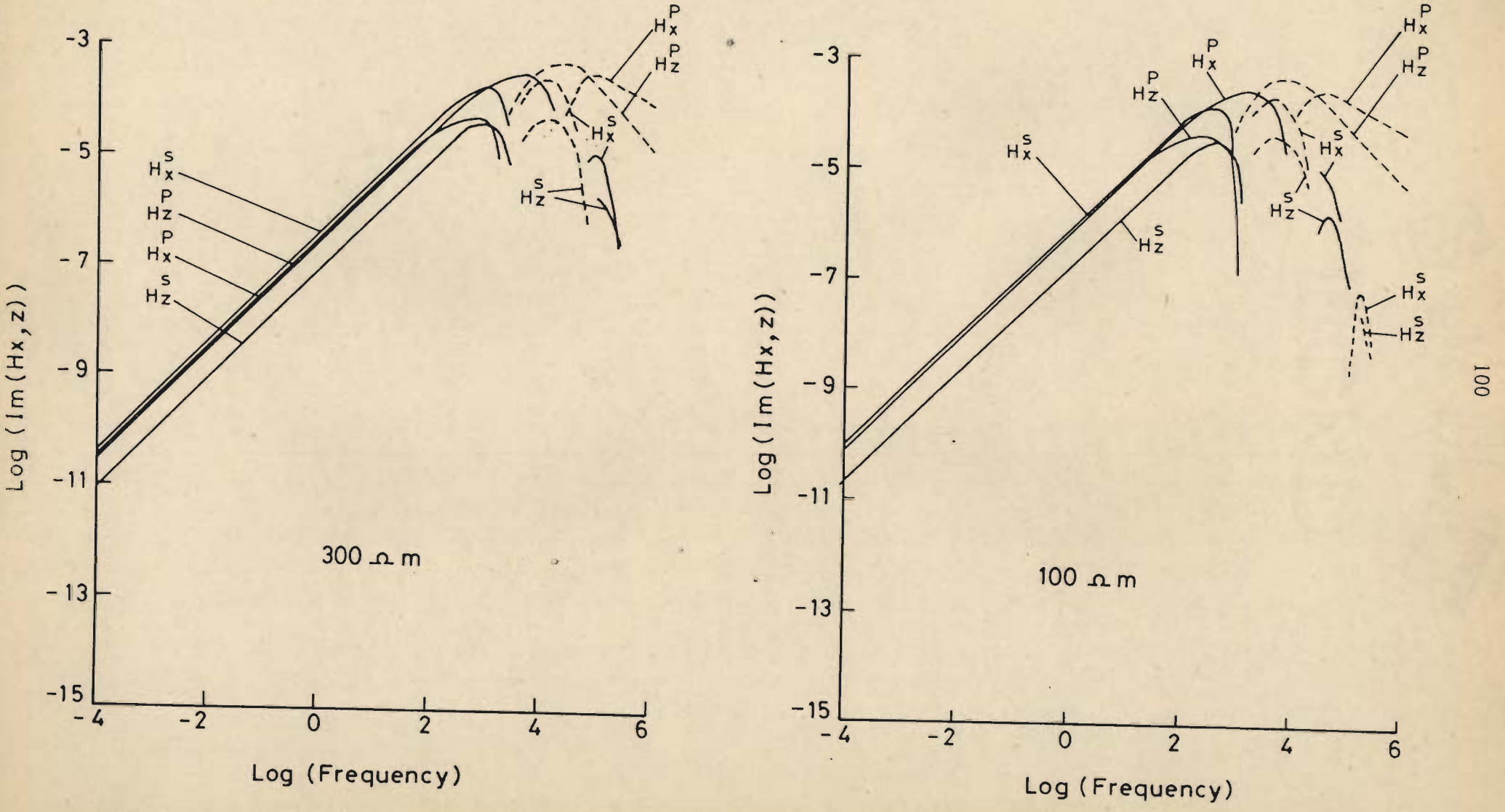

Fig. 5.11(b) The logarithmic plots of imaginary parts of the x- and z-components of the primary and secondary magnetic field for two resistivity contrasts 750 and 250 and for the receiver positioned -10 m from the centre.

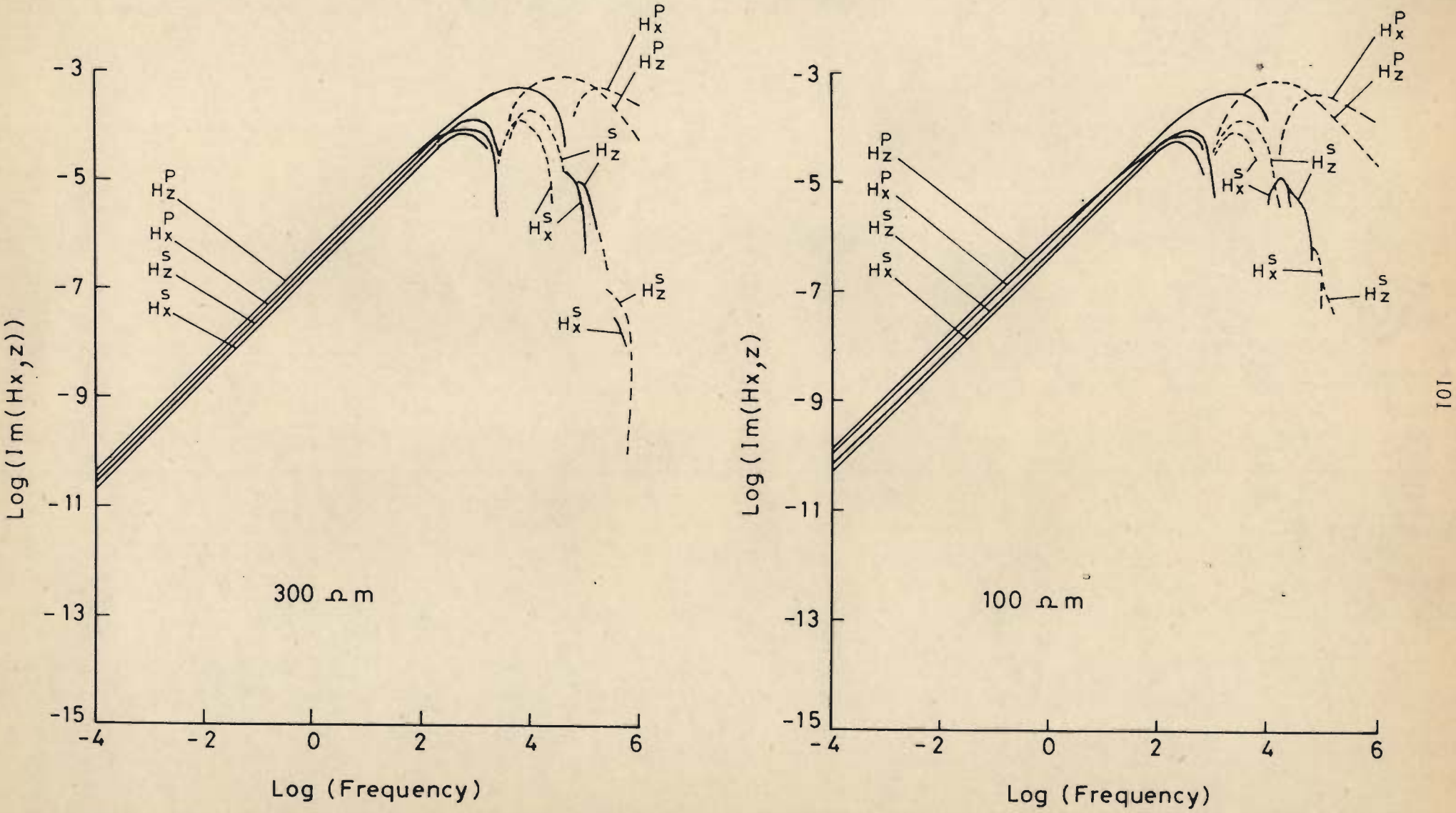

Fig. 5.11(c) The algorithmic plots of imaginary parts of the x- and z-components of the primary and secondary magnetic field for two resistivity contrasts 750 and 250 and for the receiver positioned -50 m from the centre.

liberal estimate of the range. In general, for low resistivity contrast a shorter range would suffice. In fact, in the worst example of the resistivity contrast equal to 750, the transformed early time (< 5 mS) results for primary fields obtained by using a frequency range 10-10^5 Hz were in agreement upto four significant digits with the corresponding results obtained using the wider frequency range. However, for secondary fields, there existed only one or two digit agreement. Similarly, for the resistivity contrast of 250, a three significant digit agreement was found even for 10^2 - 10^4 Hz range, for very early times (< 1 mS) in the case of primary fields and upto one or two digit agreement in the case of secondary fields. Since this study was rather limited, the wider range 10^{-2} - 10^6 Hz was chosen for subsequent studies.

In order to identify the minimum number of frequencies per decade, SAMAYA runs were made for the six cases with 10, 6, 5 and 4 frequencies per decade. Figure 5.12 presents the plots of x-component of the secondary fields for four receiver positions -110, -50, -10 and 0 m in case of resistivity contrast equal to 250. In all cases there was a four significant digit agreement between the plots for the cases of 6 and 10 frequencies per decade. Hence these were treated as standard curves. The curves for 5 frequencies per decade oscillate, mildly around the standard curves, the magnitude of oscillation increasing towards centre of the target. The curves for 4 frequencies per decade oscillate wildly around the standard curves. For receiver positions of -10 and 0 m the values change signs during the oscillations. On the basis of this analysis, 6 frequencies per decade were used in subsequent studies. Thus, in all 49 frequency responses were computed for each time domain profile. It may be added here that for low contrasts the number of frequencies less than six may suffice.

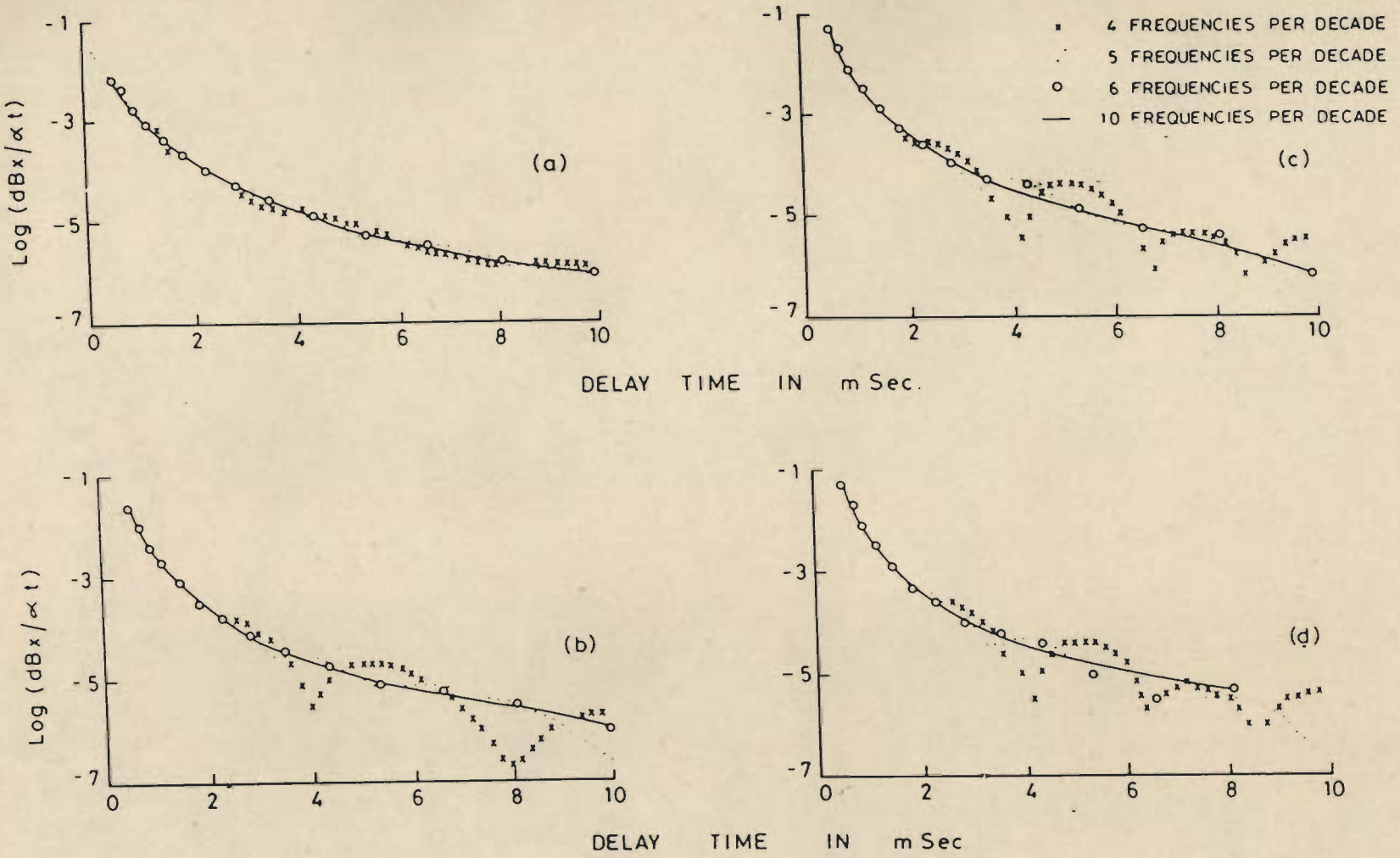

Fig. 5.12 The logrithmic decay curves for dB_x/dt for various number of frequencies per decade. For the four sets A, B, C and D the receiver is situated at -110, -50, -10 and 0 m respectively from the centre.

5.8 COMPARISON OF SAMAYA RESULTS WITH THE RESULTS FROM OTHER SOURCES

Two sets of results, that were generated by using different time-domain algorithms, were available to the author for all the six cases of the base model, discussed in the previous section. The first set was generated by San Filipo by using the 3-D time domain integral equation algorithm (vide San Filipo et.al. 1985 a). These results were computed for delay times upto 10 mS. The second set was generated by K.H. Lee (1986) by using his time-domain version, SHEET, of the 3-D thin sheet frequency domain algorithm developed by Weidelt (1981). These results were computed for delay times upto 50 mS. Besides these two sets, a third set was generated by the author by using the algorithm OZPLAT adapted by Gallagher (1985) from the algorithm PLATE of the University of Toronto (vide Dyck et.al. (1981)). This algorithm generates the time domain response of a plate like structure in free space.

The comparative plots of the results from SAMAYA and the corresponding results in each one of the three sets are given in Figs. 5.13-5.18. The symbols KHL, SAN, OZP and HYB used in the keys to the plots stand for the result sets generated, respectively, by K.H. Lee, San Filipo, the algorithm OZPLAT and by using the algorithm SAMAYA. Further, the six character title of each plot can be deciphered using the table given below :

Character number	Possible alternatives	Meaning
1	L, H	Target resistivity in Ohm m (H = 5.0 ; L = 0.4)
2 - 4	300, 100, 030	Host resistivity in Ohm m
5	X, Z	Component of dB/dt
6	1,2,3,4,5,6	Receiver positions -110, -90, -70, -50, -30 and -10 m respectively from the centre

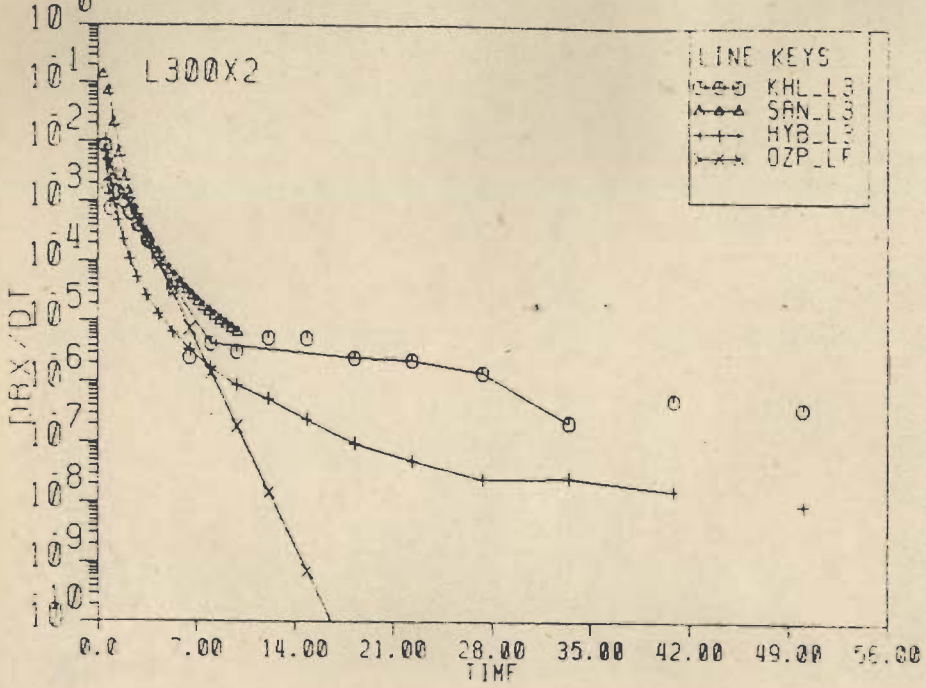

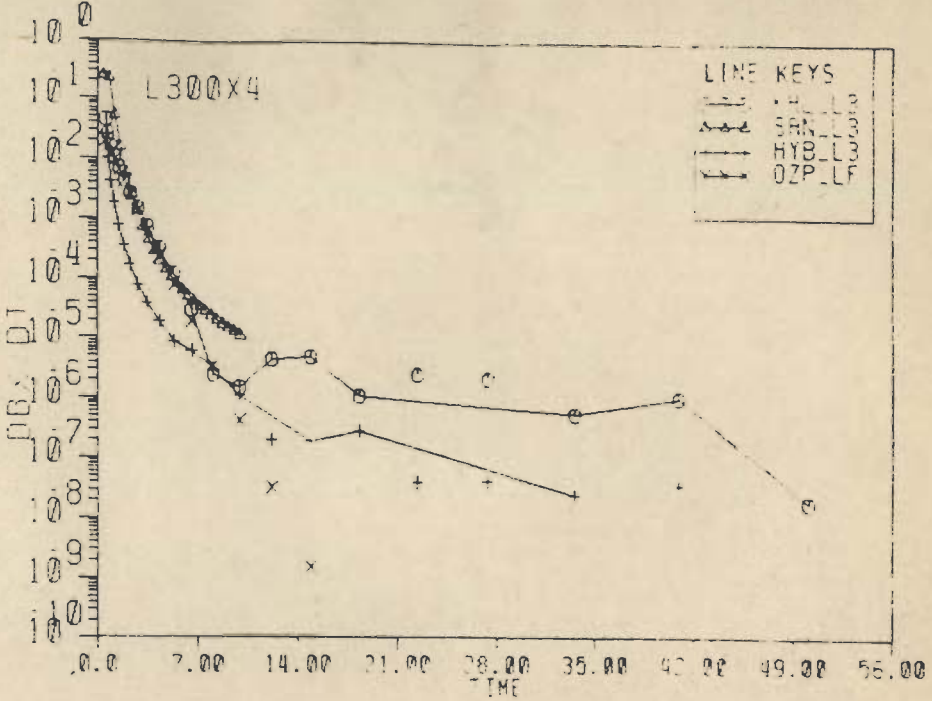

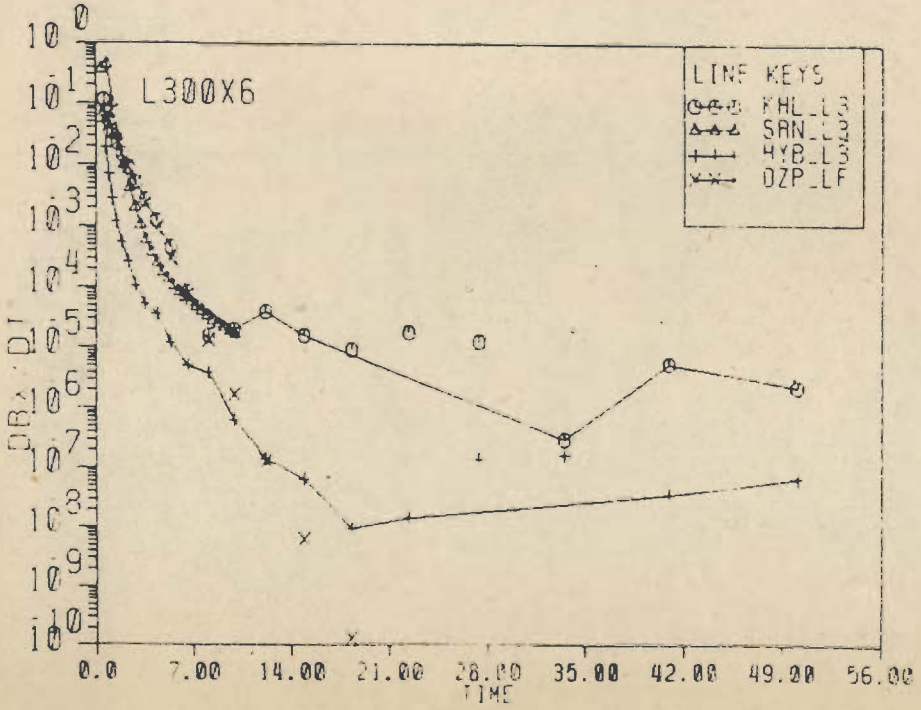

Fig. 5.13(a) The decay curves for dB_x/dt obtained using the CFEM algorithm SAMAYA (HYB), IEM algorithm (SAN), thin sheet algorithm (KHL) and the algorithm OZPLAT (OZP). The resistivity contrast is 750 . The three sets L300X2, L300X4, L300X6 correspond to receiver positions -90, -50 and -10 m from the centre.

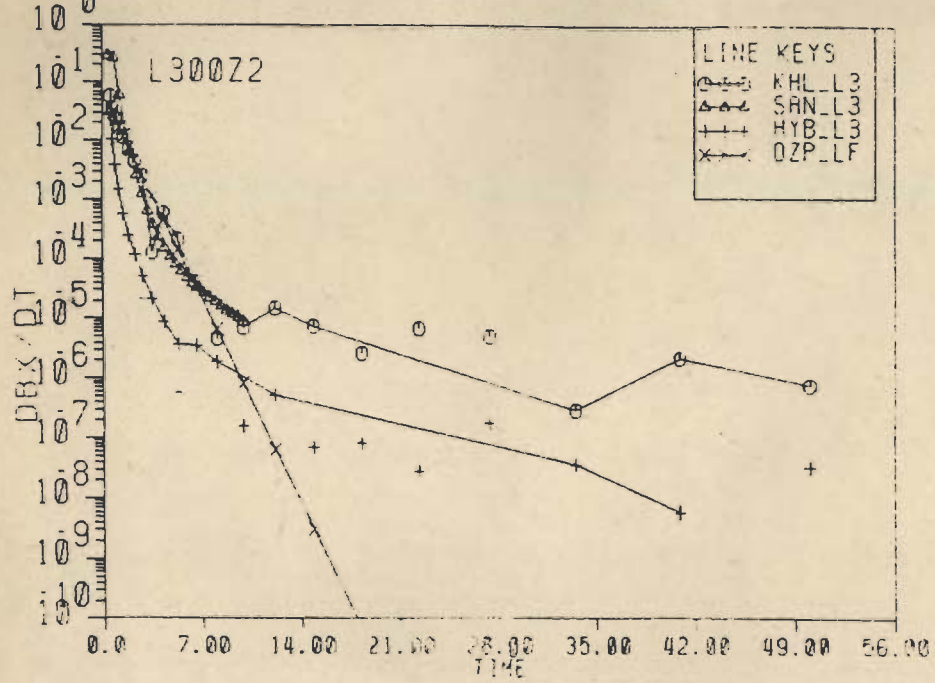

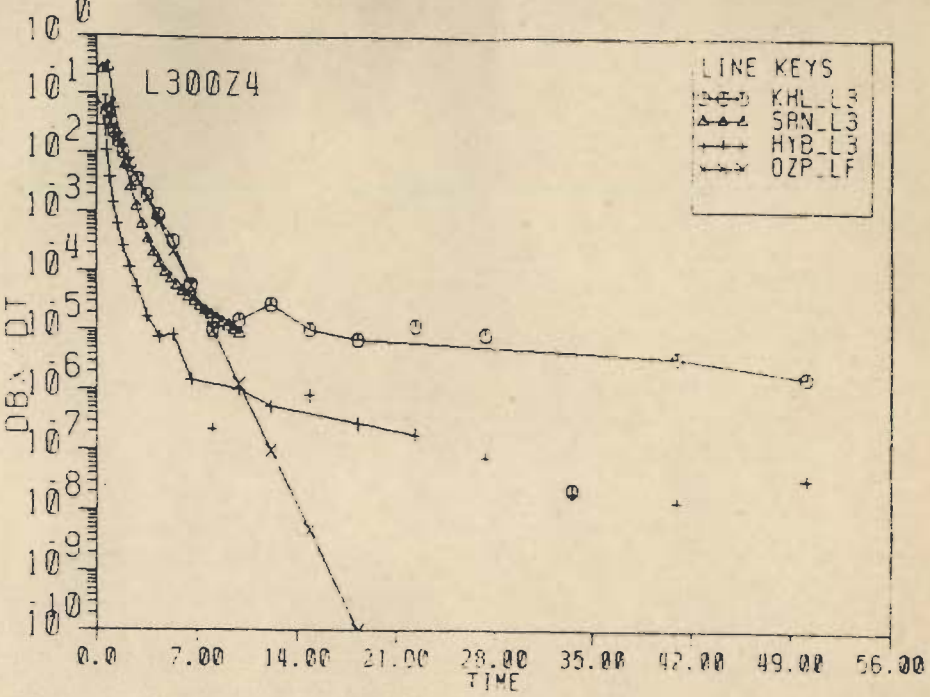

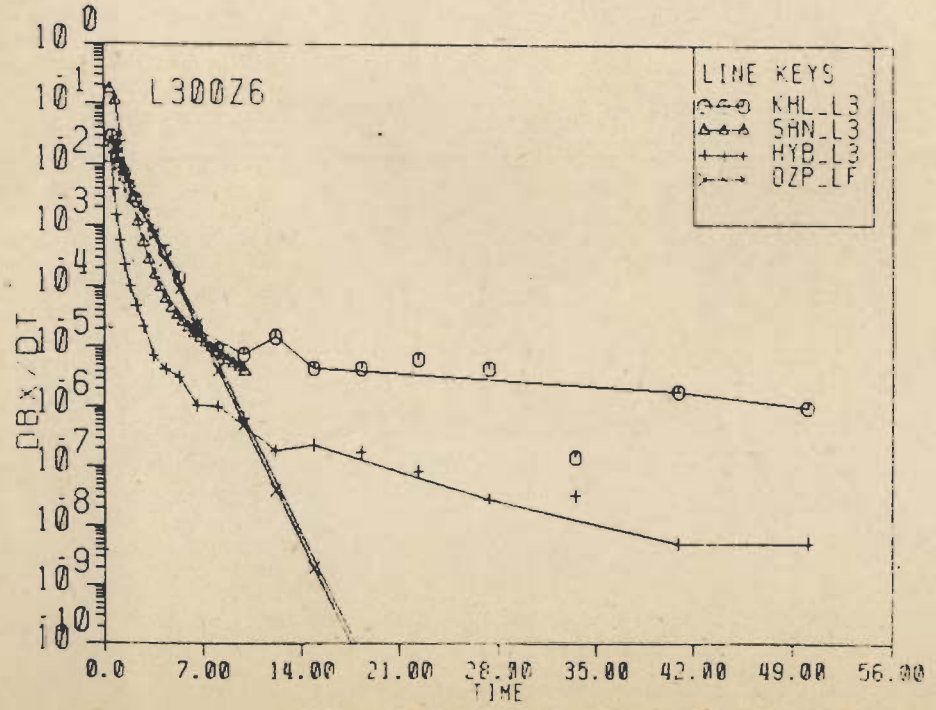

Fig. 5.13(b) The decay curves for dB_z/dt obtained using the CFEM algorithm SAMAYA (HYB), IEM algorithm (SAN), thin sheet algorithm (KHL) and the algorithm OZPLAT (OZP). The resistivity contrast is 750. The three sets L300Z2, L300Z4 and L300Z6 correspond to receiver positions -90, -50 and -10 m from the centre.

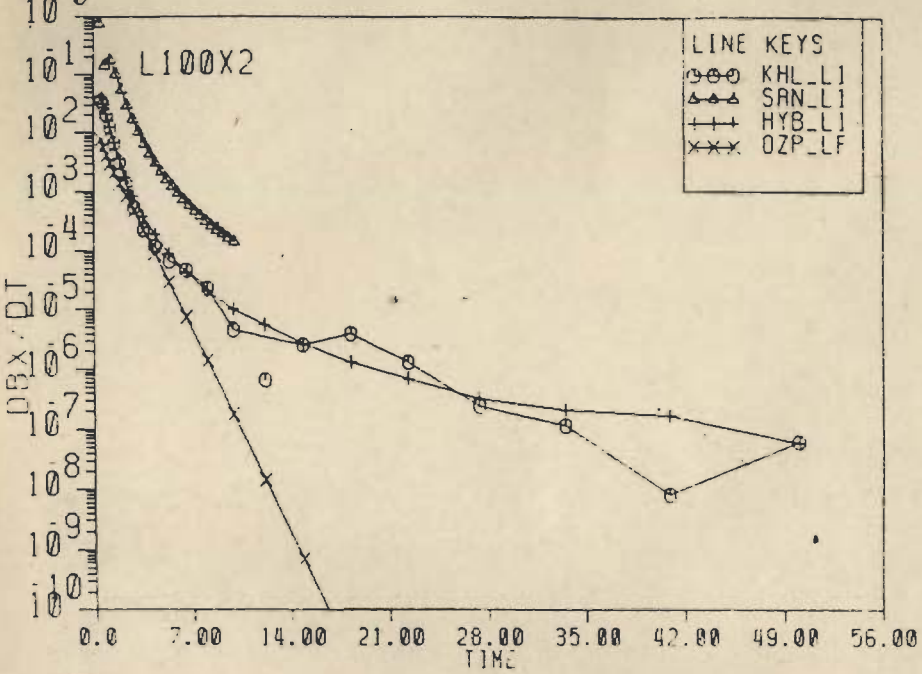

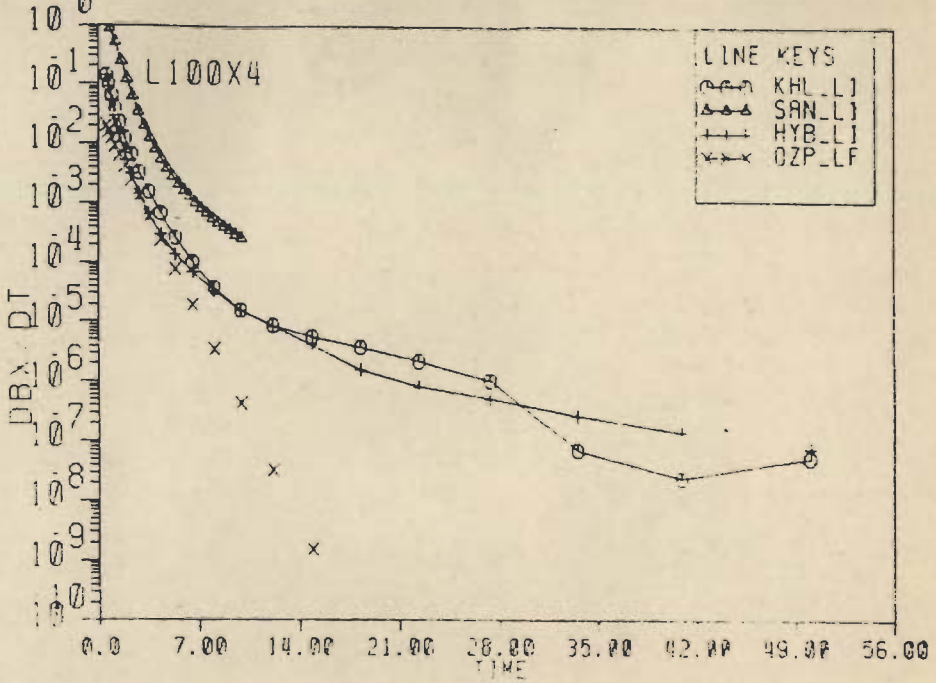

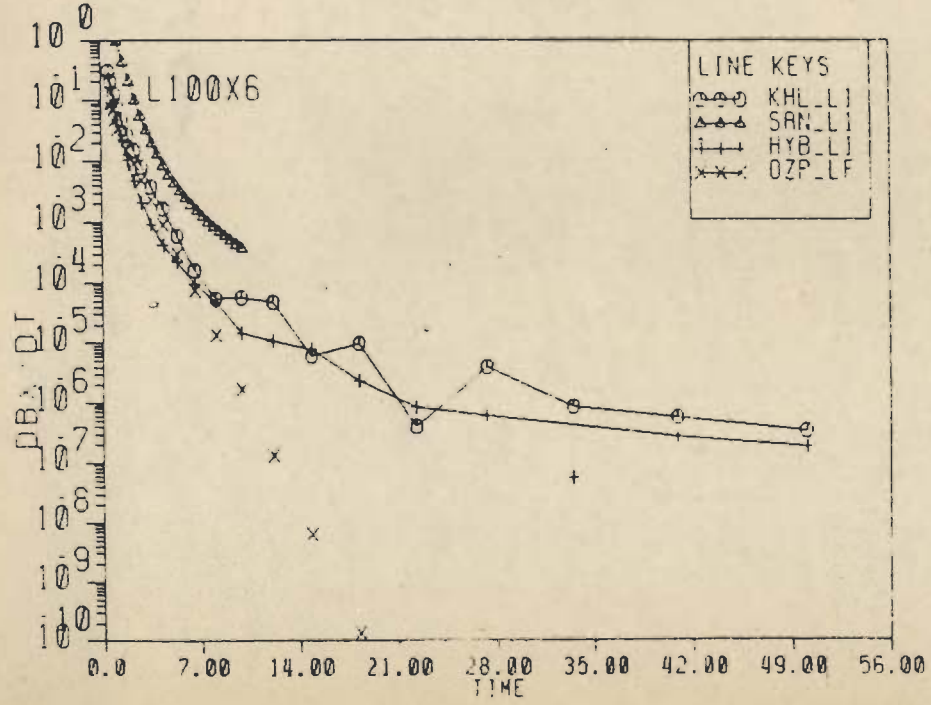

curves

Fig. 5.14(a) The decay for dB_x/dt obtained using the CFEM algorithm SAMAYA (HYB), IEM algorithm (SAN), thin sheet algorithm (KHL) and the algorithm OZPLAT (OZP). The resistivity contrast is 250. The three sets L100X2, L100X4 and L100X6 correspond to receiver positions -90, -50 and -10 m from the centre.

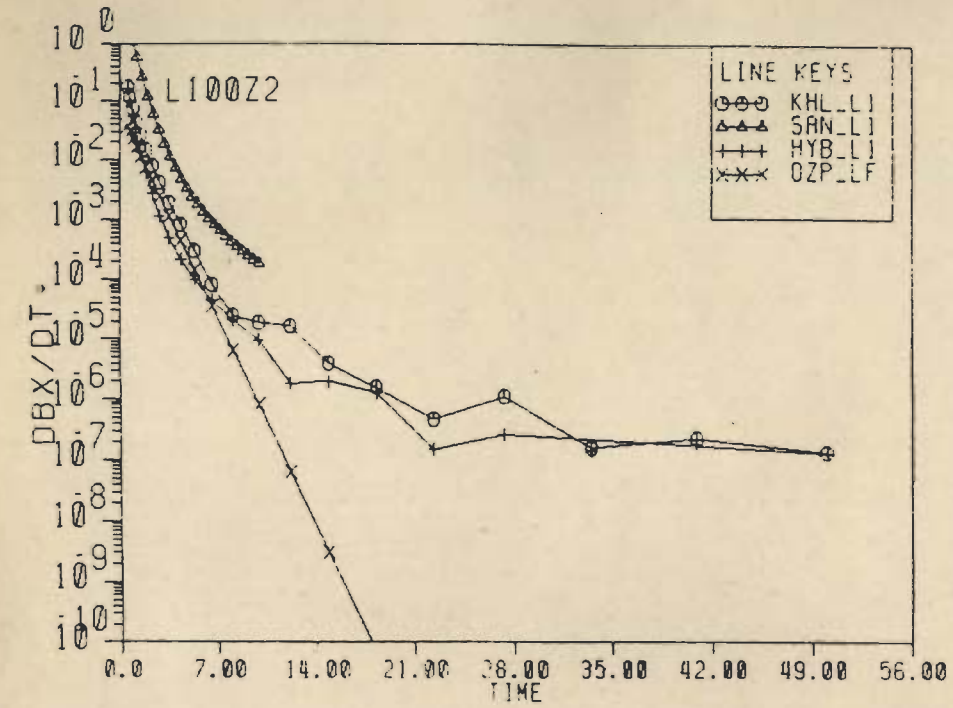

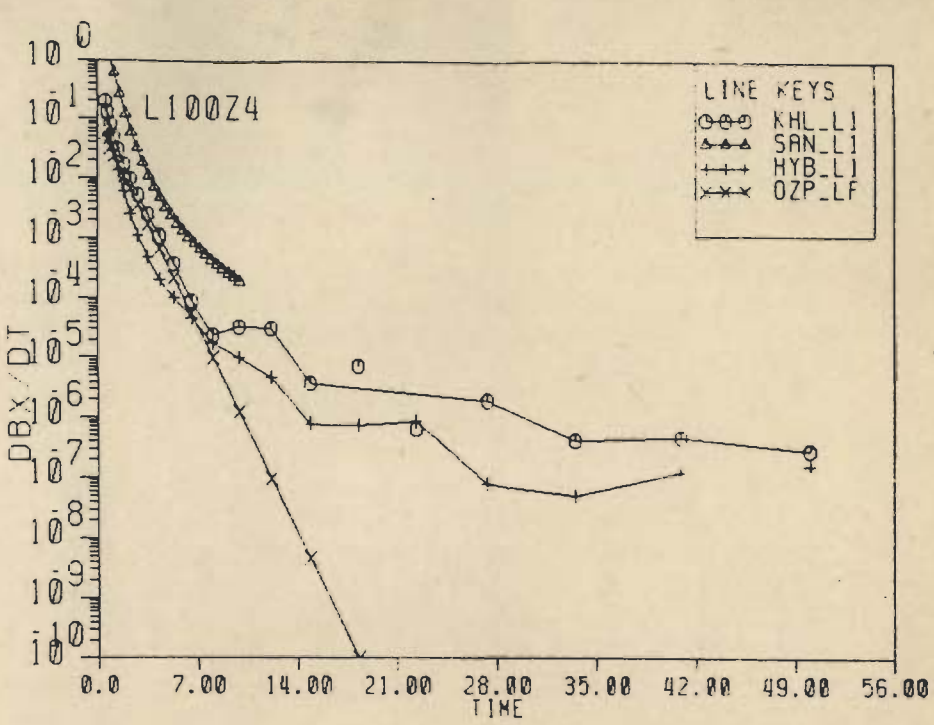

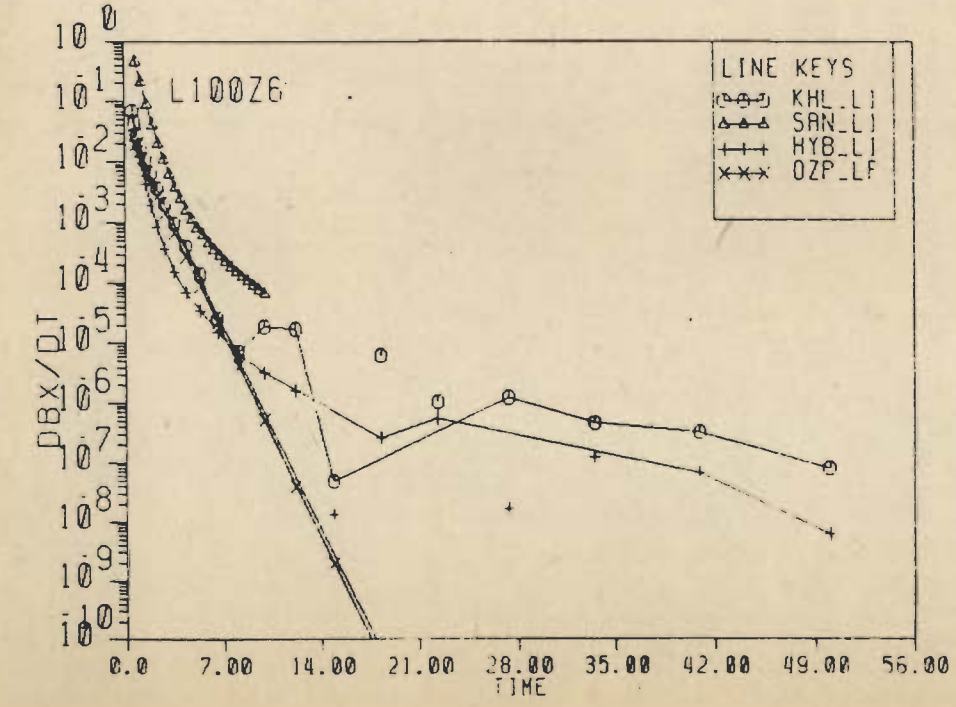

curves

Fig. 5.14(b) The decay for dB_z/dt obtained using the CFEM algorithm SAMAYA (HYB), IEM algorithm (SAN), thin sheet algorithm (KHL) and the algorithm OZPLAT (OZP). The resistivity contrast is 250. The three sets L100Z2, L100Z4 and L100Z6 correspond to receiver positions -90, -50 and -10 m from the centre.

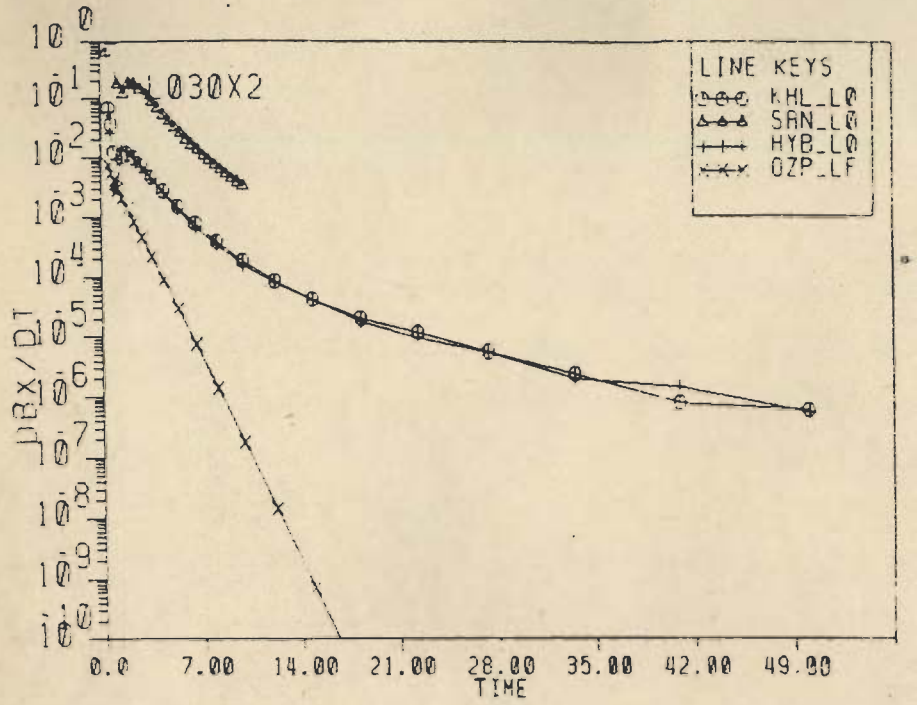

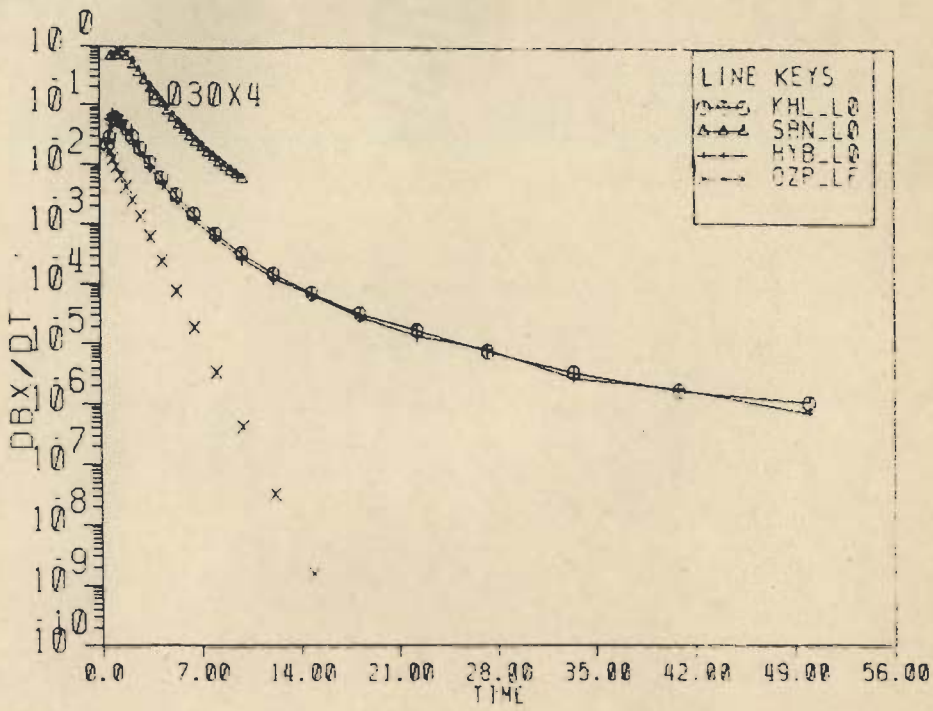

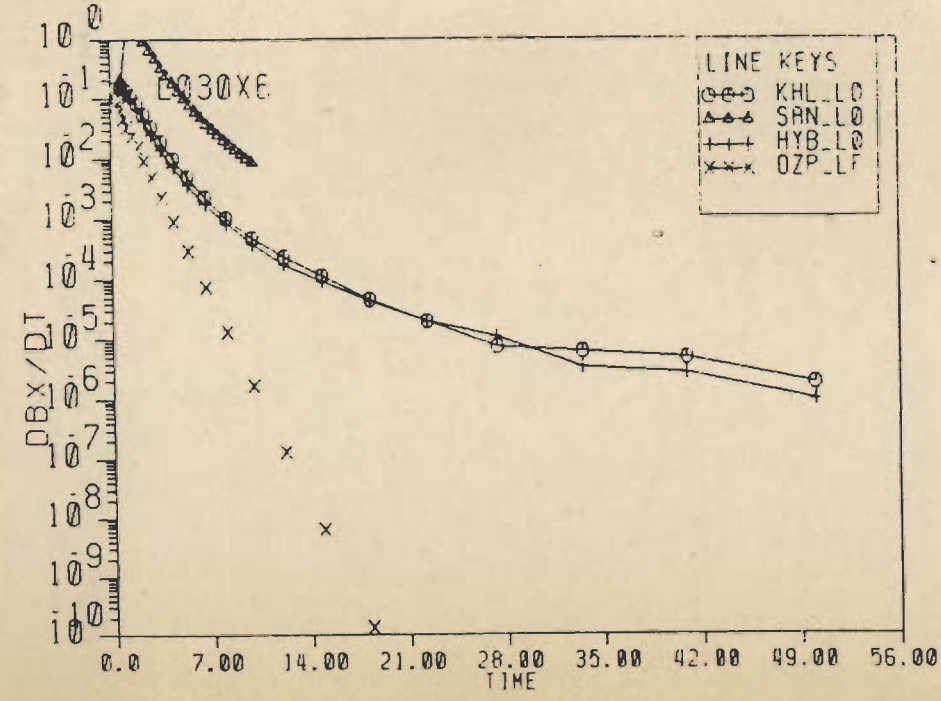

curves

Fig. 5.15(a) The decay for dB_x/dt obtained using the CFEM algorithm SAMAYA (HYB), IEM algorithm (SAN), thin sheet algorithm (KHL) and the algorithm OZPLAT (OZP). The resistivity contrast is 75. The three sets L030X2, L030X4 and L030X6 correspond to receiver positions -90, -50 and -10 m from the centre.

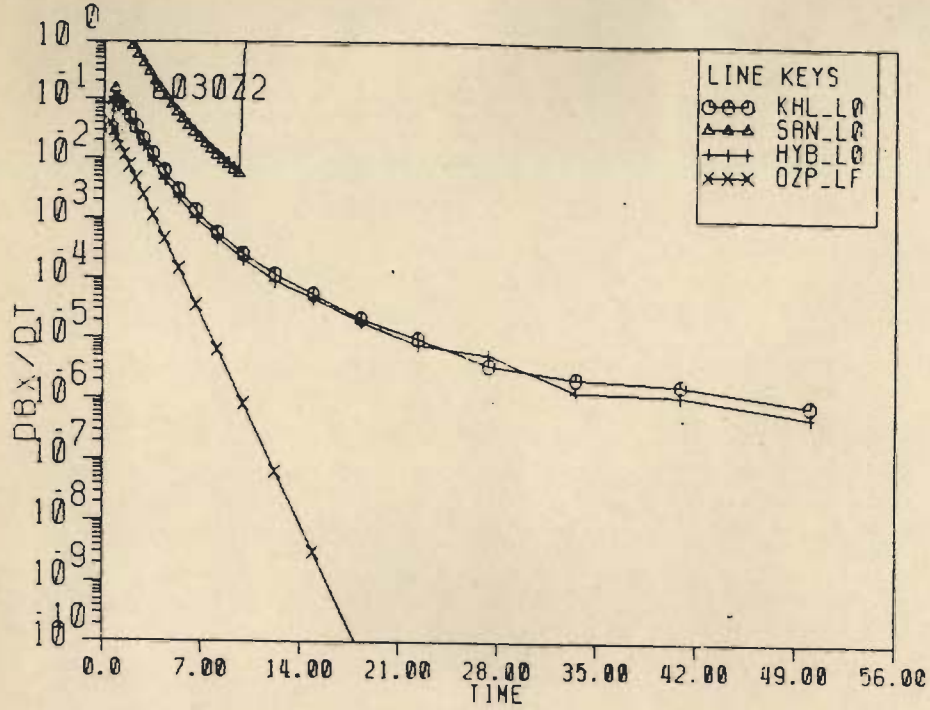

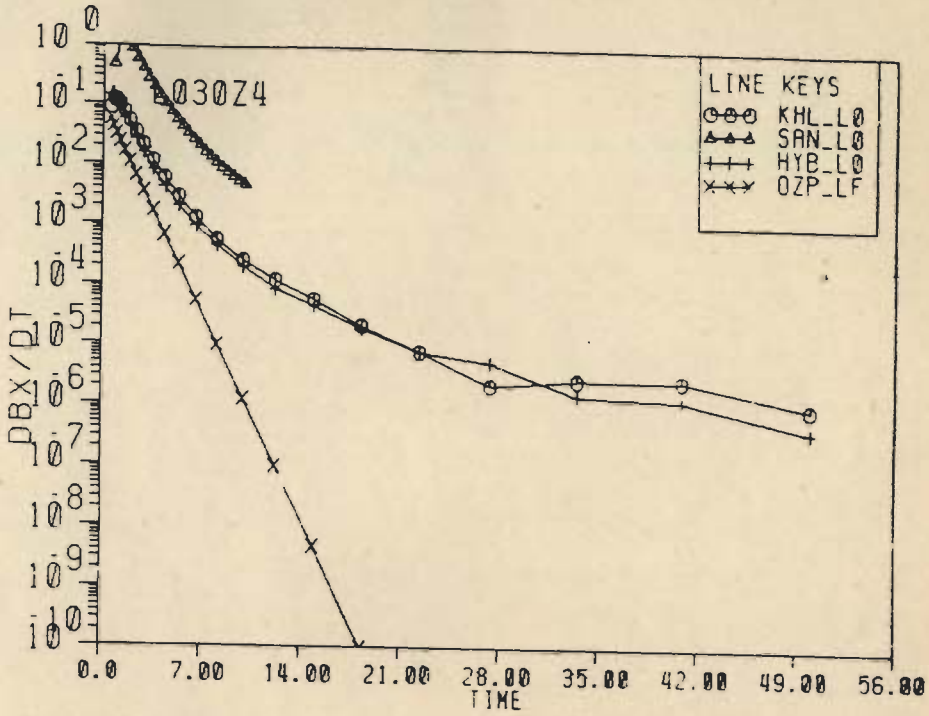

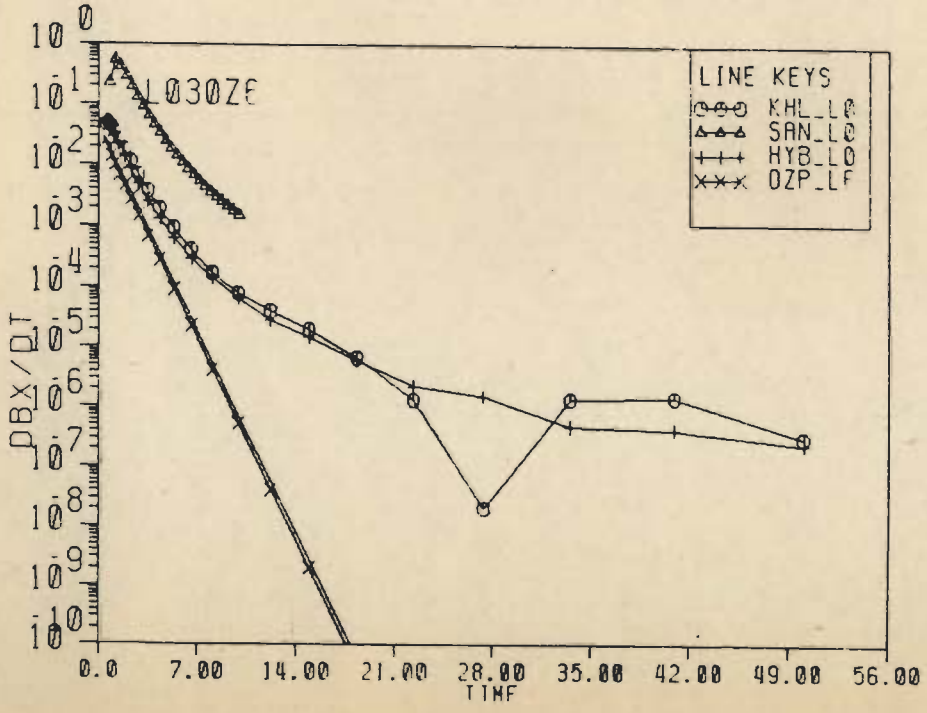

Fig. 5.15(b) The decay curves for dB_z/dt obtained using the CFEM algorithm SAMAYA (HYB), IEM algorithm (SAN), thin sheet algorithm (KHL) and the algorithm OZPLAT (OZP). The resistivity contrast is 75. The three sets L030Z2, L030Z4 and L030Z6 correspond to receiver positions -90, -50 and -10 m from the centre.

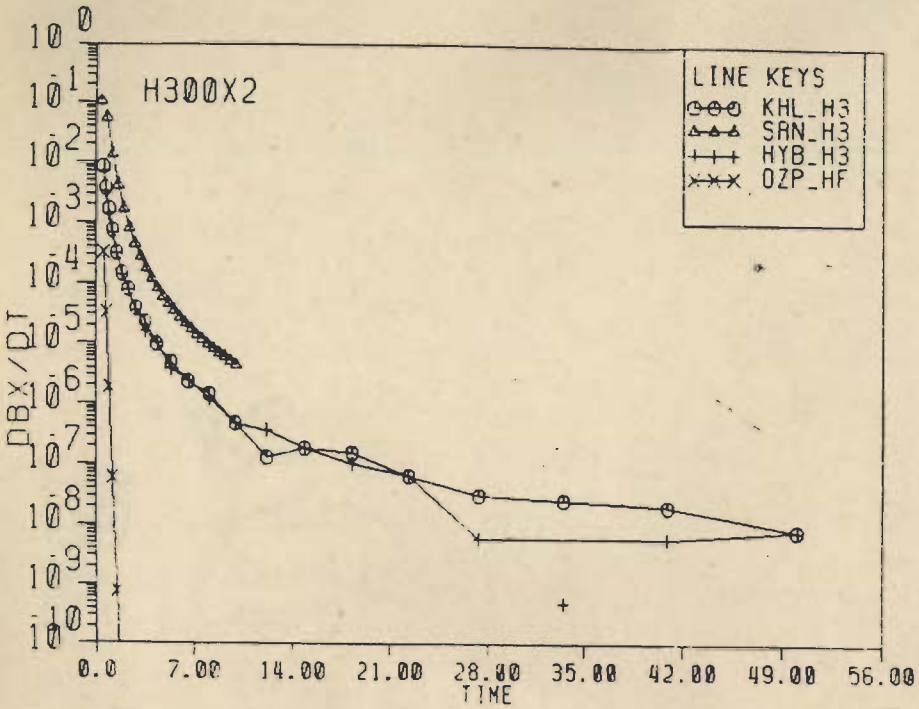

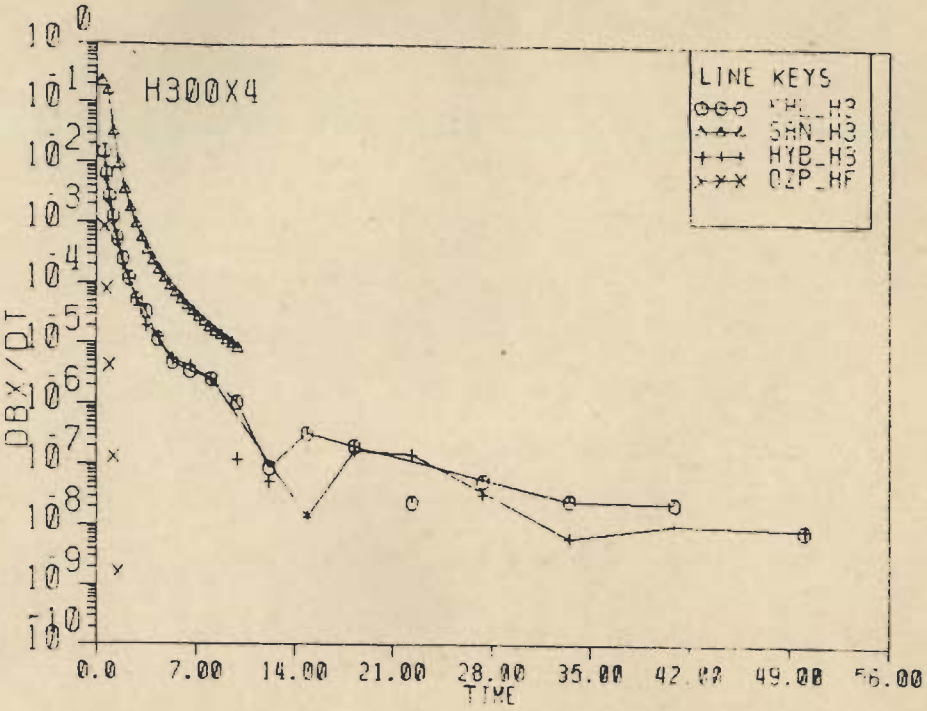

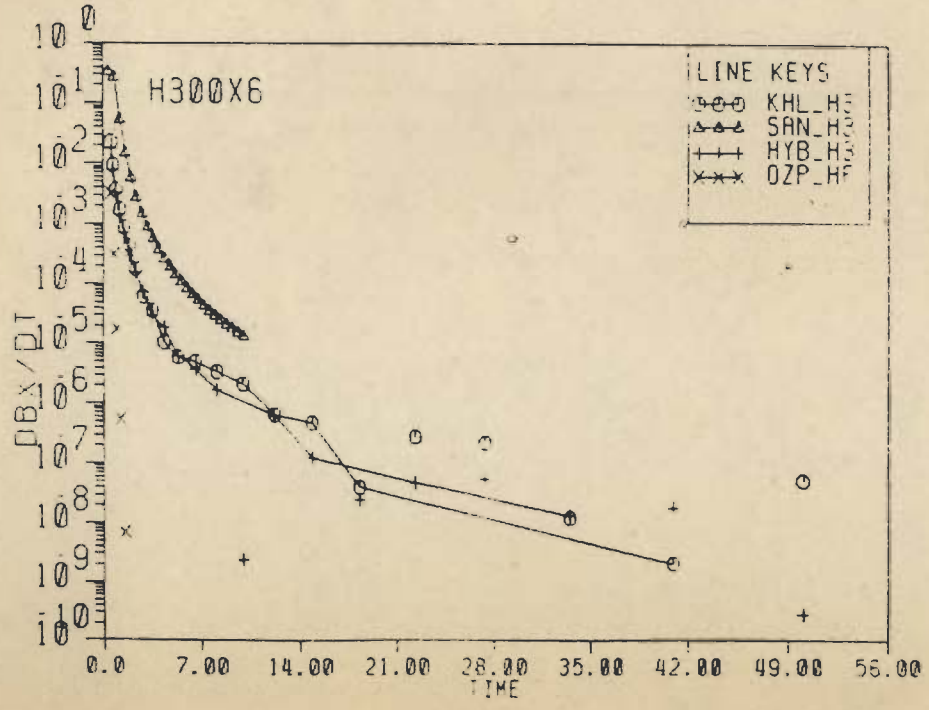

Fig. 5.16(a) The decay curves for dB_x/dt obtained using the CFEM algorithm SAMAYA (HYB), IEM algorithm (SAN), thin sheet algorithm (KHL) and the algorithm OZPLAT (OZP). The resistivity contrast is 60. The three sets H300X2,H300X4 and H300X6 correspond to receiver positions -90, -50 and -10 m from the centre.

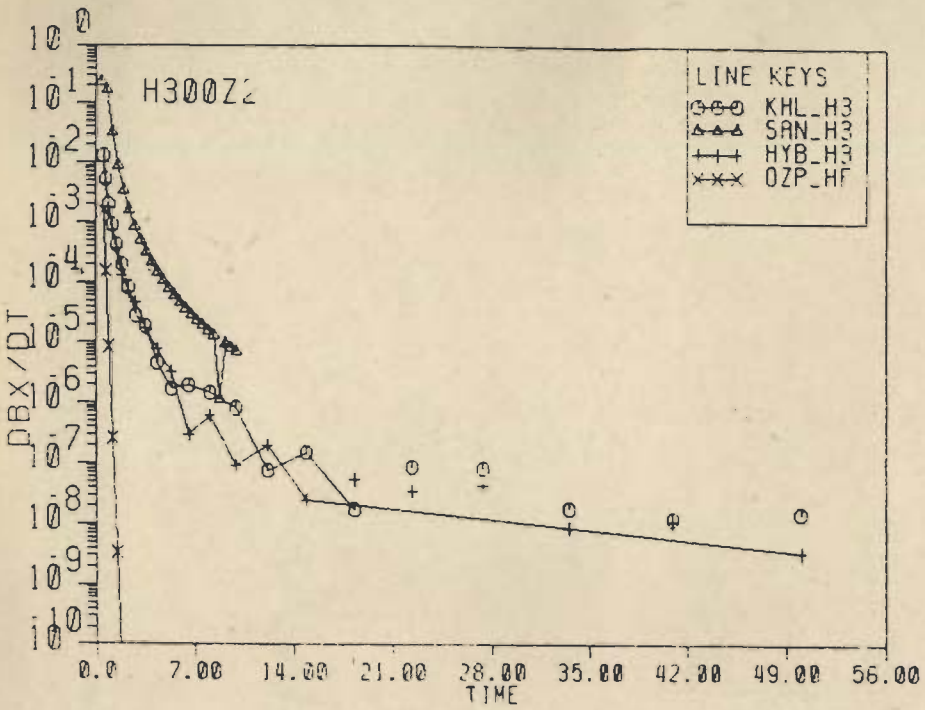

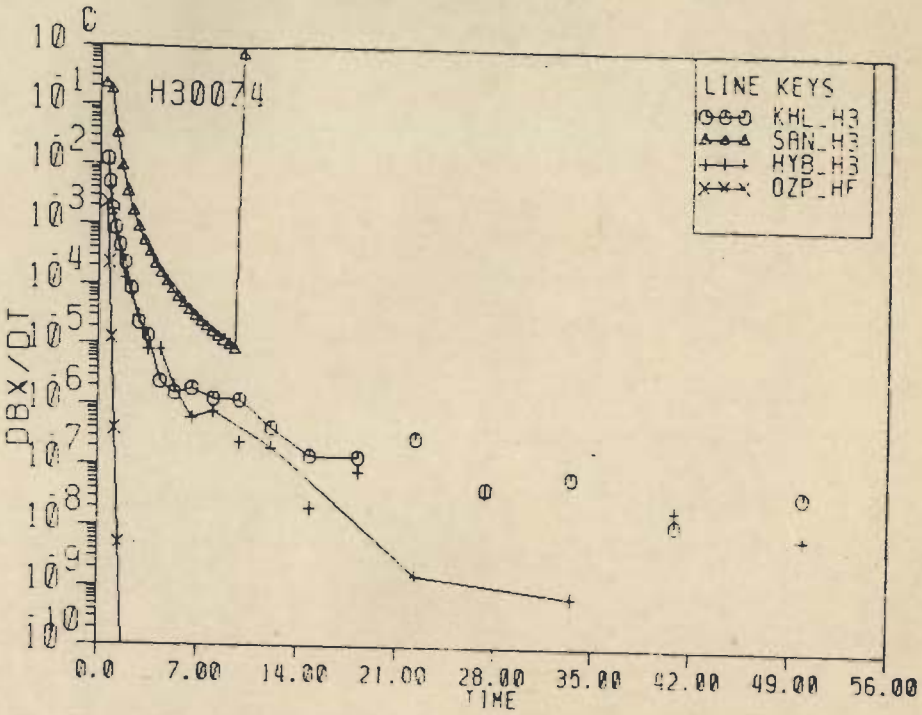

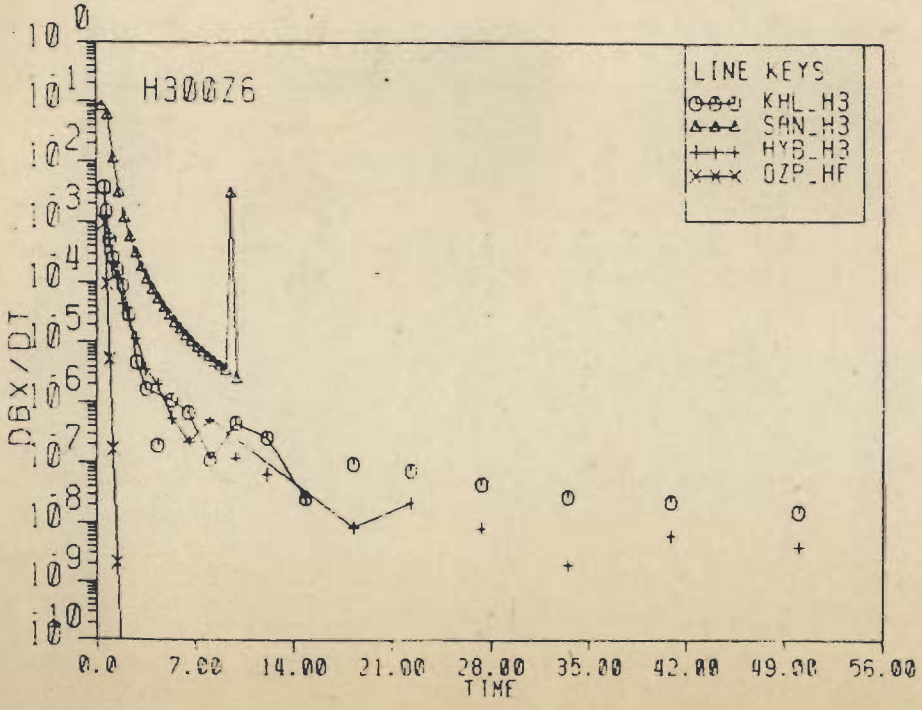

Fig. 5.16(b) The decay curves for dB_z/dt obtained using the CFEM algorithm SAMAYA (HYB), IEM algorithm (SAN), thin sheet algorithm (KHL) and the algorithm OZPLAT (OZP). The resistivity contrast is 60. The three sets H300Z2,H300Z4 and H300Z6 correspond to receiver positions -90, -50 and -10 m from the centre.

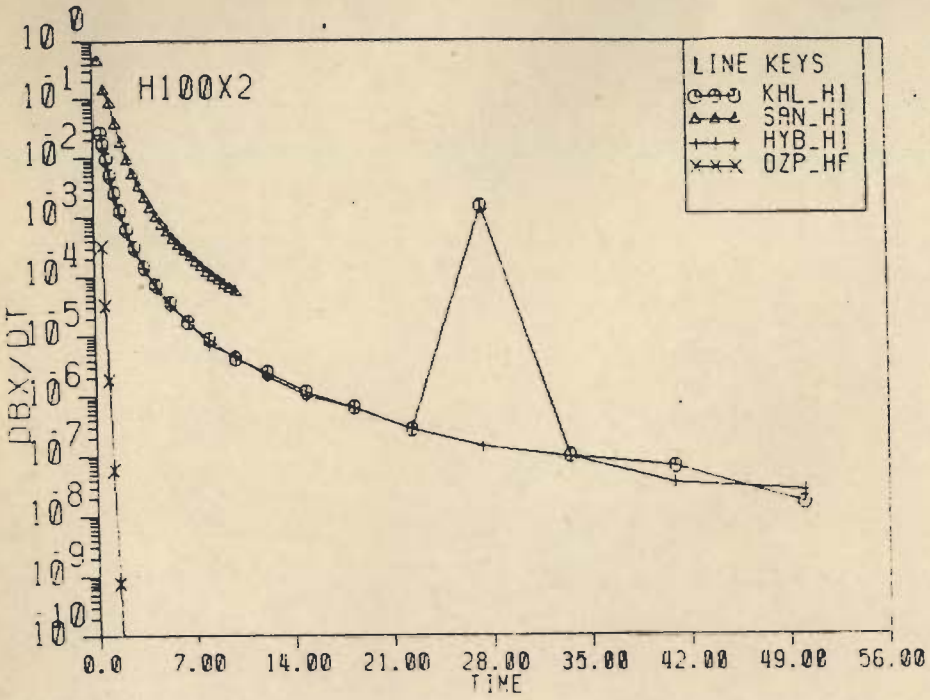

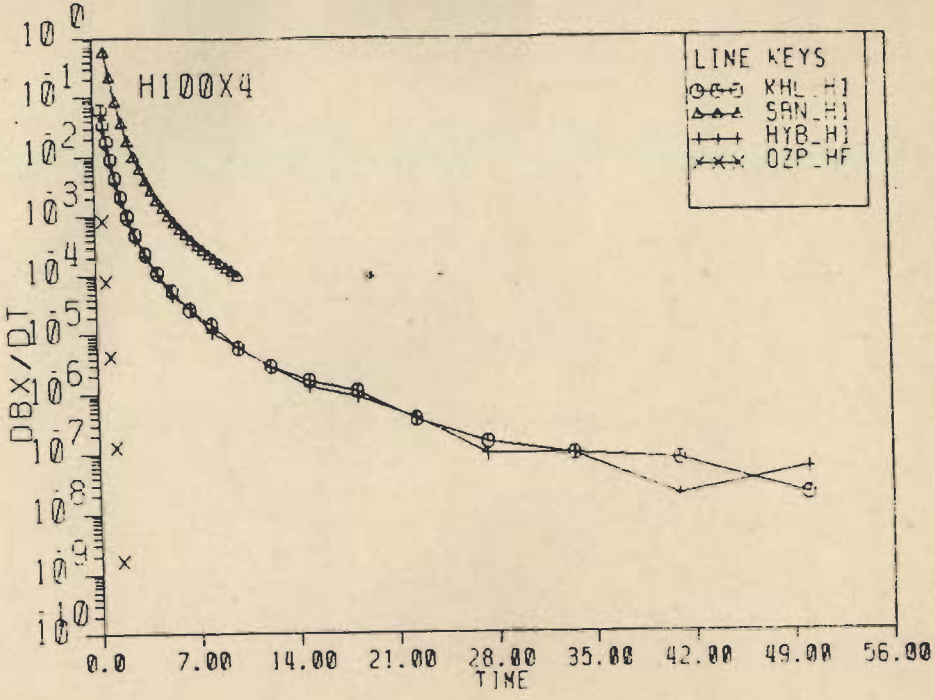

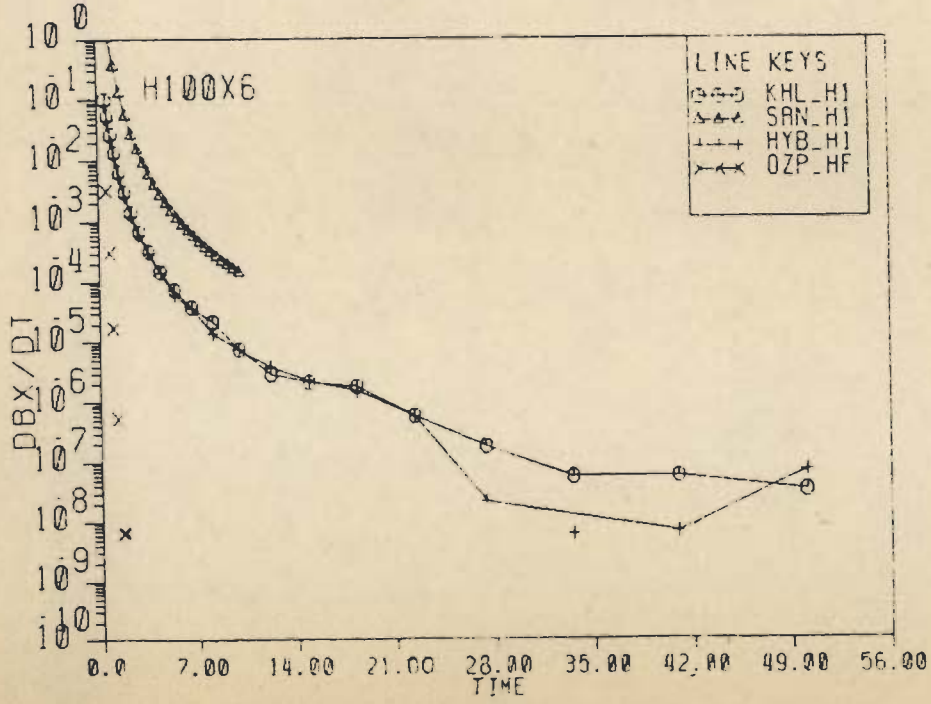

Fig. 5.17(a) The decay curves for dB_x/dt obtained using the CFEM algorithm SAMAYA (HYB), IEM algorithm (SAN), thin sheet algorithm (KHL) and the algorithm OZPLAT (OZP). The resistivity contrast is 20. The three sets H100X2,H100X4 and H100X6 correspond to receiver positions -90, -50 and -10 m from the centre.

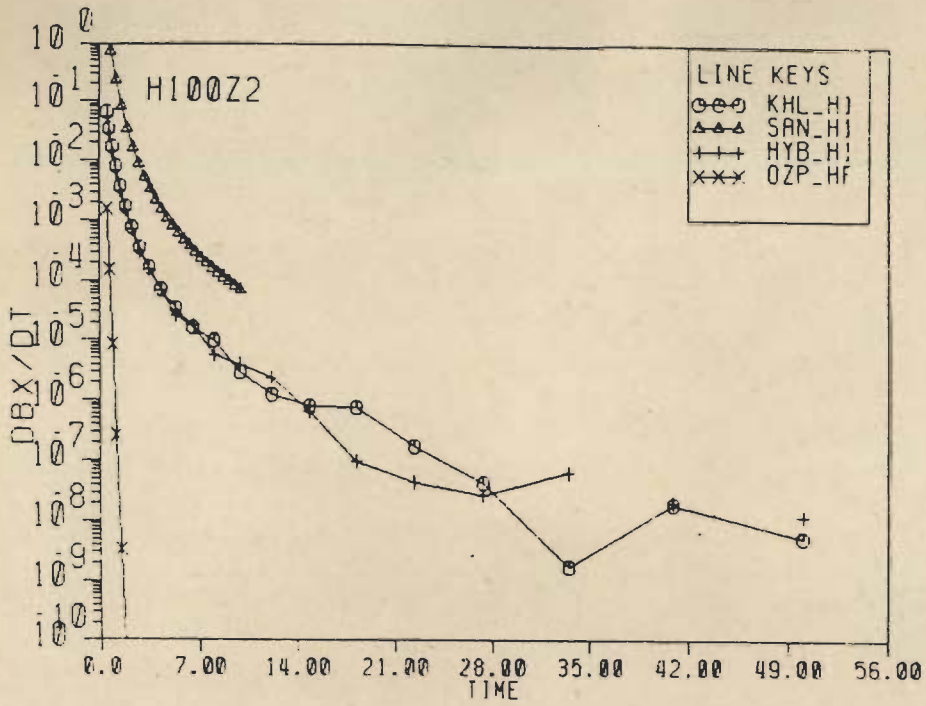

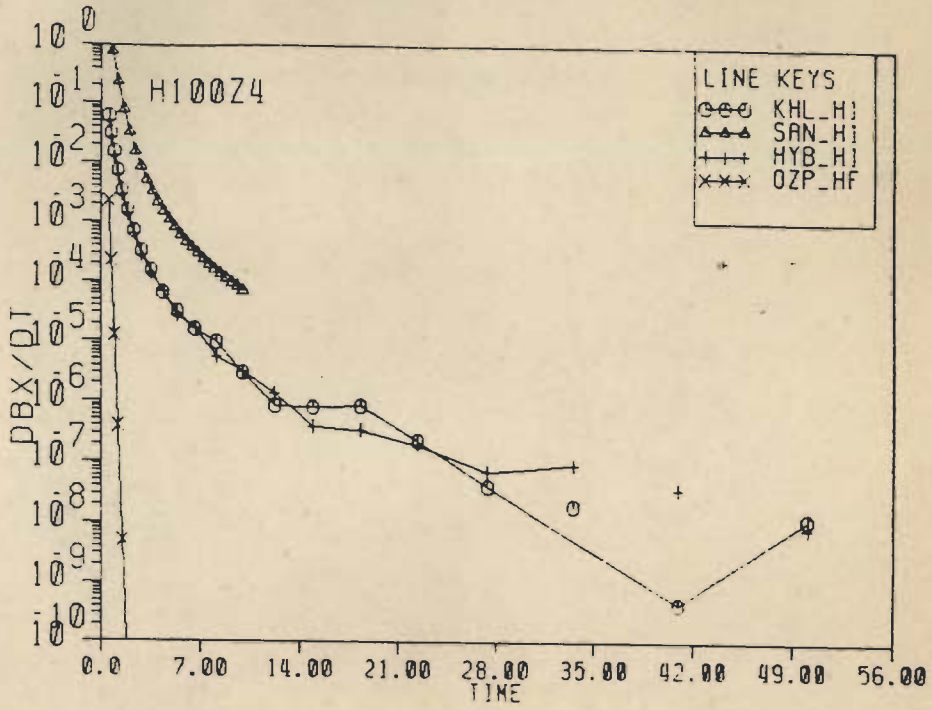

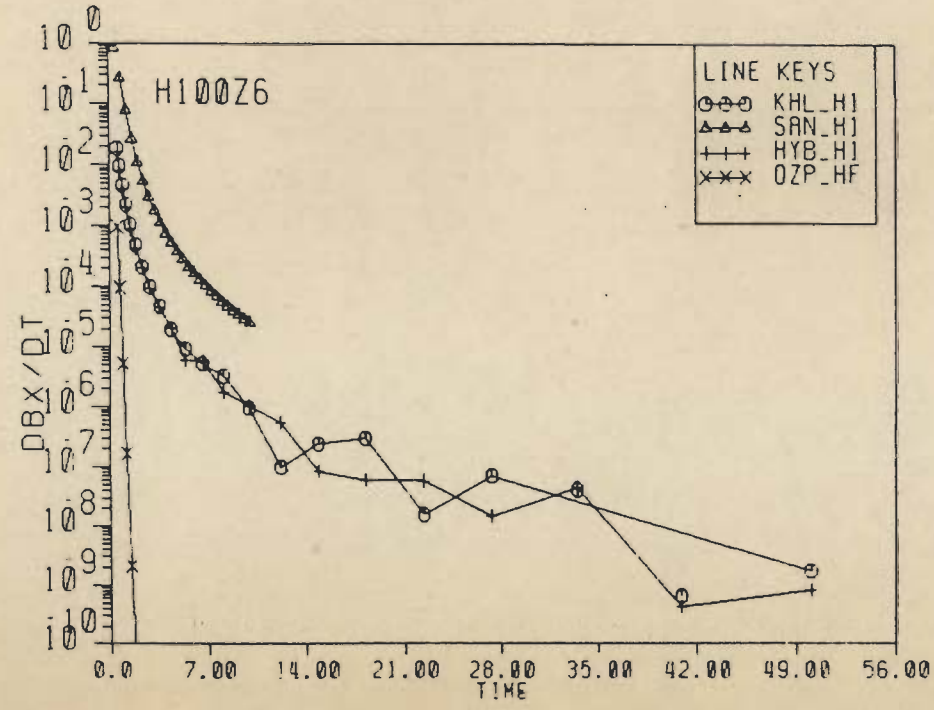

Fig. 5.17(b) The decay curves for dB_z/dt obtained using the CFEM algorithm ZSAMAYA (HYB), IEM algorithm (SAN), thin sheet algorithm (KHL) and the algorithm OZPLAT (OZP). The resistivity contrast is 20. The three sets H100Z2,H100Z4 and H100Z6 correspond to receiver positions -90, -50 and -10 m from the centre.

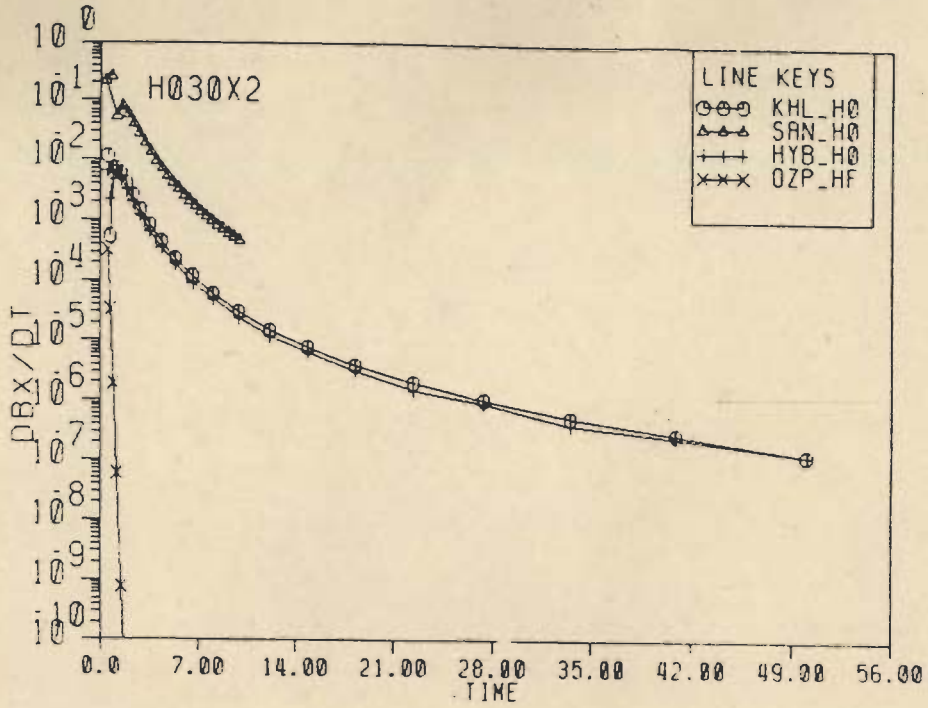

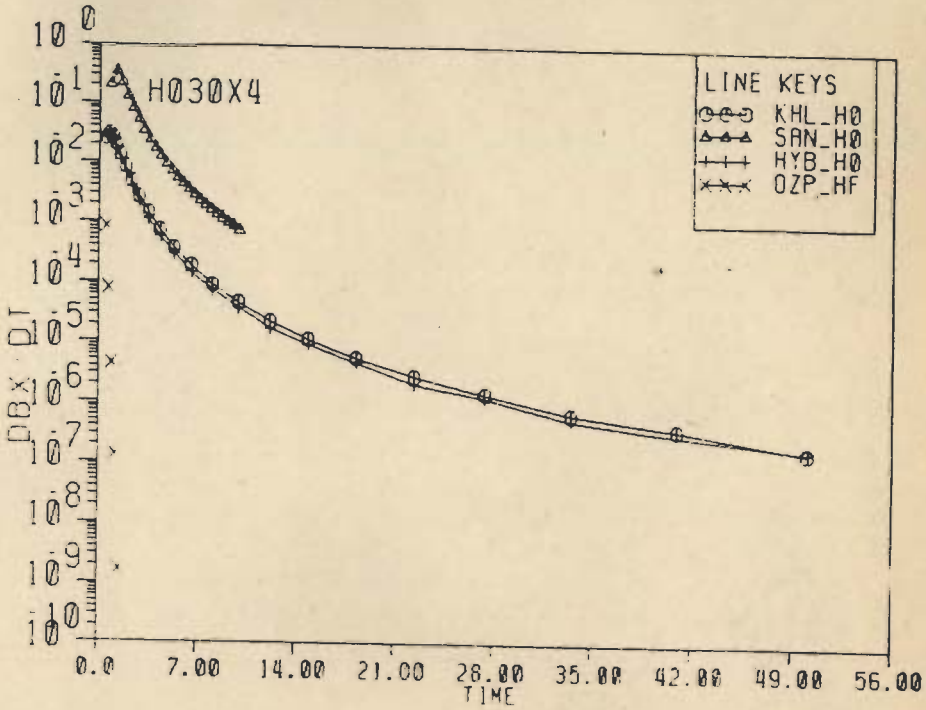

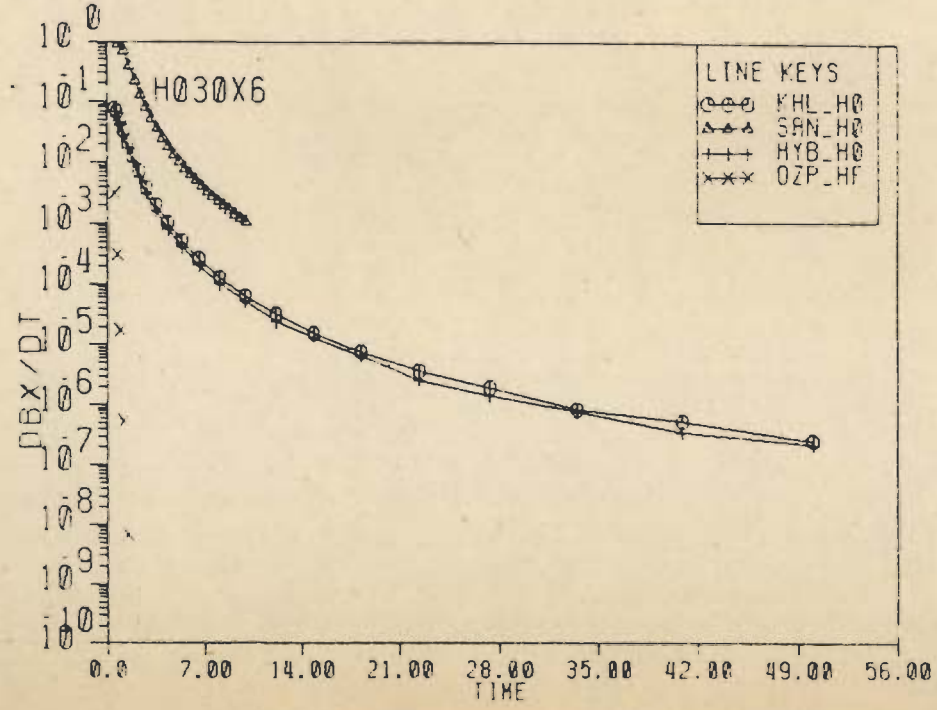

Fig. 5.18(a) The decay curves for dB_x/dt obtained using the CFEM algorithm SAMAYA (HYB), IEM algorithm (SAN), thin sheet algorithm (KHL) and the algorithm OZPLAT (OZP). The resistivity contrast is 6. The three sets H030X2,H030X4 and H030X6 correspond to receiver positions -90, -50 and -10 m from the centre.

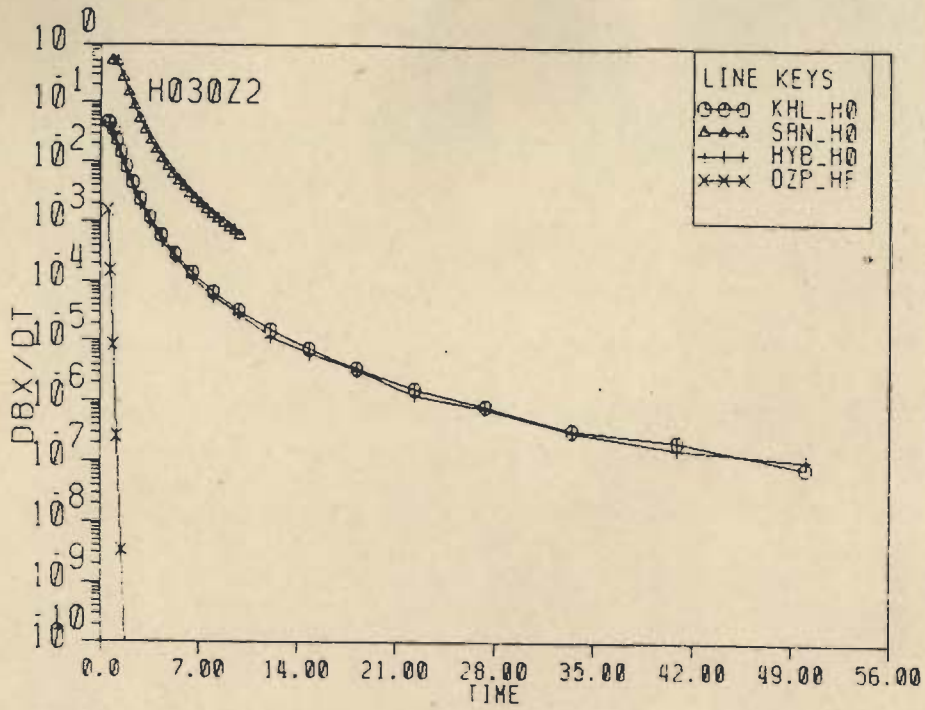

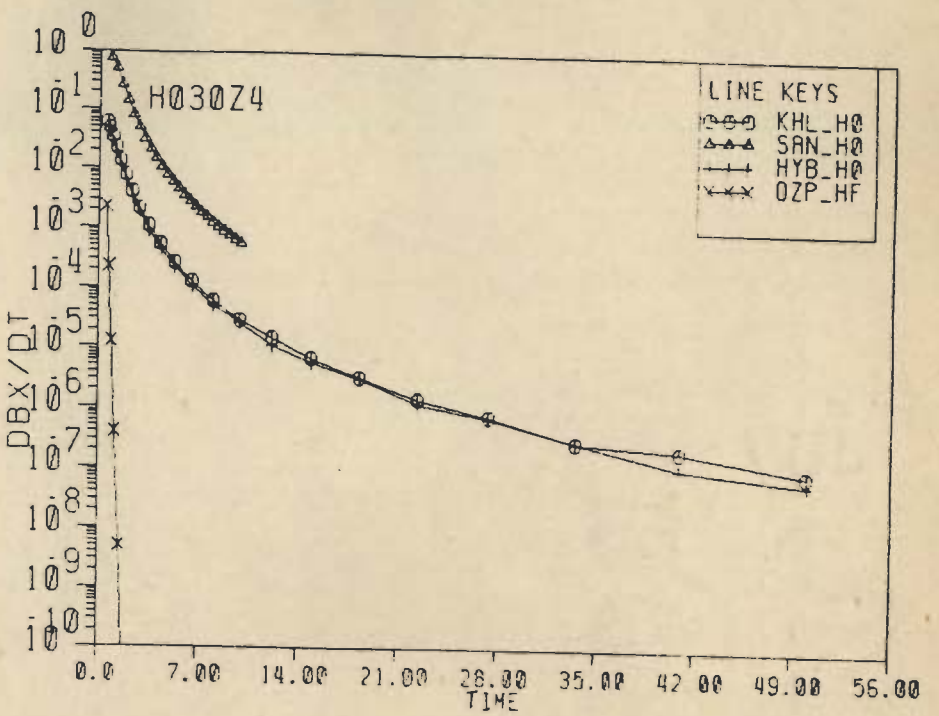

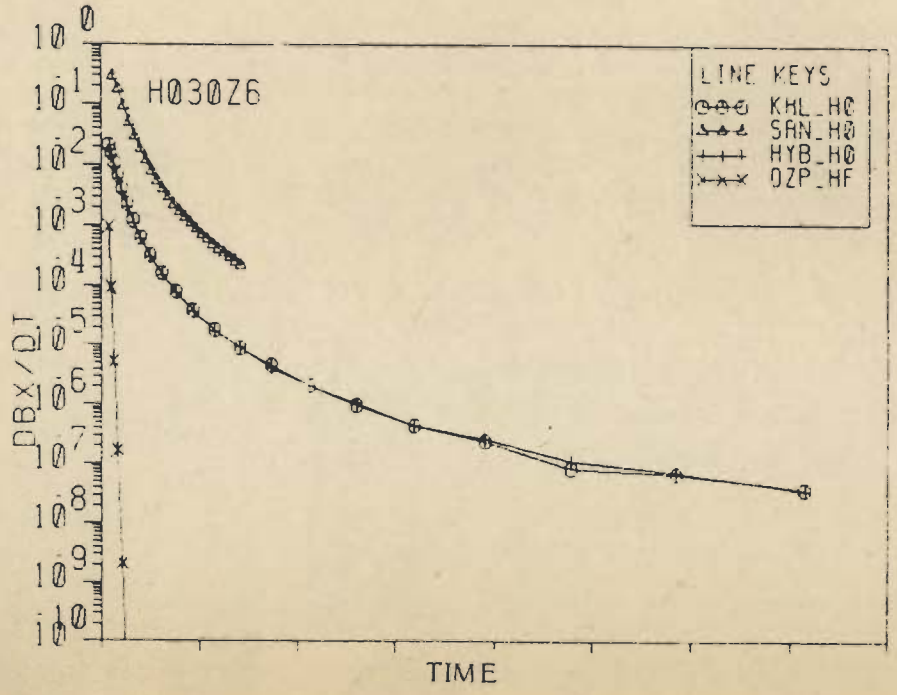

Fig. 5.18(b) The decay curves for dB_z/dt obtained using the CFEM algorithm SAMAYA (HYB), IEM algorithm (SAN), thin sheet algorithm (KHL) and the algorithm OZPLAT (OZP). The resistivity contrast is 6. The three sets H030Z2,H030Z4 and H030Z6 correspond to receiver positions -90, -50 and -10 m from the centre.

A scrutiny of Figs. 5.13-5.18 reveals the following features of the plots :

1. The numerical errors start dominating, thereby resulting in the oscillatory behaviour of the curves, after 10 mS for high resistivity contrast and after 30 mS for low resistivity contrast.

2. For resistivity contrast values upto 250, the KHL curves are closer to the HYB curves than to the SAN curves. On the other hand, for the resistivity contrast of 750, these are closer to the SAN curves than to the HYB curves. This leads to the inference that SAMAYA results deviate significantly from the 3-D thin sheet results for high resistivity contrasts. This deviation is, indeed, expected. Similar effect was encountered by Lajoie and West (1976) and Newman et.al. (1986). One explanation forwarded for this kind of behaviour is in terms of the disparity in the magnitudes of the Galvanic (charge source) and inductive (current source) components of the secondary magnetic induction. Until special schemes, like splitting the potential (Lajoie and West, 1976), are devised, the galvanic component dominates over the inductive component and the latter is all but lost during numerical computation. San Filipo et.al. (1985) and Newman et.al. (1986), following Annan (1974) and Lajoie and West (1976), used special set of basis functions to counter this effect. Another explanation can be thought of in terms of the difficulty in numerically simulating the vortex currents by means of simple shape functions. The specially designed higher order shape functions would help in this regard, one possibility is to use higher order isoparametric family of shape functions (Zienkiewicz, 1977). The disparity between the HYB and SAN curves, in case of low resistivity contrast, may be due to over compensation for inductive component in the latter.

3. In case of the x-component curves, for resistivity contrasts of 250. 750 the HYB and SAN curves respectively possess higher ordinate values than those of corresponding KHL curves for receiver positions far away from the centre of the target, while these curves possess lower values for receiver positions closer to the centre. For lower contrast values the HYB curves possess ordinate values either identical to or lower than those of the corresponding KHL curves and the same is the case for all z-component curves.

On the basis of the results presented here, it may be concluded that for contrast values less than 250, SAMAYA results are closer to true value than the corresponding integral equation results, while for higher contrast values it is the other way round. However, this conclusion must be further substantiated by comparing the two sets of results for a wide range and types of models. It may be stressed here that the deviation in the two sets of results can not be attributed to the different schemes of transformation to time domain as Newman et.al. (1986) obtained reasonable agreement between their results, which were obtained by transforming the frequency domain results to time domain and the corresponding results of San Filipo. Hence the deviation must be a result of the initial deviations in the frequency domain results from the integral equation and CFEM algorithms.

5.9 OVERBURDEN STUDY

Six cases were studied to investigate the overburden effect. The base model discussed earlier was retained with the change that the depth of burial was increased to 80 m, the layer and half-space resistivities of the two layer earth being 10 and 100 Ohm m respectively. The six cases were generated by combining one of the two values of target resistivities of 0.4 and 5 Ohm m

with one of the three values of layer thicknesses of 0, 30 and 60 m, the two cases with 0 layer thickness simulating the half-space to provide a check on the results. For the 30 and 60 m overburden cases, the results from the 3-D thin sheet algorithm SHEET were provided by K.H. Lee (1986). The comparative plots of the x and z-components of d**B**/dt for the four cases are given in Figs. 5.19 - 5.22.

From Figs. 5.19 - 5.22 it is clear that in the case of low resistivity contrast there exists excellent agreement between the KHL and HYB curves for both the components. On the other hand, in case of high resistivity contrast the agreement is good for the x-component curves and it is acceptable in the case of the z-component curves. Hence, as in the case of the half-space, SAMAYA can be successfully used for studying the overburden effect when resistivity contrast is not very high. Figures 5.23 - 5.26 compare the dB_x/dt and dB_z/dt profiles for half-space and 30 and 60 m overburden cases. Comparisons are made at five delay time values of 0.553, 0.719, 1.17, 2.85 and 14.9 mS. It may be observed from these figures that at the earliest delay time value of 0.553 mS, the half-space curves are smooth and these possess the maximum ordinate values, the 30 m curves show sign reversal with respect to half-space values at receiver positions far away from the centre and 60 m curves possess ordinate values opposite in sign to the corresponding half-space values. For later times the magnitudes of 30 and 60 m curves increase, the latter at a faster pace, in comparison to the corresponding half-space values so much so that for a delay time value of 1.17 mS, the half-space values are the least, while the 30 m values are maximum. At 2.85 mS and all subsequent delay times, the 60 m values are maximum and the half-space values are the least. This pattern exists for both the components of d**B**/dt and for all the four cases. Thus, a correlation exists between the earliest time when the curve becomes smooth and the thickness of the overburden. It is conjectured

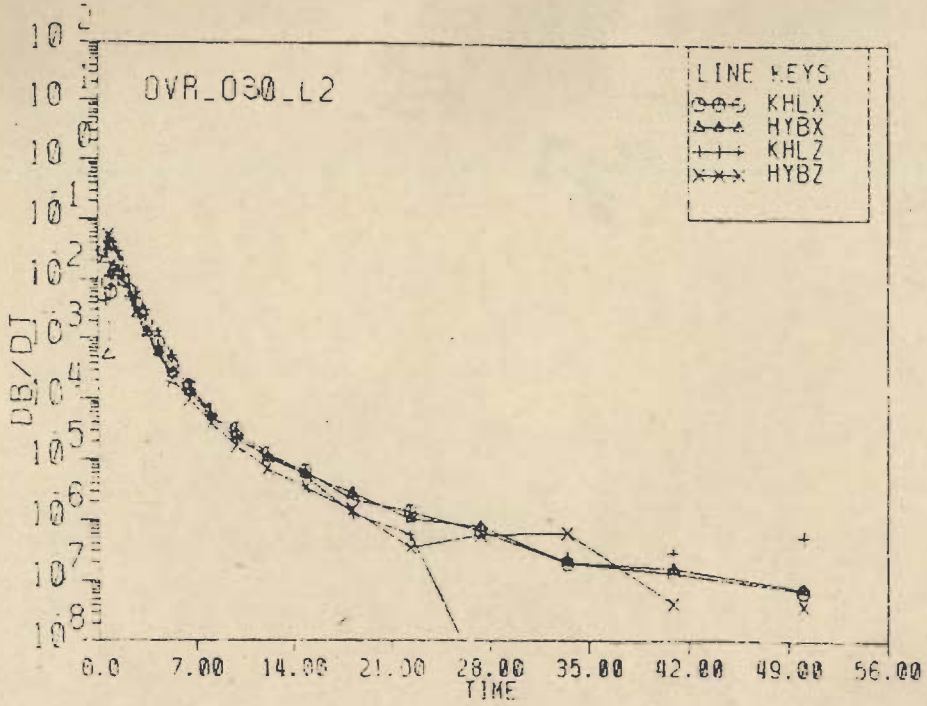

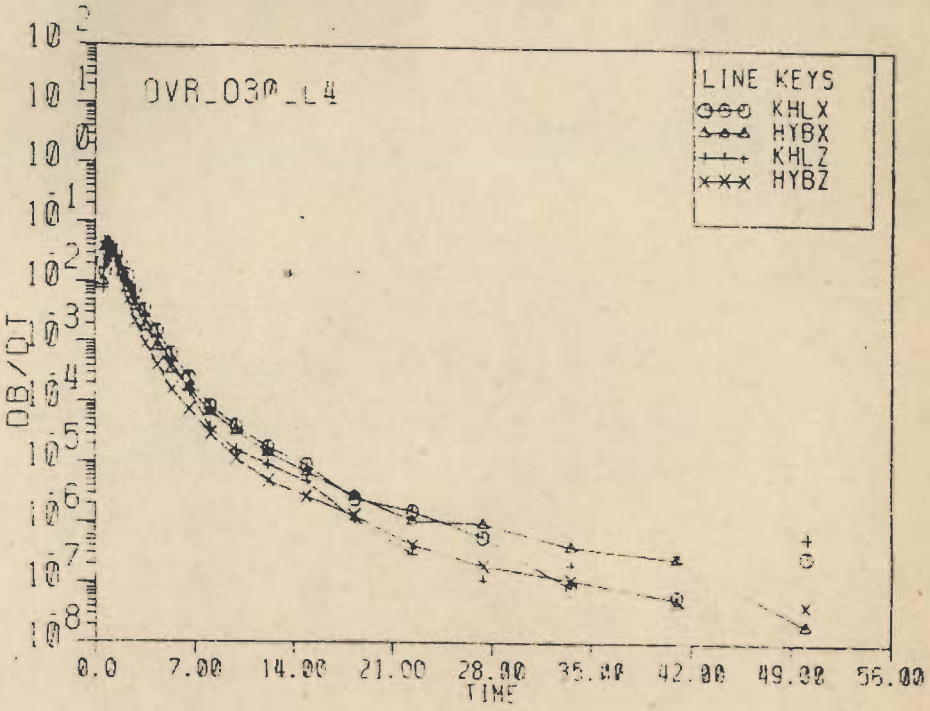

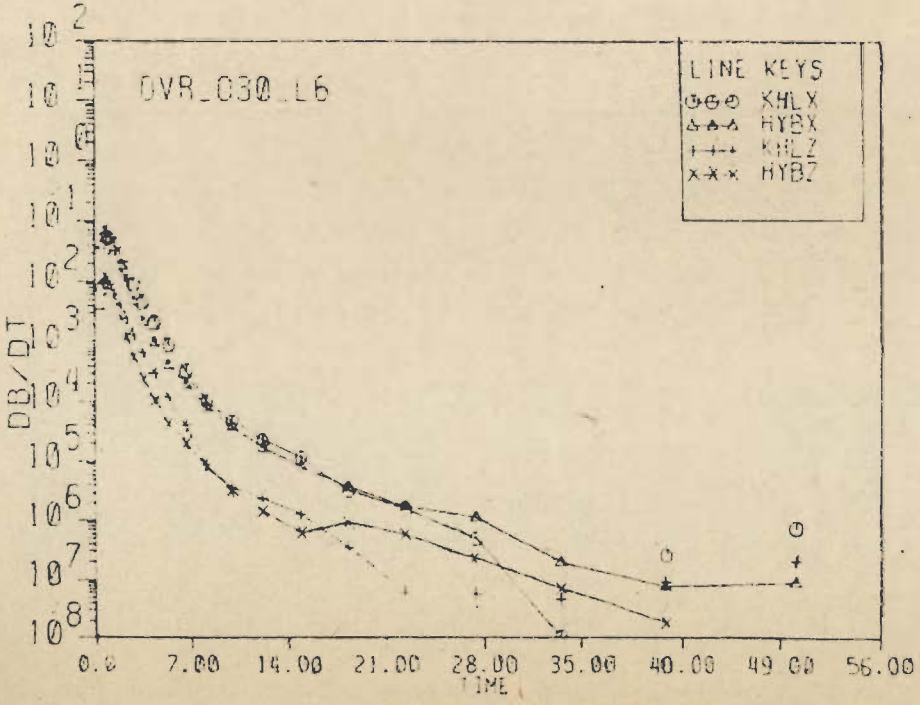

Fig. 5.19 The decay curves for dB_x/dt and dB_z/dt obtained using CFEM algorithm SAMAYA (HYBX, HYBZ) and the thin sheet algorithm (KHLX, KHLZ). The host-target resistivity contrast is 250, while the overburden resistivity is 10 Ohm m and thickness is 30 m. The three sets correspond to receiver positions -90, -50 and -10 m from the centre.

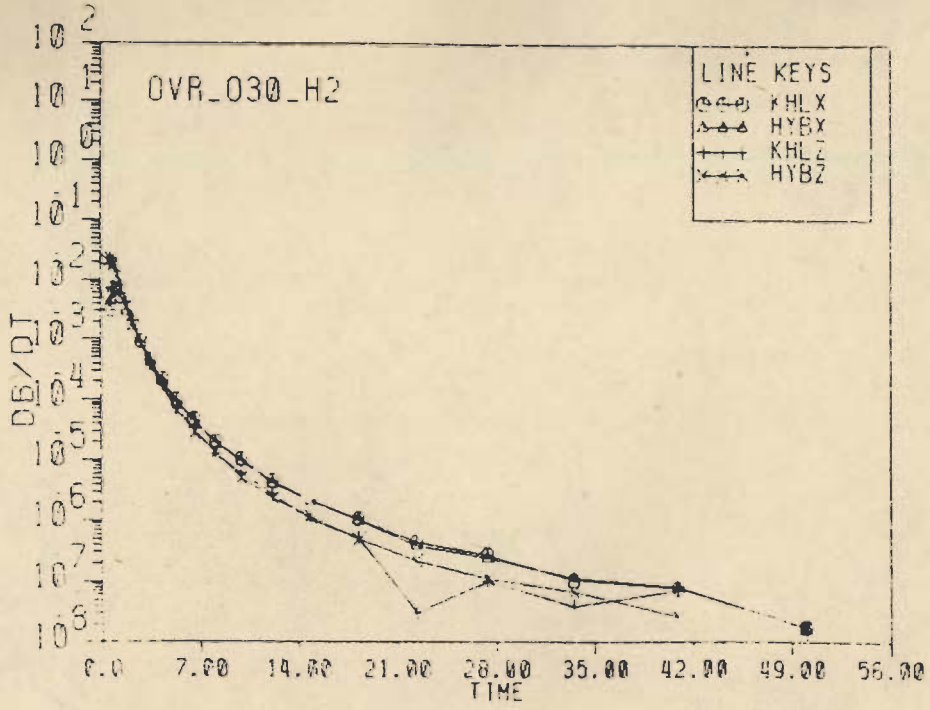

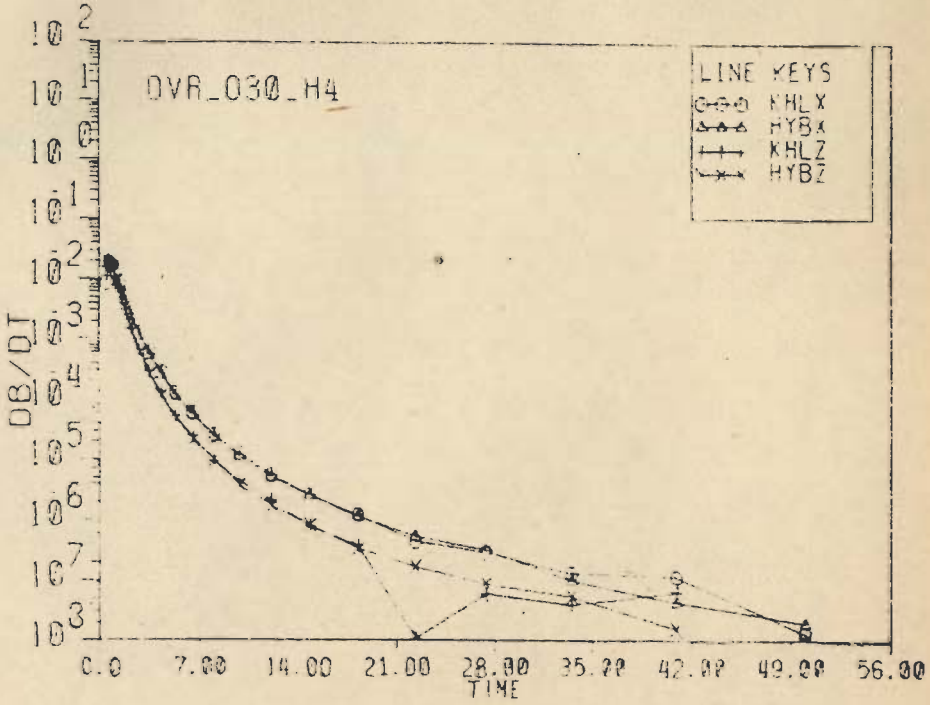

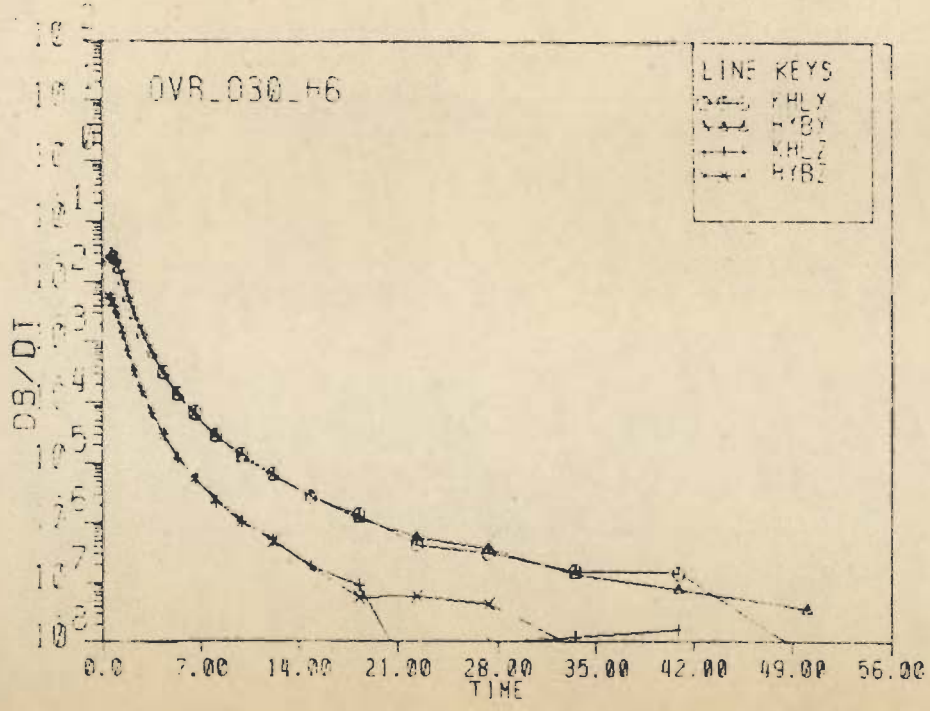

Fig. 5.20 The decay curves for dB_x/dt and dB_z/dt obtained using CFEM algorithm SAMAYA (HYBX, HYBZ) and the thin sheet algorithm (KHLX, KHLZ). The host-target resistivity contrast is 20, while the overburden resistivity is 10 Ohm m and thickness is 30 m. The three sets correspond to receiver positions -90, -50 and -10 m from the centre.

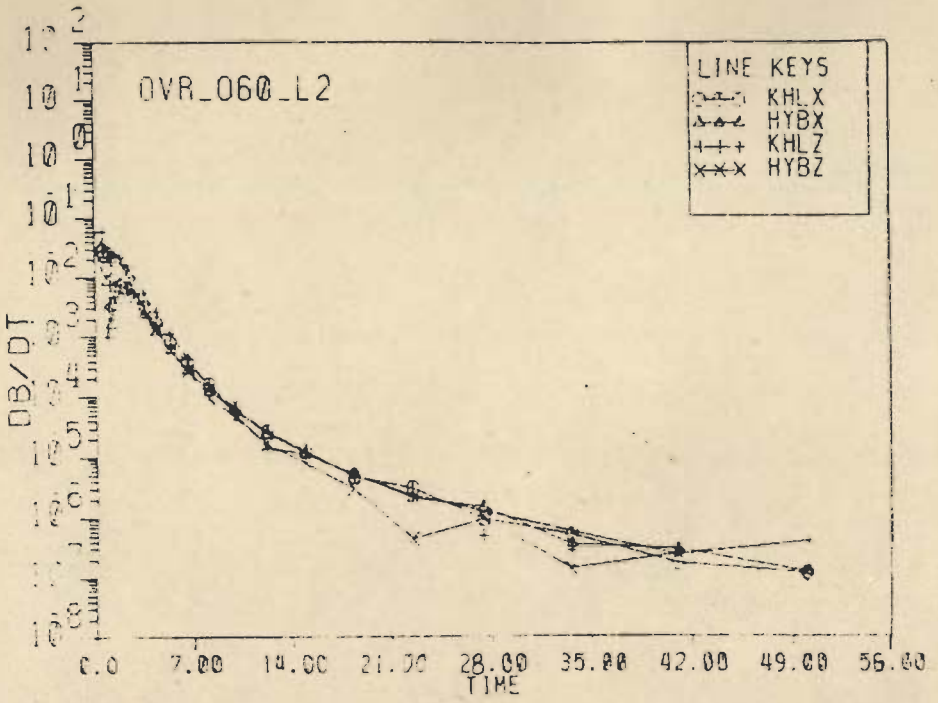

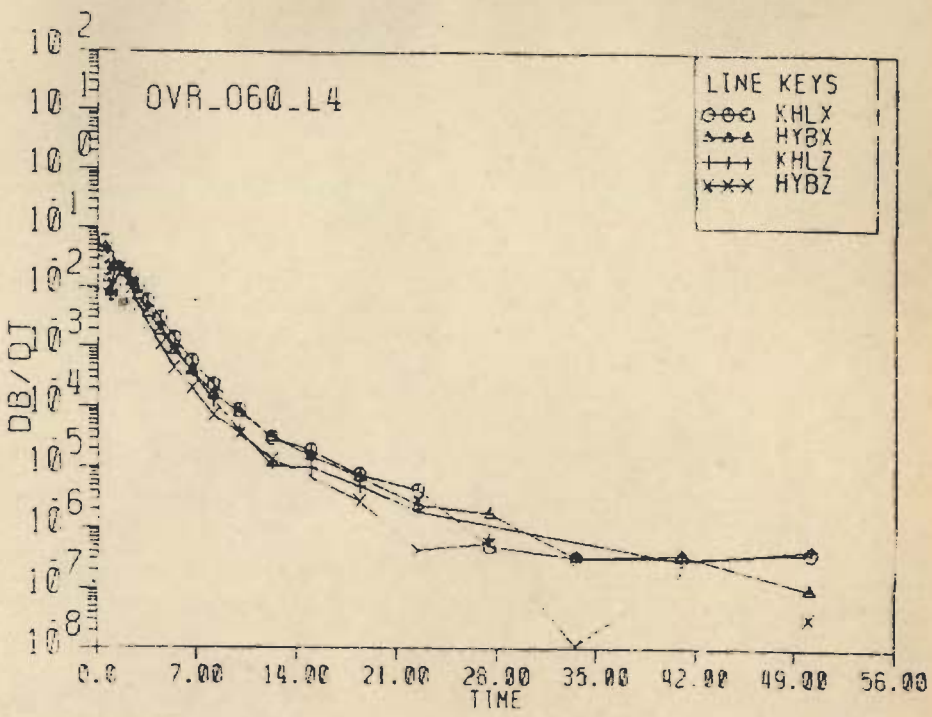

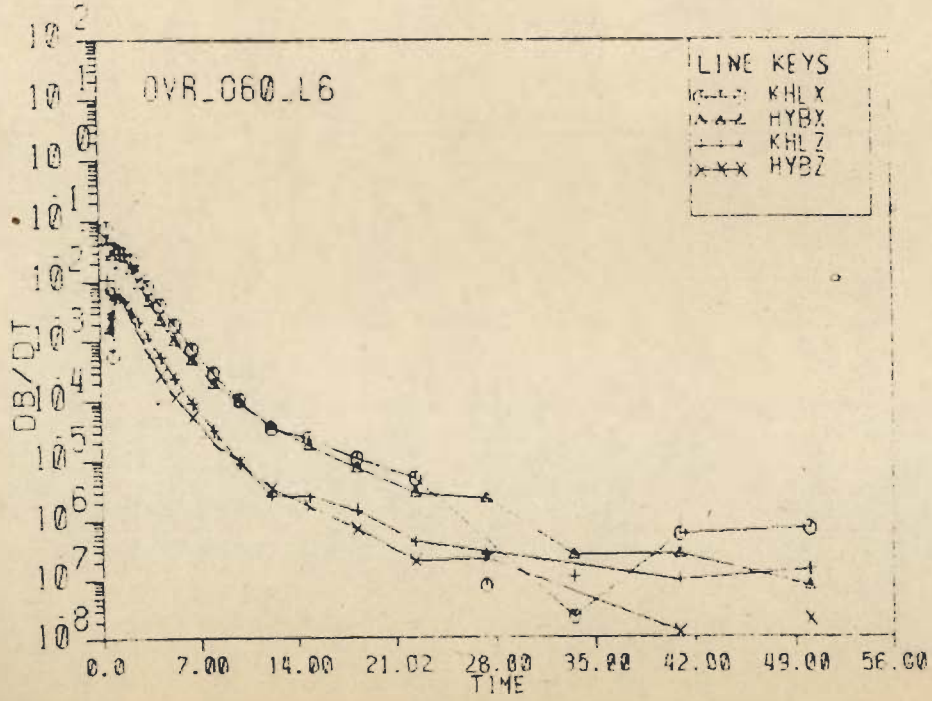

Fig. 5.21 The decay curves for dB_x/dt and dB_z/dt obtained using CFEM algorithm SAMAYA (HYBX, HYBZ) and the thin sheet algorithm (KHLX, KHLZ). The host-target resistivity contrast is 250, while the overburden resistivity is 10 Ohm m and thickness is 60 m. The three sets correspond to receiver positions -90, -50 and -10 m from the centre.

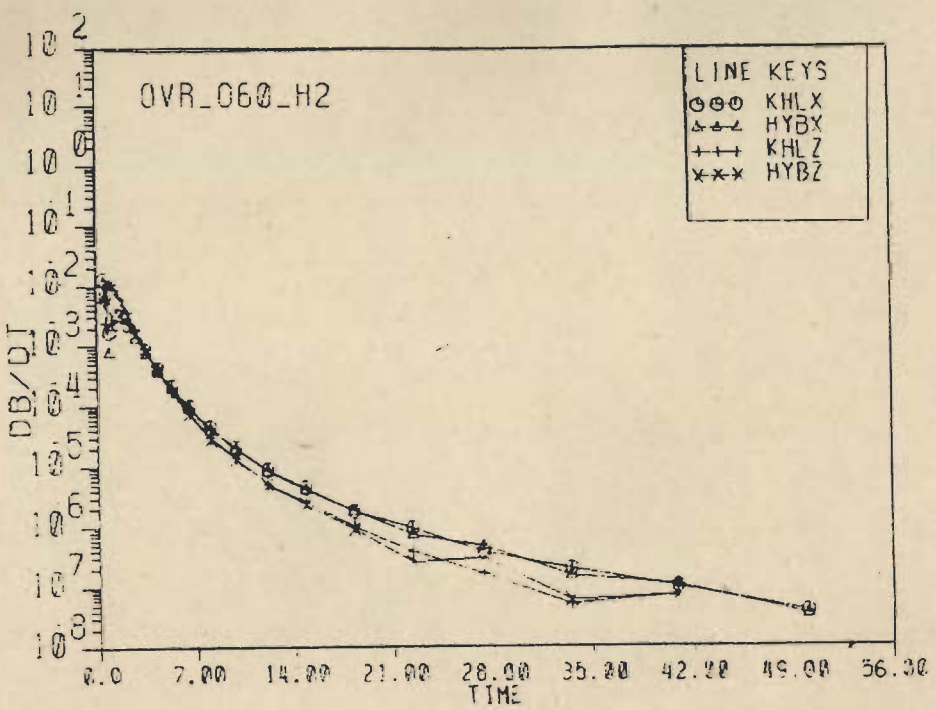

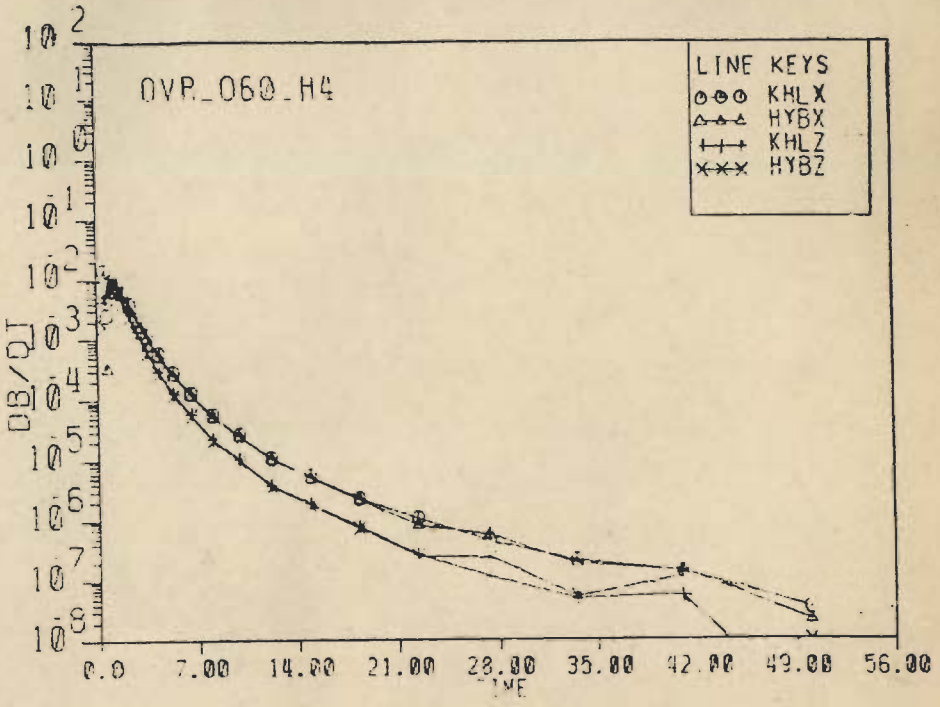

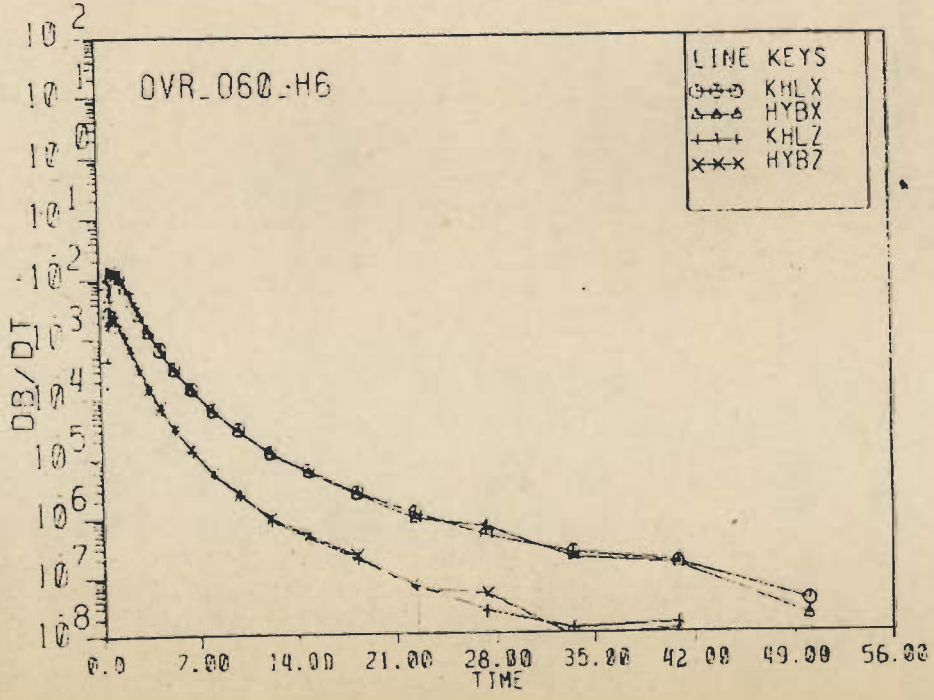

Fig. 5.22 The decay curves for dB_x/dt and dB_z/dt obtained using CFEM algorithm SAMAYA (HYBX, HYBZ) and the thin sheet algorithm (KHLX, KHLZ). The host-target resistivity contrast is 20, while the overburden resistivity is 10 Ohm m and thickness is 60 m. The three sets correspond to receiver positions -90, -50 and -10 m from the centre.

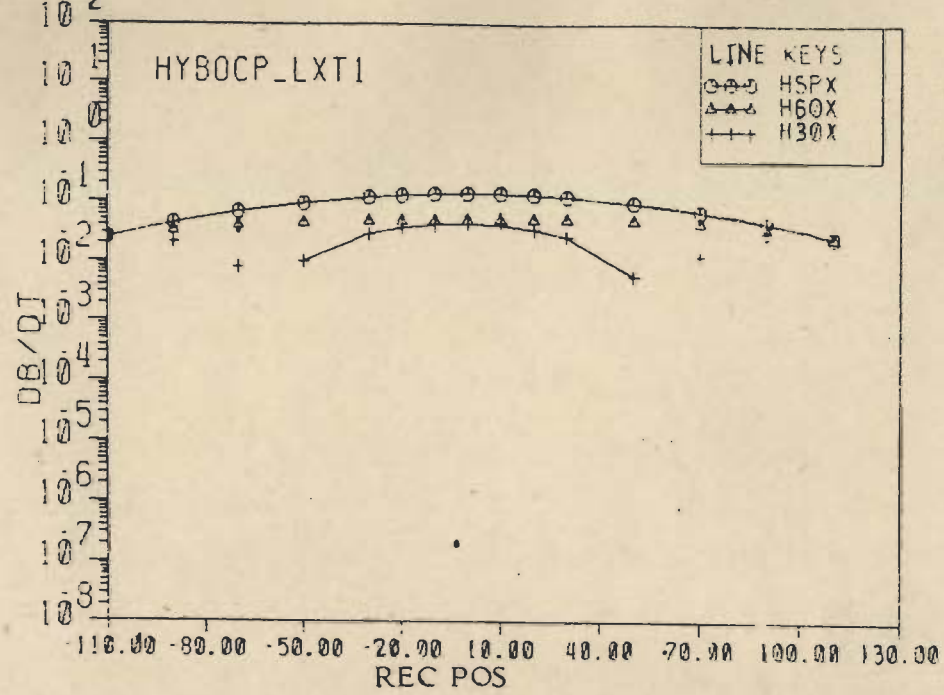

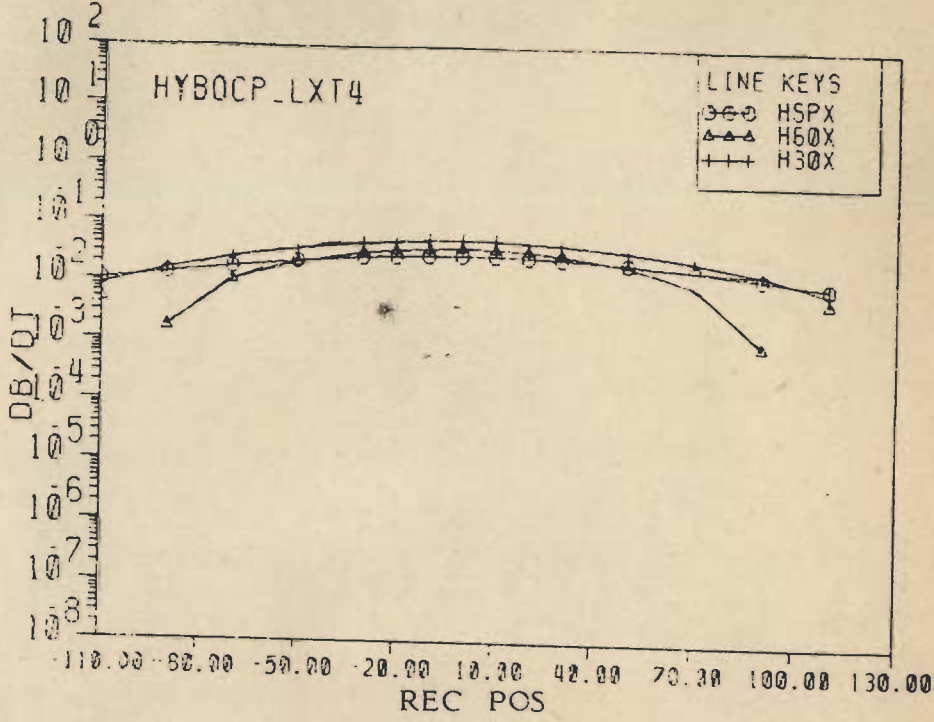

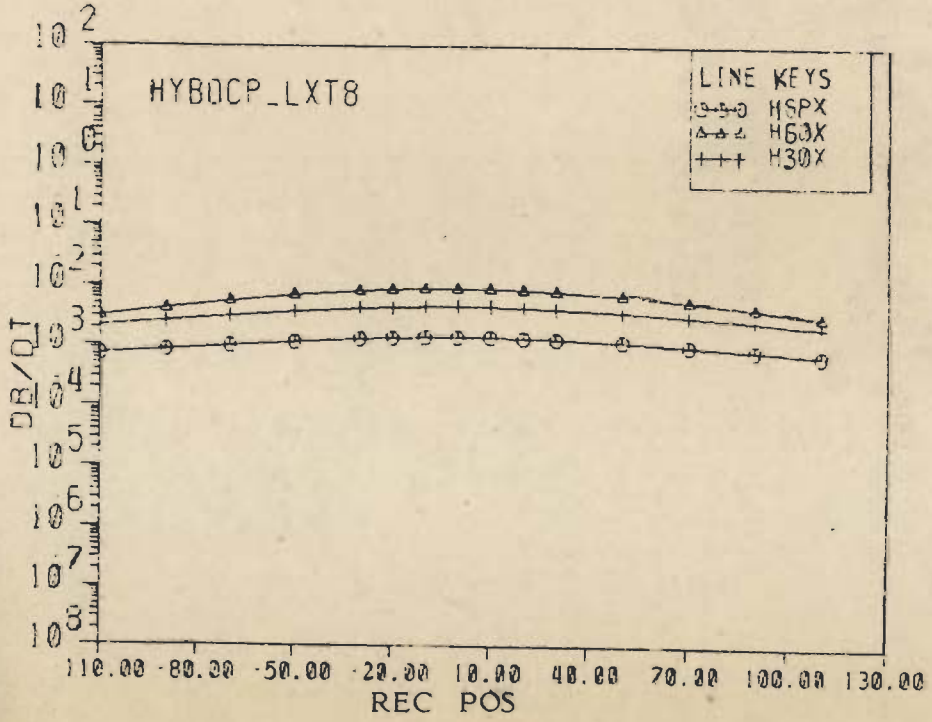

Fig. 5.23 Comparison of the dB_x/dt profiles for half-space and 30 and 60 m overburden cases. The host-target resistivity contrast is 250 and overburden resistivity is 10 Ohm m. The three sets correspond to the delay-times (from bottom of the ramp) 0.553, 1.17 and 2.85 mS.

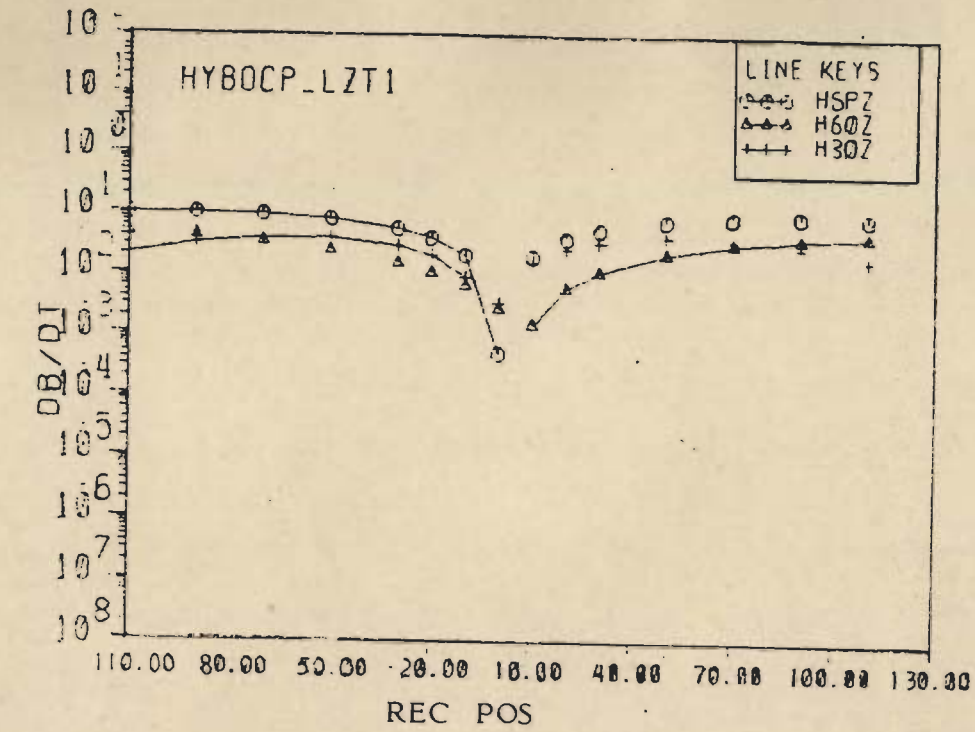

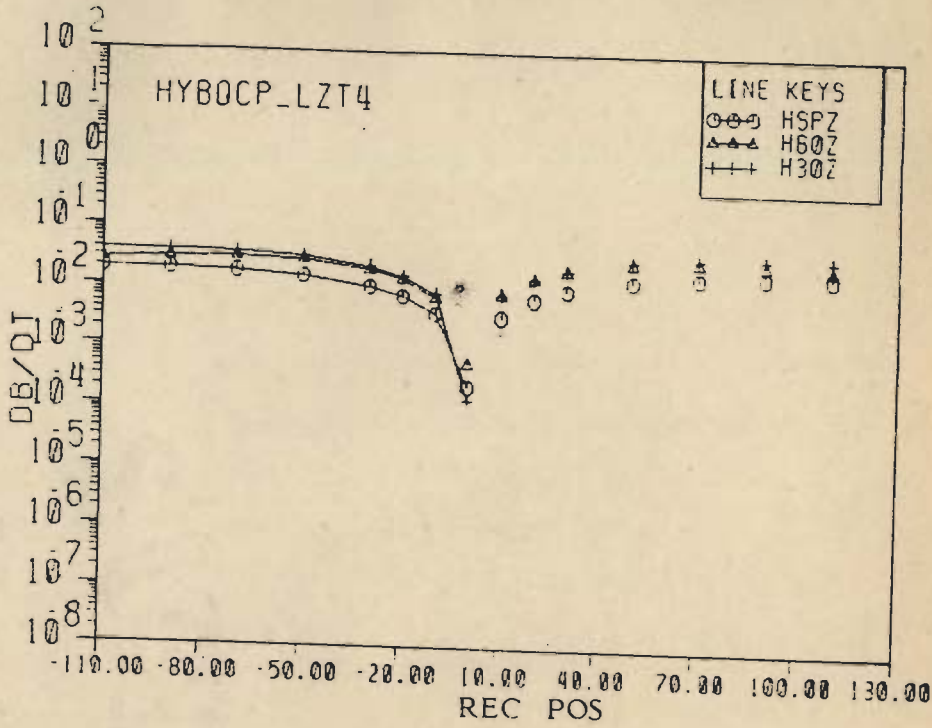

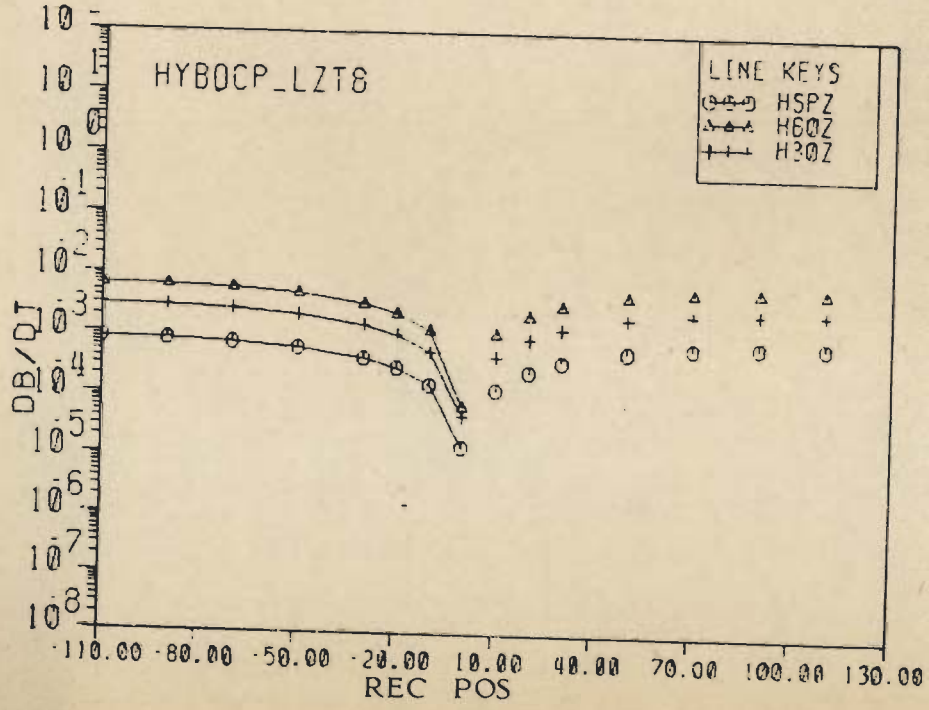

Fig. 5.24 Comparison of the dB_z/dt profiles for half-space and 30 and 60 m overburden cases. The host-target resistivity contrast is 250 and overburden resistivity is 10 Ohm m. The three sets correspond to the delay-times (from bottom of the ramp) 0553, 1.17 and 2.85 mS.

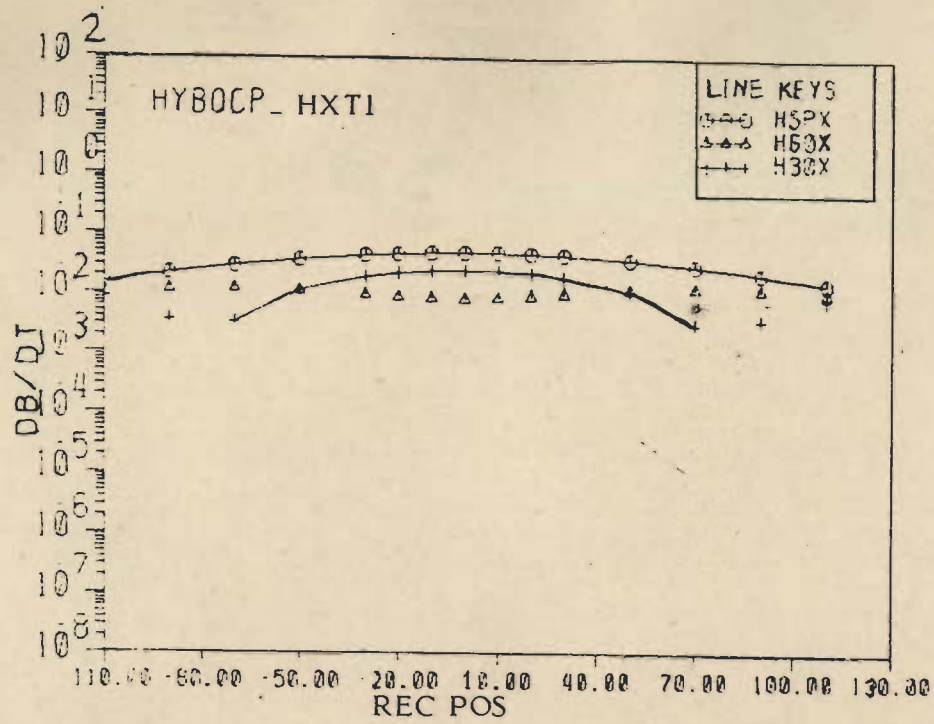

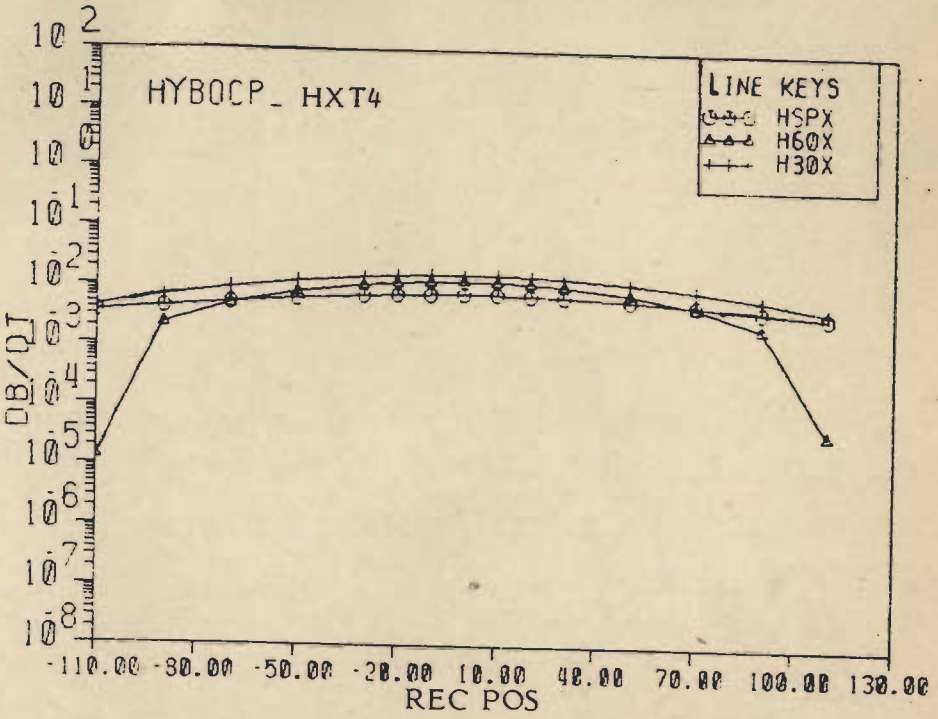

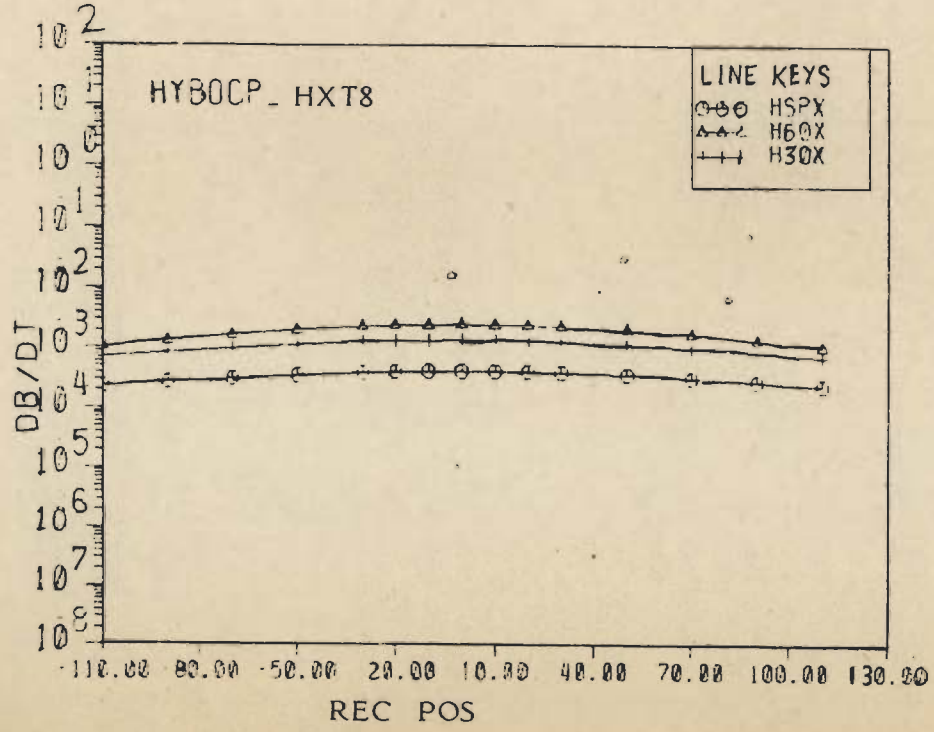

Fig. 5.25 Comparison of the dB_x/dt profiles for half-space and 30 and 60 m overburden cases. The host-target resistivity contrast is 20 and overburden resistivity 10 Ohm m. The three sets correspond to the delay-times (from bottom of the ramp) 0.553, 1.17 and 2.85 mS.

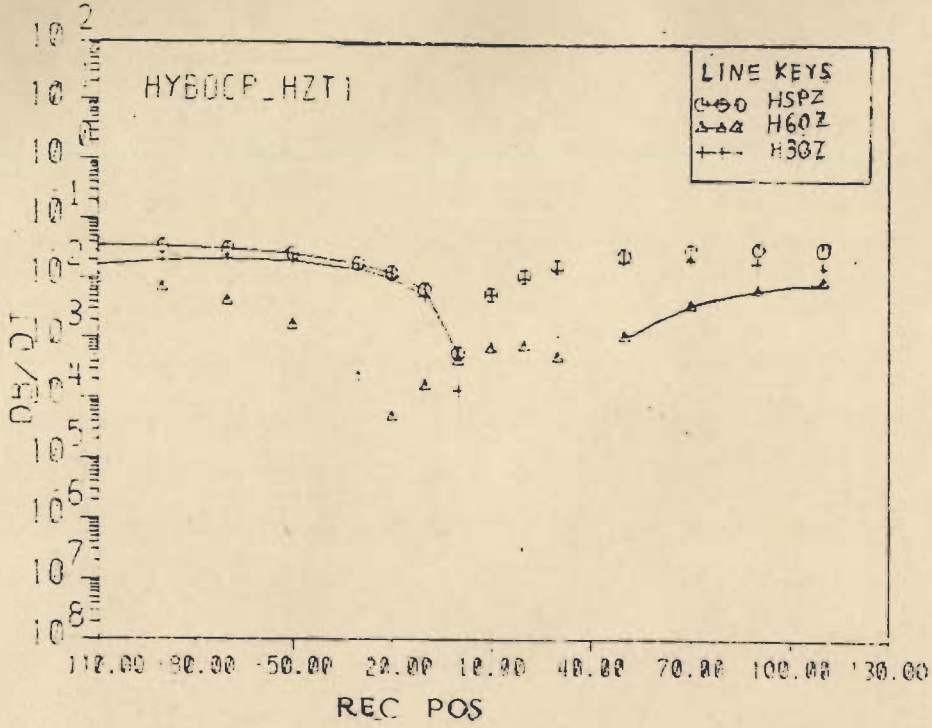

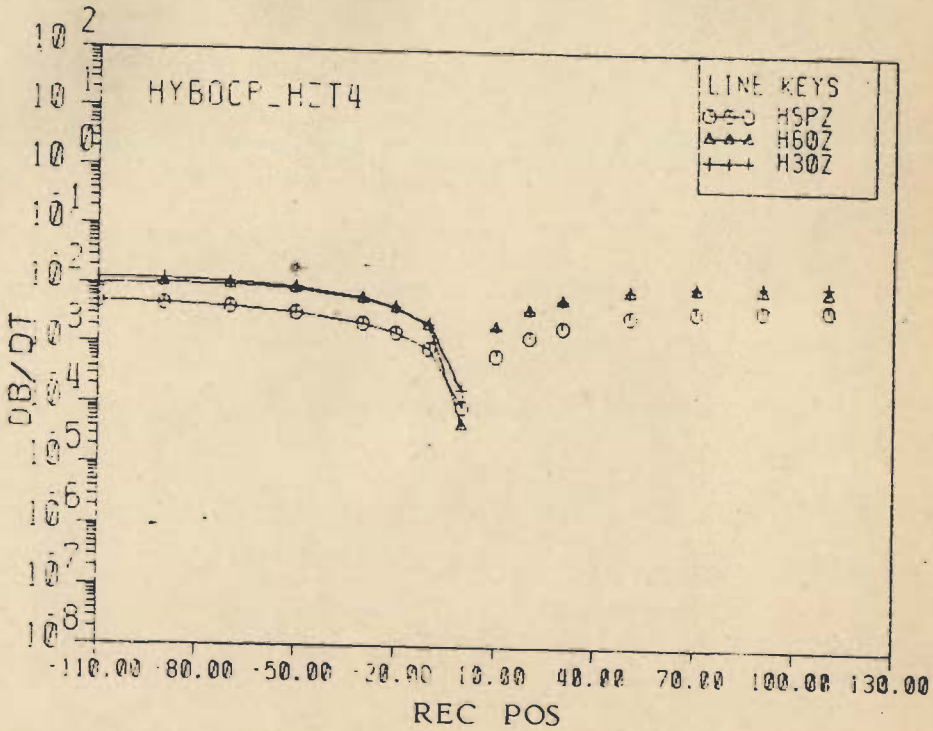

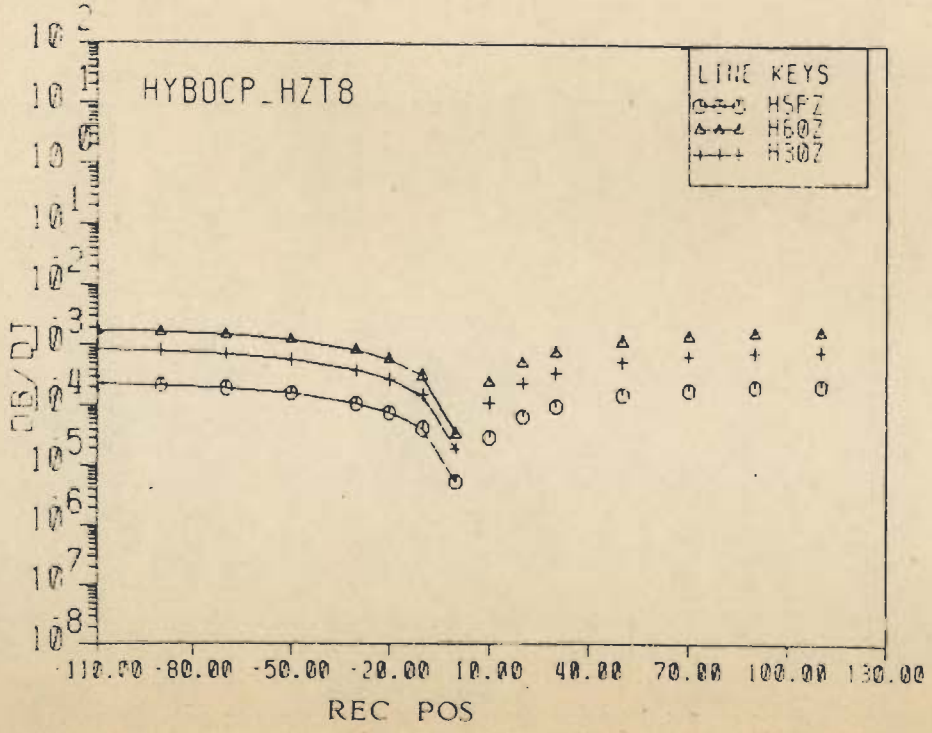

Fig. 5.26 Comparison of the dB_z/dt profiles for half-space and 30 and 60 m overburden cases. The host-target resistivity contrast is 20 and overburden resistivity 10 Ohm m. The three sets correspond to the delay-times (from bottom of the ramp) 0.553, 1.17 and 2.85 mS.

that an empirical relationship between such time value and the overburden thickness may be discovered by comparing overburden thickness and the decay parameter $\sqrt{t/\mu\sigma}$ for a large number of models, σ being the conductivity of the overburden.

5.10 DOWNHOLE STUDY

A test run was made with the base model to generate a profile along a borehole that was inclined at an angle of 45^{o} to the surface. The comparative plots of surface and downhole curves of x and z-components for three delay time values 0.553, 1.48 and 8.1 mS are given in Fig. 5.27. An interesting feature of the downhole x-component curves is that unlike their surface counterparts, these curves are almost parallel to the abscissa for all delay times. As far as, the z-component curves are concerned, the downhole ones are similar in nature to the surface ones but these possess higher magnitudes.

5.11 DISCUSSION

The results presented in sections 5.2 - 5.6 lead to the conclusion that the frequency domain algorithms HYBRIDC and SANGAM are stable, convergent and accurate. Earlier, in chapter-IV, it was shown that these algorithms are more accurate than and require less computer CPU time than the original Hybrid algorithm HYBRIDB. However, the price paid is in terms of higher memory and storage requirement than is needed for HYBRIDB. It follows that whereas cost-effectiveness of HYBRIDB and SANGAM will depend on the relative costs of CPU time and memory/storage, the higher accuracy of HYBRIDC and SANGAM justify the use of these algorithms over HYBRIDB.

The time-domain algorithm SAMAYA yields better results than the integral equation algorithm whenever the resistivity contrast is less than 250. Since the very high contrast value results can be satisfactorily approximated by

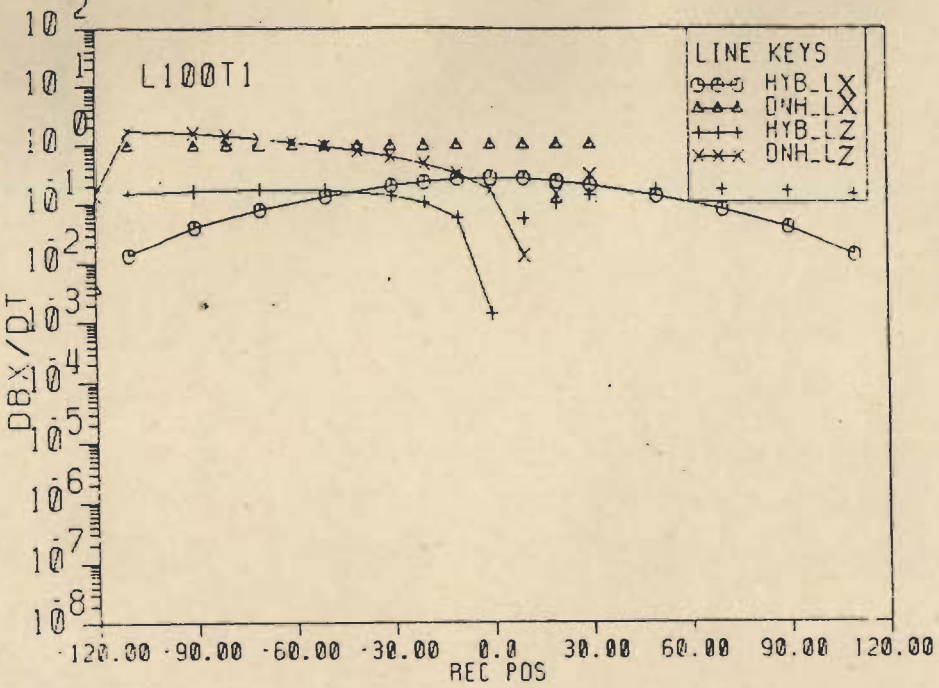

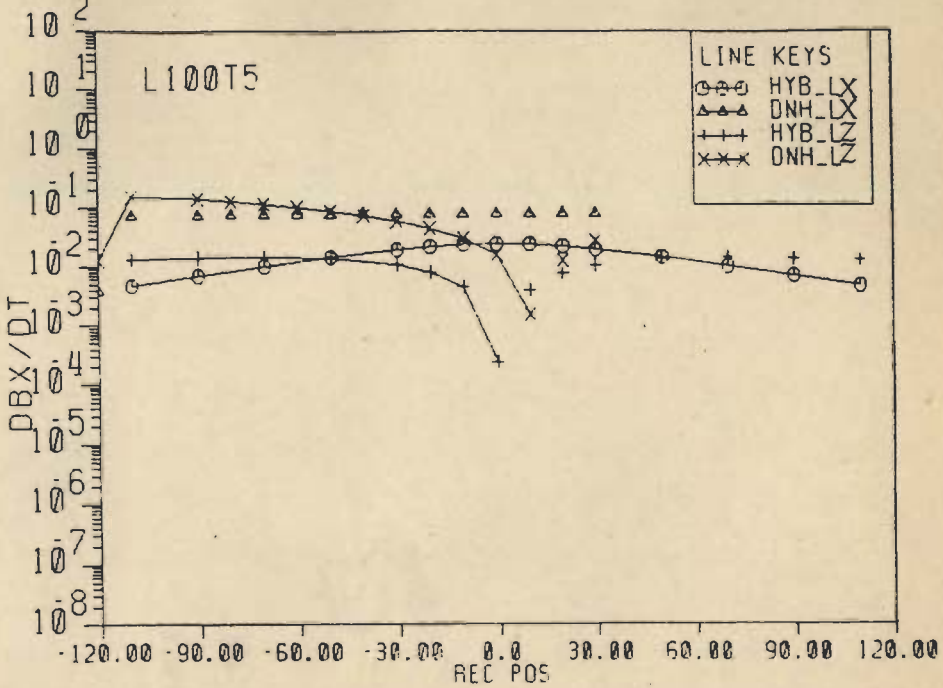

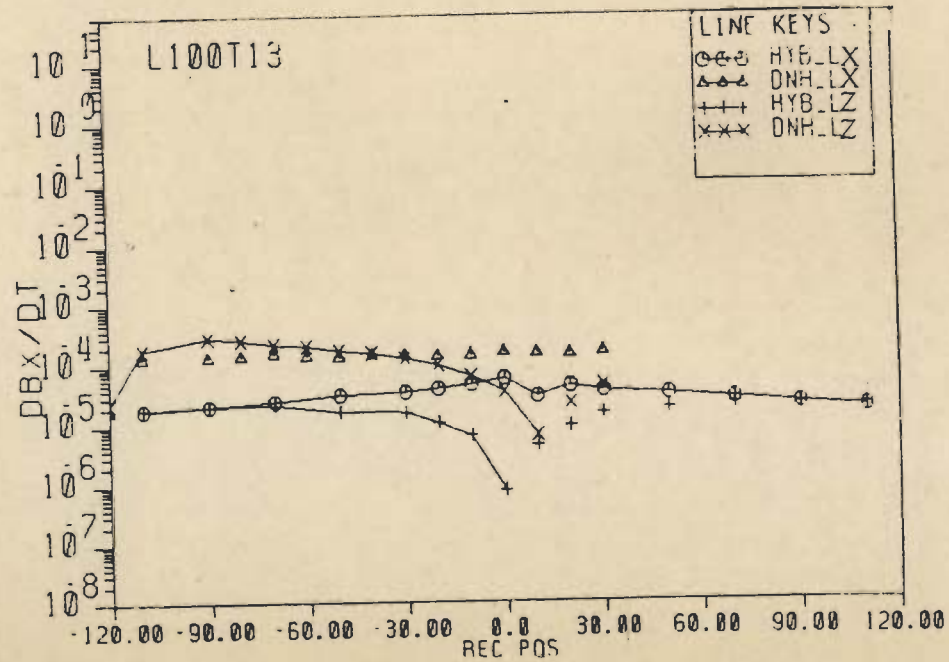

Fig. 5.27 Comparison of the dB_x/dt and dB_z/dt profiles for observations at surface (HYB-LX, HYB-LZ) and in a 45^{o} borehole (DNH-LX, DNH-LZ). The three sets correspond to the delay-times (from bottom of the ramp) 0.553, 1.48 and 8.1 mS.

the free space results, the restriction on contrast value is not a serious handicap for SAMAYA. Hence, it can be usefully employed for 3-D forward modelling of EM methods.

CHAPTER - VI

CONCLUDING REMARKS AND SCOPE FOR FUTURE WORK

6.1 CONCLUDING REMARKS

The three CFEM algorithms - HYBRIDC, SANGAM and SAMAYA - developed in this thesis offer an efficient and reliable set of software packages for 3-D forward EM modelling. The first two algorithms deal with the FDEM problem, while the third one deals with the TDEM problem. These algorithms have been as rigorously and comprehensively tested as was possible in the limited time framework of the study and under the given computing environment. All studies conducted to investigate the efficacy of these algorithms yielded encouraging results, thereby generating confidence in them. A comparison of the results obtained using these algorithms with those obtained using other algorithms further enhanced this confidence. It may be stressed here that when results from two different algorithms are not in agreement, no definite conclusion can be drawn in favour of one or the other because neither can be treated as a standard, in the absence of theoretical results. All that one can say in such a case is that at least one of these algorithms must be yielding incorrect results. On the other hand, if the two sets of results are found to be in agreement, then the faith in the correctness of both increases, particularly if the two formulations are distinctly different. The former situation arose only when SAMAYA results were compared with those from the IEM algorithm of San Filipo et.al. (1985 a). In other cases, the latter situation was obtained. Hence, a qualified faith in the algorithms HYBRIDC, SANGAM and SAMAYA is justified and further studies with these algorithms should be planned. Two important areas for such studies are - i) enhancement of the efficiency and versatility of these algorithms and

ii) use of these algorithms in developing interpretational aids for 3-D cases.

6.2 ENHANCEMENT OF EFFICIENCY OF THE ALGORITHMS

The operations consuming maximum time and storage in these algorithms pertain to the computation of the Green's functions. In fact, it was in the more efficient computation of the Green's functions that first advantage was scored over HYBRIDB. However, there is still considerable scope for improvement if efforts are directed in the following three directions :

i) towards discovering the exact relationship between (a) the (r,z) pairs for which Green's function convolution integrals need be computed, and (b) the parameters on which these depend. This will eliminate the need of search routines and thereby reduce time and storage requirements, latter significantly.

ii) towards developing a shorter and efficient set of digital filters that can be used in convolution operations. This will bring about substantial saving in computing time.

iii) towards using higher order shape functions such as parametric shape functions (Zienkiewicz, 1977). This will enhance accuracy of the algorithm.

Another important area where significant improvement is possible is that of matrix equation solving routines. Here, the Gaussian elimination in its simplest form has been employed. It is suggested that for iterative scheme (HYBRIDC), where the coefficient matrix is banded and sparse, these features, particularly sparsity, should be more efficiently exploited, for example, by using the minimum degree algorithm developed by George and Liu (1980). In case of direct scheme (SANGAM), where sparsity is not assured

a-priori, the matrix must be carefully scrutinized for a number of models and if any persistent structure can be identified, it should be exploited for judicious partitioning of matrix (else, arbitrary partitioning can be performed) and algorithms for partitioned matrices should be employed for equation solving. Further, for both the schemes, the iterative matrix equation solvers should also be tried.

In SAMAYA, the number of frequencies needed for transformation from frequency to time domain must be reduced as much as possible by developing new strategies that would need fewer frequencies and yet yield stable and accurate time domain results. One such possibility is the use of decay spectrum technique discussed by Lamontagne (1975), Tripp (1982) and Newman et.al. (1986).

Wherever possible, the possibility of pipelining and parallel computing should be brought out. One such experiment was conducted during this study, in solving a matrix equation on the Floating Point System FPS120B array processor. The resulting improvement in time was by a factor of 30 in comparison to Vax 11/780. For the main program, additional saving will accrue from the fact that whilst the array processor is performing one set of computation, the main computer would be performing another set. For such pipelining and parallel computing, the algorithms will have to be restructured.

6.3 ENHANCEMENT OF VERSATILITY OF THE ALGORITHMS

In their present form, the algorithms HYBRIDC, SANGAM and SAMAYA are capable of dealing with targets buried in the half-space of a two layered earth. This limitation can be removed by rendering the algorithms usable in cases, where the target lies anywhere in a multilayered earth, by employing the expressions of Green's functions given by Wannamaker et.al. (1984 a).

Further, an attempt should be made to develop Green's functions for primary earth models, other than the layered earth model. One such model with wide application is that of a faulted layered earth.

6.4 USE OF THE ALGORITHMS IN DEVELOPMENT OF INTERPRETATIONAL AIDS

The dream of a 3-D inversion program can not be realized until the cost of forward computations can be drastically reduced. This challenge lies behind the motivation towards a continued refinement of forward modelling algorithms. In their present form, these algorithms are unlikely to be widely used even for forward modelling, unless the high requirement of computer time and storage is significantly reduced. Until then, however, they could be profitably employed in preparing catalogues of responses for some chosen important shapes of 3-D bodies. A critical comparison of 3-D response curves with the corresponding 1-D/2-D curves can then be made with attempts to identify definitive features of 3-D response curves that discriminate these from corresponding 1-D/2-D curves. Finally, these definitive features can be correlated with the parameters of the 3-D body and some useful guidelines for 3-D interpretation can be prepared.

REFERENCES

Abbreviations used :

GE - Geophysics

GP - Geophysical Prospecting

GJRAS - Geophysical Journal of Royal Astronomical Society

JGR - Journal of Geophysical Research

Adam A., 1976, 'Geoelectric and Geothermal Studies', KAPG Geoph. Mon., Budapest: Akademiai Kiado.

Adhidjaja J.I., Hohmann G.W., Oristaglio M.L., 1985, 'Two-dimensional Transient Electromagnetic Responses', GE, **50**(12), 2849-2861.

Anderson R., Pelton W.H., 1985, 'MT Exploration in Volcanic Cover, Overthrust Belts and Rift Zones', 55th SEG Meeting Washington, MT 7, 274-276.

Anderson W.L., 1979, 'Numerical Integration of Related Hankel Transforms of Orders 0 and 1 by Adaptive Digital Filtering', GE, **44**(7), 1245-1265.

ibid, 1984, 'Computation of Green's Tensor Integrals for Three-dimensional Electromagnetic Problem Using Fast Hankel Transforms', GE, **49**, 1754-1759, 1811-1812.

Annan A.P., 1974, 'The Equivalent Source Method for Electromagnetic Scattering Analysis and its Geophysical Applications', Ph.D. Thesis submitted at the Memorial University of Newfoundland.

Arora C.L., Bose R.N., 1981, 'Demarcation of Fresh-and Saline-Water Zones Using Electrical Methods (Abohar Area, Ferozpur District, Punjab)' Jr. of Hydrology, **49**, 75-86.

Banks R.J., Beamish D., 1984, 'Local and Regional Induction in the British Isles', GJRAS, **79**, 539-553.

Barnett C.T., 1984, 'Simple Inversion of Time-Domain Electromagnetic Data', GE, **49**, 925-933.

Becker A., DeCarle R., Lazenley P.G., 1984, 'Simplified Prediction of Transient Electromagnetic Response', GE, **49**, 913-917.

Berdichevsky M.N., Dmitriev V.I., 1976, 'Distortion of Magnetic and Electrical Fields by Near-surface Lateral Inhomogeneities', Acta, Geod. Geophys. Mont. Hung., **11**, 447-483.

Berdichevsky M.N., Zhdanov M.S., 1984, 'Advanced Theory of Deep Geomagnetic Sounding', Elsevier - Amsterdem-Oxford-New York-Tokyo. ISBN 0-444-42189-0.

Berkman E., Orange A., 1985, 'Interesting Aspects of Magnetotelluric Data in Northwestern Montana', 55th SEG Meeting, Washington, MT6, 271-274.

Best M.E., Duncan P., Jacobs F.J., Scheen W.L., 1985, 'Numerical Modelling of the Electromagnetic Response of Three-dimensional Conductors in a Layered Earth', GE, **50**(4), 665-676.

De Boor C., 1978, 'A Practical Guide to Splines', Springer Verlag, New York.

Buselli G., 1985, 'Stratigraphic Mapping Applications of TEM', ASEG Bull., **16**(2/3), 177-179.

Butt G.R., 1985, 'Case Histories Showing Various Applications of a Combined INPUT - Magnetometer-Spectrometer Airborne Geophysical System in Australia', ASEG Bull., **16**(2/3), 180-182.

Cauterman M., Degauque P., Demoulin B., Gabillard R., 1978, 'Remote Sensing of Buried Resistive Inhomogeneities by Electromagnetic Transmission Measurements Between the Ground Surface and a Borehole - Theory and Experiment', Radio Science, **13**(2), 371-378.

Cermak I.A., Silvester P., 1968, 'Solution of 2-Dimensional Field Problems by Boundary Relaxation', Proc. IRE, **115**(9), 1341-1348.

Craven B.L., Hayden W.B., Smith M.J., 1985, 'A Comparison of Electromagnetic Prospecting Results at the Scuddles Cu-Zn Massive Sulphide Deposit, Golden Grove Area, Western Australia', ASEG Bull., **16**(2/3), 194-197.

Cull J.P., 1985, 'Magnetotelluric Soundings Over a Precambrian Contact in Australia', GJRAS, **80**, 661-675.

Das U.C., Verma S.K., 1981, 'Numerical Considerations on Computing the EM Response of Three Dimensional Inhomogeneities in a Layered Earth', GJRAS, **66**, 733-740.

ibid, 1982, 'EM Response of an Arbitrarily Shaped Three Dimensional Conductor in a Layered Earth-Numerical Results', GJRAS, **68**, 55-66.

Dawson T.W., Weaver J.T., 1979, 'Three-dimensional Induction in a Non-uniform Thin Sheet at the Surface of a Uniformly Conducting Earth', GJRAS, **59**, 445-462.

Degauque P., Demoulin B, Cauterman M., 1986, 'Transient Response of a Deposit Excited by a Pulse Current', IEEE Trans. on Geosci. and Remote Sensing, **GE-24**(5), 674-678.

Dey A., Morrison H.F., 1979, 'Resistivity Modeling for Arbitrarily Shaped Three-dimensional Structures', GE, **44**, 753-780.

Dodds S., Ivic D., 1985, 'Integrated Geophysical Methods Used for Groundwater Studies in the Polda and Murray Basins', ASEG Bull, **16**(2/3), 204-206.

Dyck A.V., West G.F., 1984, 'The Role of Simple Computer Models in Interpretations of Wide-band, Drill-hole Electromagnetic Surveys in Mineral Exploration', GE, **49**, 957-980.

Eaton P.A., Hohmann G.W., 1984, 'The Influence of a Conductive Host on Two-dimensional Borehole Transient Electromagnetic Responses', GE, **49**(7), 861-869.

Flores C., Edwards R.N., 1985, 'Approximate Calculation of Low-frequency 3-D Magnetotelluric Responses Using a Multiple Plate Model', 55th SEG Meeting Washington, (MT 3), 262-264.

Frischnecht F.C., 1966, 'Application of Electromagnetic Surveying to Geologic Mapping in Northern Main', SEG Minning Geophysics, Vol.I, 10-17.

Gallagher R., 1985, Private Communication.

George A., Liu W.H., 1980, 'A Minimum Storage Implementation of the Minimum Degree Algorithm', SIAM Jr. Num. Anal., **17**(1), 282-299.

Goldman Y., Hubans C., Nicoletis S., Spitz S., 1986, 'A Finite Element Solution of TEM Response of an Arbitrary 2-D Resistivity Distribution', GE, **51**(7), 1450-1461.

Goldman M.M., Stoyer C.H., 1983, 'Finite Difference Calculations of the Transient Field of an Axially Symmetric Earth for Vertical Magnetic Dipole Excitation', GE, **48**(7).

Gough D.I., 1973, 'The Geophysical Significance of Geomagnetic Variation Anomalies', Phys. Earth Planet. Inter., **7**, 379-388.

ibid, 'The Interpretation of Magnetometer Array Studies', GJRAS, **35**, 83-98.

ibid, 1983, 'Electromagnetic Geophysics and Global Tectonics', JGR, **88**(B4), 3367-3377.

Green V.R., Weaver J.T., 1978, 'Two-dimensional Induction in a Thin Sheet of Variable Integrated Conductivity at the Surface of a Uniformly Conducting Earth', GJRAS, **55**, 721-736.

Haigh J.E., Nelson R.G., 1985, 'Geophysical Investigations of Dolines in Lateritic Terrain', ASEG Bull, **16**(2/3), 224-226.

Hanneson J.E., West G.F., 1984, 'The Horizontal Loop Electromagnetic Response of a Thin Plate in a Conductive Earth: Part I - Computational Method', GE, **49**(4), 411-420.

ibid, '..... Part II - Computational Results and Examples', ibid, 421-432.

Hermance J.F., 1983, 'DC Telluric Fields in Three-dimensions : A Refined Finite Difference Simulation Using Local Integral Forms', GE, **48**, 331-340.

Hewson-Brown R.G., Kendall P.C., 1976, 'Magnetotelluric Modelling and Inversion in Three-dimensions', Acta Geodaet. Geophys. et. Mont. Acad. Hung., **11**(3-4), 427-446.

Hobbs B.A., 1975, 'Analytical Solutions to Global and Local Problems of Electromagnetic Induction in the Earth', Phys. Earth Planet. Inter., **10**, 250-261.

Hofstadter D.R., 1982, 'Godel, Escher, Bach : An Eternal Golden Braid', Penguin Books, ISBN 0140055797.

Hohmann G.W., 1975, 'Three-dimensional Induced Polarisation and Electromagnetic Modeling', GE, **40**(2), 309-324.

ibid, 1983(a), 'Numerical Modelling for Electrical Geophysical Methods', in Proc. Intl. Symp. App. Geophys. in Tropical Regions, Belem, Brazil, Sept.1-8, 1982, Ed., Lourenco JS, Rijo L.

ibid, 1983(b), 'Three-dimensional EM Modelling', Geophysical Surveys, **6**, 27-53.

Holland R., 1977, 'THREDE : A Free-field EMP Coupling and Scattering Code', IEEE Trans. Nucl. Sci., **NS-24**, 2416-21.

Holmes J.J., Balanis C.A., 1977, 'Electromagnetic Modeling of Reflections Inside an In-situ Gasified Coal Seam', Radio Science, **12**(1), 33-40.

Hoover D.B., Long C.L., Senterfit R.M., 1978, 'Some Results from Audiomagnetotelluric Investigations in Geothermal Areas', GE, **43**(7), 1501-1514.

Hutton R., 1976(a), 'Induction Studies in Rifts and Other Active Regions', Acta Geod. Geoph. Mont. Hung., **11**, 347-376.

ibid, 1976(b), 'The Electrical Conductivity of the Earth and Planets', Reports on Progress in Physics, **39**, 487-572.

Hutton V.R.S., Sik J.M., Gough D.I., 1977, 'Electrical Conductivity and Tectonics of Scotland', Nature, **266**, 617-620.

James B.A., 1985, 'Efficient Microcomputer Based Finite-Difference Resistivity Modelling via Polozhii Decomposition', GE, **50**(3), 443-465.

Jones F.W., 1973, 'Induction in Laterally Non-uniform Conductors : Theory and Numerical Models', Phys. Earth Planet. Inter., **7**, 282-293.

ibid, 1974, 'The Effect of an Island and Bay Structure on Alternating Geomagnetic Fields at Three Periods', GJRAS, **36**, 627-639.

Jones F.W., Lokken J.E., 1975, 'Irregular Coastline and Channeling Effects in Three-dimensional Geomagnetic Perturbation Anomalies', Phys. Earth Planet. Inter., **10**, 140-150.

Jones F.W. and Pascoe L.J., 1972, 'The Perturbation of Geomagnetic Fields by Three-dimensional Conductive Inhomogeneities', GJRAS, **27**, 479-485.

Jones F.W., Vozoff K., 1978, 'The Calculation of Magnetotelluric Quantities for Three-dimensional Conductivity Inhomogeneities', GE, **43**, 1167-1175.

Jupp D.L.B., Vozoff K., 1977, 'Two-dimensional Magnetotelluric Inversion', GJRAS, **50**, 333-352.

Kaikkonen P., Panjunpaa K., 1984, 'Audiomagnetotelluric Measurements Across the Lake Ladoga-Bothnian Bay Zone in Central Finland', GJRAS, **78**, 439-452.

Kamara A.Y.S., 1981, 'Review : Geophysical Methods for Kimberlite Prospecting', ASEG Bull., **12**, 43-51.

Kaufman A.A., Keller G.V., 1981, 'The Magnetotelluric Sounding Method', Elsevier-Amsterdem-Oxford-New York. ISBN 0-444-41863-6.

ibid, 1983, 'Frequency and Transient Soundings', ibid, ISBN 0-444-42032-0.

ibid, 1985, 'Inductive Mining Prospecting Part I : Theory', ibid, ISBN 0-444-42271-4.

Keller G.V., 1971, 'Natural-field and Controlled Source Methods in Electromagnetic Exploration', Geoexploration, **9**, 99-147.

Keller G.V., Frischnecht F.C., 1966, 'Electrical Methods of Geophysical Prospecting', Pergamon Press, New York, N.Y.

Koefoed O., Biewinga D.T., 1976, 'The Application of Electromagnetic Frequency Sounding to Groundwater Problems', Geoexploration, **14**(3/4), 229-241.

Kurtz R.D., Ostrowski J.A., Niblett E.R., 1986, 'A Magnetotelluric Survey Over the East Bull Lake Gabbro-Anorthosite Complex', JGR, **91**(B7), 7403-7416.

Lajoie J., West G.F., 1976, 'The Electromagnetic Response of a Conductive Inhomogeneity in a Layered Earth', GE, **41**, 1133-1156.

ibid, 1977, 'Two Selected Field Example of EM Anomalies in a Conductive Environment', GE, **42**, 655-660.

Lamontagne Y., 1975, 'Applications of Wideband Time-domain Electromagnetic Measurements in Mineral Exploration', Ph.D. Thesis, Univ. of Toronto.

Laterraca G.A., Madden T.R., Korringa J., 1985, 'An Analysis of the Magnetotelluric Impedance for Three-dimensional Conductivity Structures', 55th SEG Meeting Washington, (MT5), 267-271.

Lee K.H. (1986), Private Communication.

Lee K.H., Pridmore D.F., Morrison H.F., 1981, 'A Hybrid Three-Dimensional Electromagnetic Modelling Scheme', GE, **46**, 796-805.

Lines L.R., Jones F.W., 1973(a), 'The Perturbation of Alternating Geomagnetic Fields by Three-dimensional Island Structures', GJRAS, **32**, 133-154.

ibid, 1973(b), 'The Perturbation of Alternating Geomagnetic Fields by an Island Near a Coastline', Can. Jr. Earth Sci., **10**, 510-518.

Lytle R.J., Lager D.L., 1976, 'Theory Relating to Remote Electromagnetic Probing of a Nonuniform Thickness Coal Seam', Radio Science, **11**(5), 465-475.

Lytle R.J., Lager D.L. Laine E.F., Salisbury J.D., Okada J.T., 1981, 'Fluid-flow Monitoring Using Electromagnetic Probing', GP, **29**, 627-638.

Lytle R.J., Laine E.F., Lager D.L., Davis D.T., 1979, 'Cross-borehole Electromagnetic Probing to Locate High-contrast Anomalies', GE, **44**(10), 1667-1676.

Macnae J.C., 1979, 'Kimberlites and Exploration Geophysics', GE, **44**, 1395-1416.

Macnae J.C., Lamontagne Y., West G.F., 1984, 'Noise Processing Techniques for Time-domain EM Systems', GE, **49**(7), 934-948.

Mbipom E.W., Hutton V.R.S., 1983, 'Geoelectromagnetic Measurements Across the Moine Thrust and the Great Glen in Northern Scottland', GJRAS, **74**, 507-524.

McKirdy D., Weaver J.T., 1984, 'Induction in a Thin Sheet of Variable Conductance at the Surface of a Stratified Earth-I. Two-dimensional Theory', GJRAS, **78**, 93-103.

McNeill J.D., Edwards R.N., Levy G.M., 1984, 'Approximate Calculations of the Transient Electromagnetic Response from Buried Conductors in a Conductive Half-space', GE, **49**, 918-924.

Mozeley E.C., 1982, 'An Investigation of the Conductivity Distribution in the Vicinity of a Cascade Volcono', Ph.D. Thesis submitted at LBL, University of California.

Nabighian M.N., 1983, 'A Review of Time-domain Electromagnetic Exploration', in Proc. Intl. Symp. App. Geophys. in Tropical Regions, Belem Brazil, Sept. 1-8, 1982, Ed. Lourenco BS, Rijo L.

Newman G.A., Hohmann G.W., 1985, 'On the Bias of 1-D TEM Inversions Over 3-D Structures for the Central Loop Configuration', 55th SEG Meeting Washington, EM5, 131-133.

Newman G.A., Hohmann G.W., Anderson W.L., 1986, 'Transient Electromagnetic Response of a Three-dimensional Body in a Layered Earth', GE, **51**(8),1608-1627.

Oristaglio M.L., Hohmann G.W., 1984, 'Diffusion of Electromagnetic Fields into a Two-dimensional Earth : A Finite Difference Apparoach', GE, **49**(7), 870-894.

Oristaglio M.L., Worthington M.N., 1980, 'Inversion of Surface and Borehole Electromagnetic Data for Two-dimensional Conductivity Model', GP, **28**, 633-637.

Palacky G.J., 1981, 'The Airborne Electromagnetic Method as a Tool of Geological Mapping', GP, **29**, 60-88.

ibid, 1983, 'EM Prospecting in Tropical Region', in Proc. Intl. Symp. Applied Geophysics in Tropical Regions, Belem Brazil, Sept. 1-8, 1982, Ed. Lourenco JS, Rijo L.

Palacky G.J., Ritsema I.L., de Jong S.J., 1981, 'Electromagnetic Prospecting for Groundwater in Precambrian Terrains in the Republic of Upper Volta', GP, **29**, 932-955.

Park S.K., 1985, 'Distortion of Magnetotelluric Sounding Curves by Three-dimensional Structures', GE, **50**(5), 785-797.

Park S.K., Orange A.S., Madden T.R., 1983, 'Effects of Three-dimensional Structure on Magnetotelluric Sounding Curves, GE, **48**, 1402-1405.

Patra H.P., 1970, 'Central Frequency Sounding in Shallow Engineering and Hydro-geological Problems', GP, **18**(2), 236-254.

Patra H.P., Mallick K., 1980, 'Geosounding Principles : Time-varying Geoelectric Soundings', Elsevier Amsterdem-Oxford-New York, ISBN 0-444-41704-4.

Peacock J., King A., 1985, 'Central Loop Transient Electromagnetic Soundings', ASEG Bull., **16**(2/3), 261-265.

Poddar M., 1981, 'Multifrequency Turam Measurements Over a Sulfide Deposit', GE, **46**(9), 1269-1277.

ibid, 1982, 'Interpretation of Pulse EM Anomalies Over Gani Conductors, Kurnool, India', GP, **30**, 86-100.

Poddar M., Dhansekaran P.C., 1986, 'Electromagnetic Sounding of the Kapurdi Lignite Deposit in Western Rajasthan, India', GP, **34**(4), 580-594.

Polozhii G.N., 1965, 'The Method of Summary Representation for Numerical Solution of Problems of Mathematical Physics', Pergamon Press Oxford, London, Edinburgh, New York, Paris, FrankFurt, 283 pp.

Porstendorfer G., 1975, 'Principles of Magnetotelluric Prospecting', Geoexploration Monograph, Series I, No.5, Berlin-West, Stuttgart.

Praus O., 1975, 'Numerical and Analogue Modelling of Induction Effects in Laterally Non-uniform Conductors', Phys. Earth. Planet. Inter., **10**, 262-270.

Pridmore D.F., 1978, 'Three-dimensional Modelling of Electric and Electromagnetic Data Using the Finite Element Method', Ph.D. Thesis, Dept. of Geol. and Geophys., University of Utah.

Pridmore D.F., Hohmann G.W., Ward S.H., Sill W.R., 1981, 'An Investigation of Finite Element Modelling for Electrical and Electromagnetic Data in Three-dimensions', GE, **46**(7), 1009-1024.

Rai S.S., Bhattacharya B.B., 1986, 'Quantitative Interpretation of Pulse EM Measurements Over a Weathered Kimberlite Diatreme', GP, **34**(2), 220-231.

Raiche A.P., 1974, 'An Integral Equation Approach to Three-dimensional Modelling', GJRAS, **36**, 363-376.

Ramaswamy V., Nienaber W., Dosso H.W., Jones F.W., Law L.K., 1975, 'Numerical and Analogue Model Results for Electromagnetic Induction for an Island Situated Near a Coastline', Phys. Earth Planet. Inter., **10**, 81-90.

Ranganayaki R.P., Madden T.R., 1980, 'Generalized Thin Sheet Analysis in Magnetotellurics : An Extension of Price's Analysis', GJRAS, **60**, 445-457.

Reddy I.K., Rankin D., Phillips R.J., 1977, 'Three-dimensional Modelling in Magnetotelluric and Magnetic Variational Sounding', GJRAS, **51**, 313-325.

Rijo L., 1983, 'Mathematical Modelling of Applied Geoelectromagnetism', in Proc. Intl. Symp. Applied Geophysics in Tropical Regions, Belem, Brazil, Sept. 1-8, 1982, Eds. Louranco J.S., Rijo L.

Rikitake T., 1966, 'Electromagnetism and the Earth's Interior', Elsevier, Amsterdem, London, New York : p. 308.

Ritz M., 1984, 'Electrical Resistivity Structure of Senegal Basin as Determined from Magnetotelluric and Differential Geomagnetic Soundings', GJRAS, **79**, 635-649.

Rozenberg G., Pesowski M., Eaton D., 1985, 'Combined Transient Electromagnetic Survey for Mineral Exploration : A case History', 55th SEG Meeting, Washington, MIN 2.7, 257-258.

Rokityansky I.I., 1982, 'Geoelectromagnetic Investigation of the Earth's Crust and Mantle', Springer-Verlag, Berlin-Heidelberg-New York, ISBN 3-540-10630-8.

Rutter H., Staltari G., 1984, Proc. of a Workshop on Electromagnetics in Mineral Exploration, held in March 1984 in Australia.

San Filipo W.A., Eaton P.A., Hohmann G.W., 1985, 'The Effect of a Conductive Half-space on the Transient Electromagnetic Response of a Three-dimensional Body', GE, **50**(7), 1144-1162.

San Filipo W.A., Hohmann G.W., 1985, 'Integral Equation Solution for the Transient Response of a Three-dimensional Body in a Conductive Half-space', GE, **50**(5), 798-809.

Scheen W.L., 1978, 'EMMMMA, A Computer Program for Three-dimensional Modeling of Airborne Electromagnetic Surveys', proc. Workshop on Modeling of Electrical and Electromagnetic Methods, LBL-7053, p. 53.

Society of Exploration Geophysicists, 1966, 'Mining Geophysics, Vol.I, Case Histories', Published by SEG.

ibid, 1967, 'Mining Geophysics, Vol.II', ibid.

Silic J., Eadie E.T., Jack D.J., 1985, 'Application of Time-domain Electromagnetic Methods in the Discovery of the Hellyer Ore Deposit, Tasmania, Australia', 55th SEG Meeting, Washington, MIN 2.1, 241-243.

Stodt J.A., Hohmann G.W., Ting S.C., 1981, 'The Telluric-magnetotelluric Method in Two and Three-dimensional Environments', GE, **46**, 1137-1147.

Stoyer C.H., Greenfield R.J., 1976, 'Numerical Solutions of the Response of a Two-dimensional Earth to an Oscillating Magnetic Dipole Source', GE, **41**, 519-530.

Tabbagh A., 1985, 'The Response of a Three-Dimensional Magnetic and Conductive Body in Shallow Depth Electromagnetic Prospecting', GJRAS, **81**, 215-230.

Taflove A., Umashankar K., 1982, 'A Hybrid Moment Method/Finite Difference Time-domain Approach to Electromagnetic Coupling and Aperture Penetration into Complex Geometries', IEEE Trans., **AP-30**, 617-627.

ibid, 1983, 'Radar Cross-section of General Three-dimensional Scatterers', IEEE Trans. Electromagnetic Compatibility, **EMC-25**(4), 433-440.

Tarlowski C.Z., Raiche A.P., Nabighian M., 1984, 'The Use of Summary Representation for Electromagnetic Modeling', GE, **49**(9), 1506-1516.

Ting S.C., Hohmann G.W., 1981, 'Integral Equation Modelling of Three-dimensional Magnetotelluric Response', GE, **46**, 182-197.

Tripp A.C., 1982, 'Multidimensional Electromagnetic Modelling', Ph.D. Thesis submitted at the Dept. of Geology and Geophysics, University of Utah.

Tripp A.C., Ward S.H., Sill W.R., Swift C.M.Jr., Petrick W.R., 1978, 'Electromagnetic and Schlumberger resistivity Sounding in the Roosevelt Hot Springs KGRA', GE, **43**(7), 1450-1469.

Umashankar K.R., Taflove A., 1982, 'A Novel Method to Analyze Electromagnetic Scattering of Complex Objects', IEEE Trans. EM Compatibility, **EMC-24**, 397-405.

Vozoff K., 1983, 'On the State of the Art of Magnetotelluric Methods', in Proc. Intl. Symp. Appl. Geophys. in Tropical Regions, Sept. 1-8, 1982, Belem, Brazil, Ed. Lourenco JS, Rijo L.

Vozoff K., Moss D., LeBrocq K.L., McAllister K., 1985, 'LOTEM Electric Field Measurements for Mapping Resistive Horizons in Petroleum Exploration', ASEG Bull., **16**(2/3), 309-312.

Wait J.R., 1982, 'Geo-Electromagnetism' Academic Press, New York-London-Paris-San Diego-San Fransisco-Sao Paulo-Sydney-Tokyo-Toronto, ISBN 0-12-730880-6.

Wannamaker P.E., Hohmann G.W., 1984, 'Magnetotelluric Responses of Three-dimensional Bodies in Layered Earths', GE, **49**(9), 1517-1533.

Wannamaker P.E., Hohmann G.W., San Filipo W.A., 1984, 'Electromagnetic Modeling of Three-dimensional Bodies in Layered Earths Using Integral Equations', GE, **49**(1), 60-74.

Ward S.H., 1967, 'Electromagnetic Theory', in Society of Exploration Geophysicists Mining Geophysics Vol.II.

ibid, 1980, 'History of Geophysical Exploration - Electrical, Electromagnetic and Magnetotelluric Methods', GE, **45**, 1659-1666.

Ward S.H., Peeples W.J., Ryu J., 1973, 'Analysis of Geoelectromagnetic Data', in Methods in Computational Physics, **13**, and in GE, **38**(5), 1109-1129.

Ward S.H., Ryu J., Glenn W.E., Hohmann G.W., Dey A., Smith B.D., 1974, 'Electromagnetic Methods in Conductive Terraines', Geoexploration, **12**, 121-183.

Weidelt P., 1975, 'Electromagnetic Induction in Three-dimensional Structures', Jr. Geophys., **41**, 85-109.

ibid, 'Inversion of Two-dimensional Conductivity Structures', Phys. Earth Planet. Inter., **10**, 282-291.

ibid, 1981, 'Dipole Induction in a Thin Plate with Host Medium and Overburden', Research project NTS 83, No. 69727, BGR, Hannover, FRG.

West G.F., Edwards R.N., 1985, 'A Simple Parametric Model for the Electromagnetic response of an Anomalous Body in a Host Medium', GE, **50**(12), 2542-2557.

White A., Polatayko D.W., 1985, 'Electrical Conductivity Anomalies and Their Relationship with the Tectonics of South Australia', GJRAS, **80**, 757-771.

Wright P.M., Ward S.H., Ross H.P., West R.C., 1985, 'State of the Art Geophysical Exploration for Geothermal Resources', GE, **50**(12), 2666-2696.

Wynn J.C., 1986, 'Archeological Prospection An Introduction to Special Issue', GE, **51**(3), 533-537.

Yee K.S., 1966, 'Numerical Solution of Initial Boundary Value Problems Involving Maxwell's Equations in Isotropic Media', IEEE Trans., **AP-14**(3), 302-307.

Zhdanov M.S., Golubev N.G., Spichak V.V., Varentsov Iv M., 1982, 'The Construction of Effective Methods for Electromagnetic Modelling', GJRAS, **68**, 589-607.

Zhdanov M.S., Frenkel M.A., 1983, 'Electromagnetic Migration', in Hjelt SE (Ed), The development of the deep geoelectric model of the Baltic shield, Part 2, Proc. of the 1st project symposium Oulu.

Zienkiewicz O.C., 1977, 'Finite Element Method', published by McGraw Hill.

Ziolkowski R.W., Madsen N.K., Carpenter R.C., 1983, 'Three-dimensional Computer Modelling of Electromagnetic Fields : A Global Lookback Lattice Truncation Scheme', Jr. Comp. Phys., **50**, 360-408.